Study on Fabrication of Cibacron Blue-Modified Nanofiber Fabric and Its Application for Protein Separation

(シバクロンブルー修飾ナノファイバー不織布の作製およびタンパク質分離への応用に関する研究)

LIU　Song

Contents

Preface

In this research, polyvinyl alcohol (PVA) nanofiber fabrics were prepared through electrospinning, and the affinity of the PVA nanofiber fabrics was enhanced using Cibacron Blue F3GA (CB). Bovine serum albumin (BSA) and bovine hemoglobin (BHb) were used as model proteins for separation study. The effects of the physical and chemical structure of nanofiber fabrics and adsorption environmental conditions on the adsorption properties of proteins were clarified. Also, the adsorption mechanism of proteins on the surface of PVA nanofiber fabrics was examined.

In chapter 1, the development history of nanofiber fabrics is reviewed, common protein separation methods are introduced, and the research background of the topic is presented. The most typical characteristics of nanofibers are high specific surface area. The superior mechanical strength, wide range of raw material sources and large porosity are also the advantages of nanofibers. Electrospinning is a versatile, convenient, and easy way for the nanofiber preparation. In the production process of protein products, the separation and purification operations directly determine the purity and biological activity of the target protein. The complicated process of biological product recovery dramatically impacts the final product cost because separation and purification accounts for 70% to 80% of the total biological process cost. The development of nanofiber fabrics has brought a promising solution for protein separation and purification.

In chapter 2, fabrication of CB-modified PVA nanofiber fabrics was introduced. Electrospinning polymer solution was prepared by dissolving PVA in water, and maleic acid was added as a cross-linking agent. Then PVA nanofibers were prepared using the electrospinning method. The PVA nanofiber fabric surface was observed by SEM. The chemical structures of the original and CB-modified PVA nanofiber fabrics were

detected with FTIR.

In chapter 3, the static adsorption performance of CB-modified PVA nanofiber fabrics on BSA was investigated. The adsorption amount growed with the BSA initial concentration. The equilibrium isotherm data was analyzed by the Langmuir and Freundlich isotherms, respectively. The saturation adsorption amounts of the PVA nanofiber fabrics increased 4 times after CB modification. The influences of pH value and strength of ions on the adsorption performance were studied. In the desorption test with 1.0 M NaCl at pH 10, the desorption ratio of BSA- adsorbed PVA nanofiber fabrics reached 97.3%. The affinity PVA nanofiber fabrics showed no significant decrease in adsorption performance during repeated adsorption-desorption cycles and exhibited excellent reusability.

In chapter 4, the effects of adsorption conditions on the BSA dynamic adsorption process, such as modification of CB, BSA concentration in the permeate liquid, and permeation rate, were examined with a continuous system. Kinetic studies of adsorption processes were used to describe the rate of solute adsorption by the adsorbent and to fit the data by kinetic models in order to investigate the adsorption mechanism. Adsorption process is usually affected by solute diffusion and chemical interaction between adsorbent and adsorbate, which is one of the focuses of kinetic research. Therefore, Adsorption results were fitted using the adsorption kinetics of the pseudo-first-order kinetic and the pseudo-second-order kinetic. All kinetic parameters and correlation coefficient values were compared between the pseudo-first-order kinetic and the pseudo-second-order kinetic. The higher correlation coefficient values of the pseudo-second-order kinetic model demonstrated that the adsorption rate of BSA on the nanofiber surface is not proportional to the concentration driving force but proportional to the square of the driving force, and the adsorption rate is controlled by the chemical

adsorption mechanism. In order to provide a design basis for adsorption operation, the static and dynamic adsorption efficiencies were compared by the fitting curves according to the experimental data.

In chapter 5, selective adsorption studies were performed using the CB-modified PVA nanofibers with BHb and BSA as model proteins. The molecular weights of BHb and BSA are 64500 and 67000, respectively, and the sizes of BHb and BSA are too close to be effectively separated by conventional filtration operations. The static and dynamic adsorption behaviors of the PVA nanofiber fabrics on BHb before and after CB modification were investigated. The maximum adsorption amounts for BHb and BSA on the CB-modified PVA nanofiber fabrics appeared at pH = 6.8 and pH = 5.0, respectively. However, the maximum difference of the adsorption amounts for the two proteins was observed at pH 6.8, which is corresponding to the isoelectric point of BHb. The selective separation experiments of the BHb-BSA binary solution were carried out at pH = 6.8, and a high selectivity factor for BHb was achieved. Finally, the reusability of the nanofiber fabric was examined by three adsorption-elution cycle tests.

In chapter 6, the research of the thesis is summarized comprehensively. This research demonstrates that Cibacron Blue-modified PVA nanofiber fabrics with simple preparation process, low cost and high protein adsorption capacity have great potential for protein separation and purification.

Chapter 1 Introduction and Background

1.1 Introduction of nanofiber

Nanometer (nm) is one of the units of measuring length, 1 nm is equal to 10^{-9} m. This size is small if compared to the normal things around us, but it is not particularly small at the atomic scale. In fact, distances between individual atoms are typically a tenth of a nanometer (1 Ångström), so a piece of a material with a side of a nanometer may contain hundreds or even a thousand atoms. Nanomaterials are structural materials that have at least one dimension in three dimensions at the nanoscale [1].

The ideas and concepts behind nanoscience and nanotechnology began with a lecture given by the physicist Richard P. Feynman during the 1959 American Physical Society meeting at the California Institute of Technology. In the lecture entitled “There’s Plenty of Room at the Bottom”, Feynman pointed out that if the arrangement of things on a small scale can be controlled, substances will acquire an enormously greater range of possible properties [2]. Nanotechnology is a technology for developing, synthesizing, characterizing and applying materials and devices by modifying their size and shape at the nanoscale [3]. Nanotechnology is a multidisciplinary science involving physics, chemistry, materials science and other engineering sciences. Compared to the bulk material, nanomaterials exhibit new magnetic, optical, electrical, mechanical, and chemical properties due to their shape and size. Applications of nanomaterials are spreading in almost all branches of science and technology. The golden era of nanotechnology began in the 1980s, and after decades of development, nanotechnology has become the foundation for significant industrial applications and exponential growth

[4].

With the rapid advancement in the field of nanotechnology, a large number of nanomaterials have been developed. These nanomaterials can be identified on the basis of structure, shape, size and chemical constituent [5]. Summarily, nanomaterials can be classified into four categories, which are carbon nanomaterials, metal and metal oxide nanomaterials, polymeric nanomaterials, and nanocomposites. Figure 1-1 displays several typical nanomaterials.

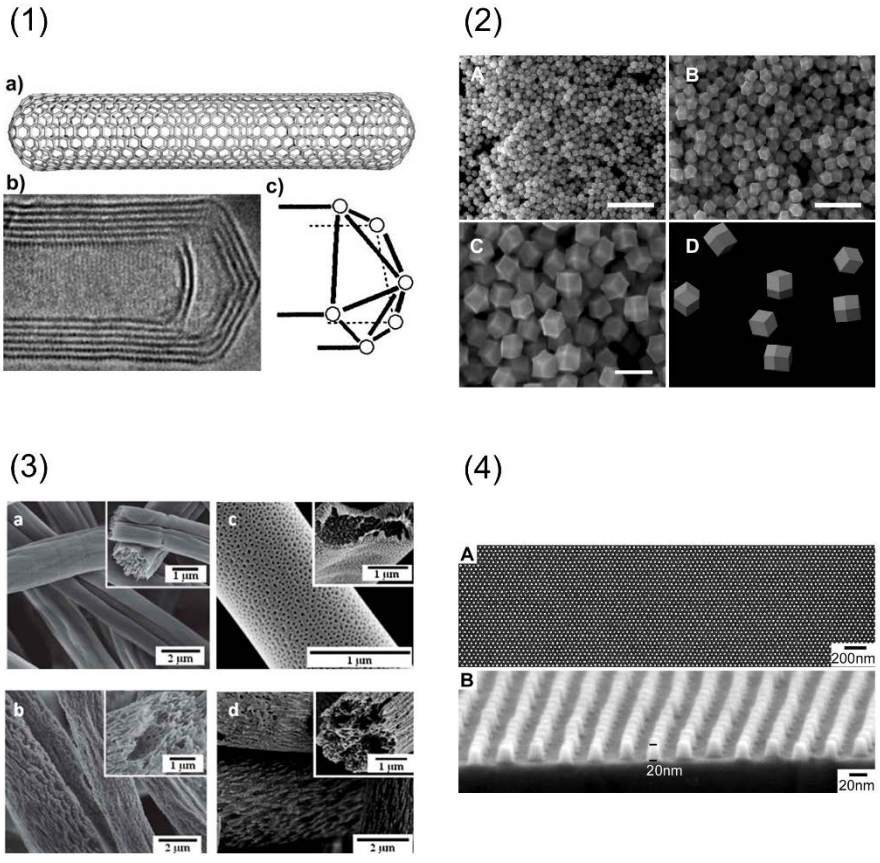

Fig. 1-1 Several typical nanomaterials: (1) carbon nanotube [6]; (2) gold nanocrystals [7]; (3) polystyrene nanofibers [8]; (4) Chromium-deposited copolymer plates [9].

Human beings have a very long history of using and processing fibers. Since ancient times, cotton, linen, wool and silk have been obtained from plants and animals to meet the needs of clothing and keeping warmth. After entering the industrial society, more and more synthetic fibers have been manufactured, not only for the traditional clothing industry, but also for environmental, energy, biomedical and construction applications. Nanofibers are narrowly defined as fibers with a diameter equal to or less than 100 nm. However, in a broad definition, fibers with a diameter less than 1 μm (1000 nm) are usually regarded as nanofibers [10]. Nanofibers have the characteristics of high specific surface area, large porosity, superior mechanical strength, and wide source of raw materials and so on. Therefore, they have received extensive attention from scientists all over the world and play an important role in the field of nanotechnology.

1.2 Electrospinning

There are many ways for the fabrication of nanofibers, such as self-assembly, conjugate spinning, template synthesis, chemical vapor deposition, and electrospinning [10]. Among these methods, electrospinning is regarded as the most versatile, convenient, and simple way for fabricating nanofibers. Electrospinning is a mechanical and electrical technique that uses high voltage electric field to produce ultrafine fibers from melts or polymer solution [11].

1.2.1 History of electrospinning

The first modern electrospinning patent was published by the American inventor Cooley in 1900. In this patent, Cooley proposed four types of indirectly charged spinning

heads, which were conventional head, coaxial head, air assisted model, and spinneret featuring a rotating distributor [12]. Formhals focused on the development of electrospinning methods and the design of apparatus, and contributed significantly to the electrospinning advancement with 22 patents granted in America, France, Britain and Germany between 1931 and 1944 [13]. In the 1960s, Taylor devoted himself to the theoretical study and made enormous contributions to the mathematical modeling of electrospinning [14,15,16]. His description of the characteristic droplet shape is generally known as the “Taylor cone”. The critical applied voltage for electrospinning was given as:

$$V_k^2 = \frac{4H^2}{L^2}\left(\ln\frac{2L}{R} - \frac{3}{2}\right)(1.30\pi R\gamma)(0.09) \qquad (1\text{-}1)$$

where V_k is the critical voltage, H is the distance between two electrodes, L is the distance of nozzle extending from electrode plate, R is the nozzle radius, and γ is the surface tension.

Larrondo et al. prepared polypropylene (PP) and polyethylene (PE) fibers by electrospinning of polymer melts. The effects of electric field strength and the temperature or viscosity of the polymer melt were investigated. Their results are groundbreaking for the melt electrospinning study [17].

Since the 1990s, with the successful acquisition of nanoscale electrospun fibers, institutions and research groups have gradually shifted their focus from the early development and improvement of spinning devices to the preparation and application of nanofiber materials. Currently, hundreds of polymer materials have been used to prepare electrospun fibers for applications in tissue engineering scaffolds, nanocatalysis, biosensors, wound dressings, filtration, pharmaceutical, healthcare, energy engineering,

security and defense [18].

1.2.2 Electrospinning processes

The basic electrospinning setup includes a high voltage power supply, a syringe pump system, a syringe, a needle, and a nanofiber fabric collector, as shown in Fig. 1-2.

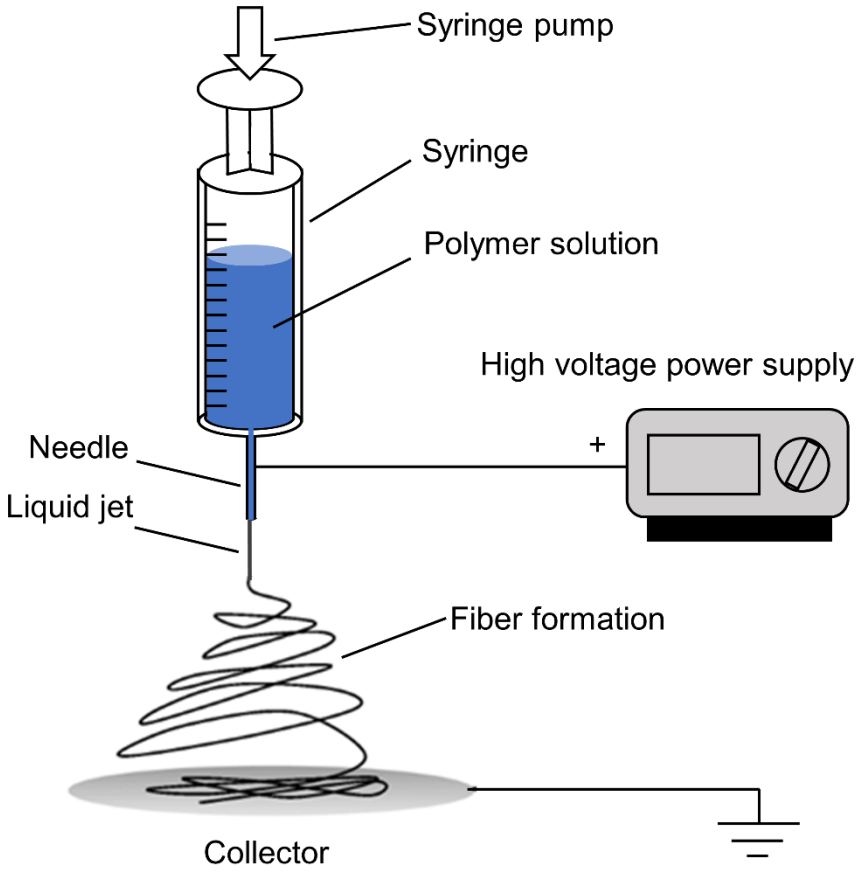

Fig. 1-2 Schematic illustration of the basic setup for electrospinning [19].

In brief, polymer solution is pumped out by the syringe pump at a constant flow rate. Two electrodes are connected to the spinning solution and the fiber collector. An optimized electrical potential is applied to the spinneret, and the droplets formed at the

spinneret tip is charged and become cone shape. Once the electrostatic force exceeds the viscoelastic force and the surface tension of the polymer droplets, the charged polymer solution is ejected from the spinneret tip. The initial straight-line jet, with the occurrence of whipping movement, transforms into a thinner form. Due to mutual repulsion, the different polymer strands in the jet get separated. During the process, the solvent evaporates as the jet moves toward the collector which decreases the jet radius and increases the polymer concentration and viscosity. After the evaporation of the solvent evaporates, the solid fibers deposit on the grounded collector [19,20].

1.2.3 Factors impacting electrospinning

The variety of polymers corresponds to the variety of solvates that can be selected. Due to the limitations of melt electrospinning, electrospinning from polymer solutions is the main way to obtain nanofibers. The morphology, strength, porosity and fiber diameter of electrospun nanofibers are influenced by many factors, which can be grouped into three categories: polymer solution properties, environmental conditions, setup and operation parameters [21].

1.2.3.1 Impact of polymer solution properties

(1) Molecular weight of polymers

The polymer used for electrospinning can be synthetic or natural polymers. Molecular weight of the polymer has a significant effect on the viscosity, surface tension, and dielectric strength of the solution. Polymers with high molecular weight are more suitable for electrospinning, but the diameter of fibers produced from polymers with too molecular weight becomes thicker [22].

(2) Concentration, viscosity, surface tension of solution

When the concentration of the polymer as a solute becomes higher, the viscosity of the polymer solution also increases. In the case of insufficient concentration and viscosity, beads of polymer are obtained instead of fibers. Zong et al. [23] reported the changes in the microstructure of electrospun poly(D,L-lactic acid) nanofibers for the solution concentration range of 20% ~ 35%, and the results are shown in Fig. 1-3.

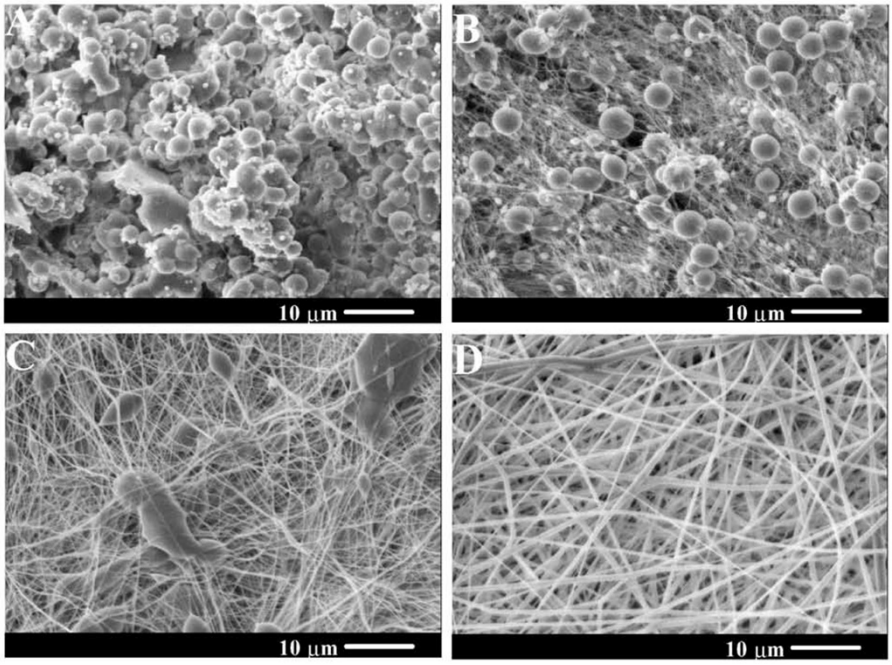

Fig. 1-3 Concentration effect on electrospun poly(D,L-lactic acid) nanofibers: (A) 20 wt%; (B) 25 wt%; (C) 30 wt%; (D) 35 wt% [24].

When the concentration and viscosity of the solution are higher than a certain critical value, continuous fiber structures are obtained because the degree of entanglement between the molecular chains increases and is less likely to break when subjected to the

tensile force of electric forces. Surface tension not only affects the formation of the Taylor cone, but also affects the motion and splitting of jets in the high voltage electric field [24]. Increasing the concentration leads to a decrease in surface tension of the solution. In addition, adjusting the solvent composition also affects the surface tension.

(3) Solvent

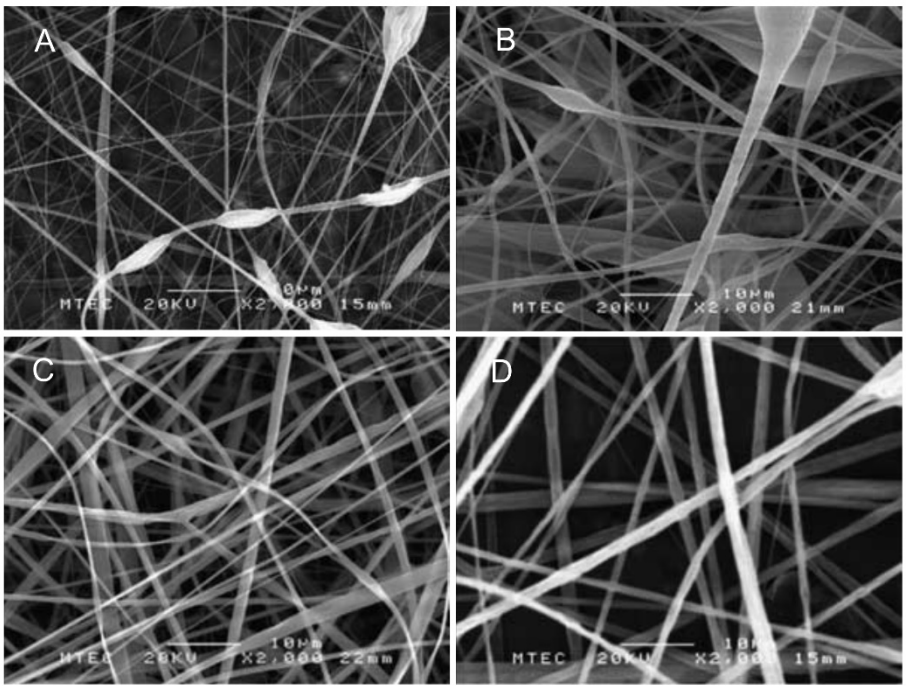

Fig. 1-4 Polystyrene nanofibers from solutions of polystyrene in various solvents (20%w/v): (A) 1,2-dichloroethane; (B) dimethylformamide; (C) methylethylketone; (D) tetrahydrofuran [26].

The main function of the solvent is to break apart the molecular chains of the polymer. During the electrospinning process, as the solvent evaporates, the polymer molecular chains are rearranged and jets finally solidifies into polymer fibers. Hydrophilic polymers are electrospun by dissolving in water, strong acids or polar organic solvents, while

hydrophobic polymers require the selection of suitable organic solvents for dissolution [25]. Jarusuwannapoom et al. [26] investigated the effects of various solvents on the structural morphology of polystyrene nanofibers, as shown in Fig. 1-4. The formation of beads was a function of viscoelasticity and surface tension. Solvents that are not evaporate fast enough before the charged jet reaches the collector caused local shrinkage of the moist fibers.

1.2.3.2 Environmental conditions

(1) Temperature

Electrospinning process is usually carried out at room temperature. Raising the ambient temperature enhances the volatilization rate of solvent, which causes jets to cure rapidly, thus weakening the stretching effect of the electric force on the jets. In addition, elevating the feed temperature reduces the viscosity and surface tension of the solution [27].

(2) Humidity

The effect of ambient humidity on nanofiber formation is closely related to the polymer and solvent properties. When the solvent on the surface of the jet evaporates, the solvent interior of it is also diffusing to the surface. Increasing the humidity inhibits the solvent removal, which makes the fiber diameter increase. When the humidity is too high, the hydrophilic groups of some polymers absorb water, causing adhesion of the fibers [28].

1.2.3.3 Setup and operation parameters

(1) Voltage

Voltage is a crucial factor in the electrospinning process. The high voltage induces the solution to generate an electric charge and creates an external electric field. When the

electrostatic force overcomes surface tension and adhesion, the polymer solution generates a jet that initiates the electrospinning. At a certain concentration of polymer solution, as the voltage increases, the charge density of the solution jet surface rises, which can intensify the stretching effect on the jet, resulting in a decrease in fiber diameter. However, the electric force acting on the jet is in competition with the viscous stress of the jet solution, and the effect of voltage on electrostatic spinning is not entirely the same for different polymer solutions [29,30]. However, high voltages are necessary to maintain the stability of the Taylor cone. Also, high voltage affects the degree of crystallization of polymer fibers [31].

(2) Feeding flowrate

The feeding flowrate is an important parameter affecting the jet velocity and mass transfer, and to some extent determines the output of the electrospinning. A feeding flowrate facilitates solvent volatilization and reduces fiber adhesion. For different polymer-solvent systems, there exists a minimum flow rate for electrospinning occurring. At a given voltage, the fiber diameter increases within a certain range with the feeding flowrate. If feeding flowrate is too high, it will lead to incomplete solvent volatilization and insufficient jet stretching, which will affect the fiber morphology [32].

(3) Collector

In the electrospinning process, the charged jet travels towards the collector from the nozzle under the force of high-voltage electric field. The collector is usually made of aluminum foil, copper plate, stainless steel and so on. The collector of conductive material facilitates the formation of a stable electric field between the nozzle and the electrode plate, and also makes the residual charge on the fiber dissipate quickly. Fibers collected

on collectors of non-conductive materials tend to have a lower packing density than those of conductive materials. The structure of the collector also affects the formation of fibers. Compared to flat collectors, rotary collectors facilitate the acquisition of dry fibers because the fibers get more time to evaporate [33,34].

(4) Needle

A necessary consideration in the jet excitation process is the critical voltage value. This value is related to the size of the droplet and decreases as the droplet size over decreases. The role of the needle in the electrospinning process is to create small droplets and to provide a base for the jet formation. Depending on the way in which the droplets are generated, the jet formation system can be usually divided into a needle system and a needleless system [35].

In the needle system, the intensity of the electric field at the mouth of the needle decreases as the diameter of the needle increases. A smaller needle diameter reduces needle clogging and creates a smaller fiber diameter [36]. Figure 1-5 displays several common electrospinning needles. In the multi needle system, on the one hand, the spinning efficiency is dramatically improved by increasing the number of needles; on the other hand, it is possible to fabricate fibers from the same polymer but with different morphologies and diameters, or composite nanofibers from multiple polymers [37].

The needleless electrospinning is a process of fabricating nanofibers by electrospinning a polymeric solution directly from an open liquid surface [38]. The advantage of needleless electrospinning technology over the electrospinning with needles is that it solves the problem of production efficiency and enables mass production. In addition, the needleless electrospinning technology avoids electrostatic interference between needles

in a multi-needle system and does not suffer from needle clogging.

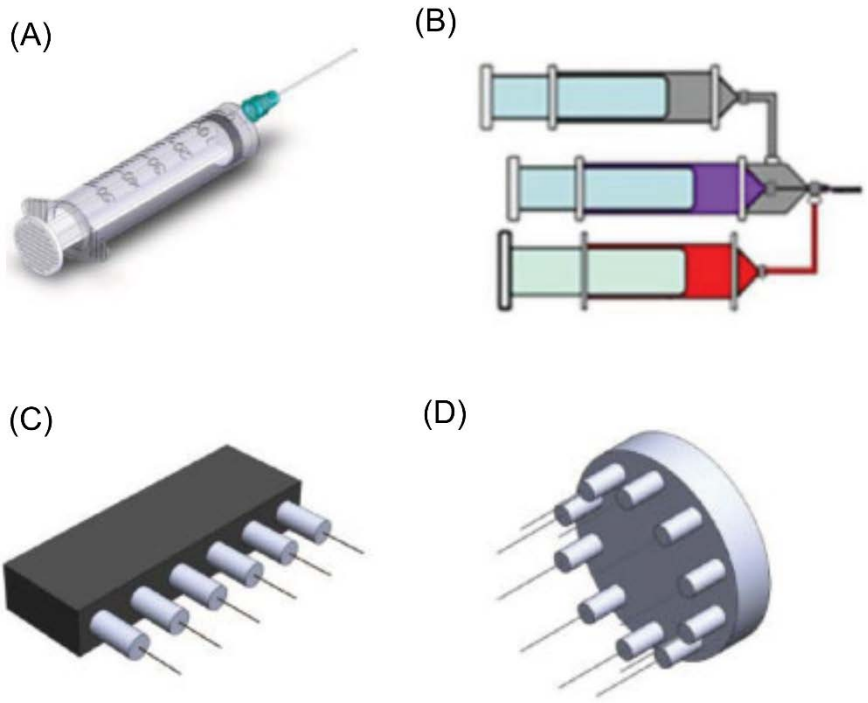

Fig. 1-5 Illustrations of several electrospinning needles: (A) single needle; (B) tri-axial; (C) linear multi needle; (D) circular multi needle [37].

1.3 Types of electrospun nanofiber

At the early stage of the development of electrospinning, researches were mainly focused on the preparation and process optimization of organic nanofibers. As the importance of composite nanofibers is gradually recognized, more and more metal and inorganic substances are added to polymer matrix to obtain composite nanofibers with special functions [39,40].

1.3.1 Organic nanofibers

Organic nanofibers can be classified into single-component nanofibers and multi-component nanofibers. So far, hundreds of natural and synthetic polymers have been prepared into nanofibers by electrospinning. As renewable resources, natural polymers mostly have good biocompatibility and are especially suitable for biomedical applications. The natural polymers that have been used to prepare nanofibers are mainly hyaluronic acid [41], cellulose [42], gelatin [43], chitin [44], chitosan [45], and so on. A wide variety of synthetic polymers are used to prepare nanofibers by electrostatic spinning, such as polyethylene glycol (PEG) [46], PVA [47], polyvinylpyrrolidone (PVP) [48], polyacrylonitrile (PAN) [49], polystyrene (PS) [50], polypropylene (PP) [51], polyurethane (PU) [52], and so on.

1.3.2 Polymer/inorganic composite nanofibers

Polymer/inorganic nanofibers are composite nanofibers formed by dispersing inorganic nanomaterials in polymer nanofibers. The inorganic materials used to prepare composite nanofibers are mainly focused on inorganic oxides [53,54], metal sulfides [55,56], metals [57,58], carbon materials [59,60], and so on. The polymer matrix serves to fix the inorganic nanocomponents for better exerting their performances. Inorganic components can endow polymers with excellent optical, electrical, catalytic, and adsorption properties. Polymer/inorganic nanofiber material is a multifunctional material because it combines the characteristics of polymer and inorganic components.

Mukai et al. [61] fabricated nanocarbon-supported nanofibers for purification of contaminated water, and Fig. 1-6 shows the images of the PAN and nanocarbon/PAN

composite nanofibers. The maximum methylene blue (MB) adsorption capacities of the PAN nanofiber, nanocarbon/PAN composite nanofiber and oxidized nanocarbon/PAN nanofibers were 1.9, 5.0 and 96.2 mg/g, respectively. Although nanocarbon particles have been demonstrated to be an excellent adsorbent for diverse organic compounds including dyes, the secondary pollution of sludge has to be considered when they are used for adsorption alone. The oxidized nanocarbon/PAN nanofiber takes advantage of the high specific surface area of nanofiber and excellent adsorption of carbon particles, which perfectly solve the problem of secondary pollution of carbon particles.

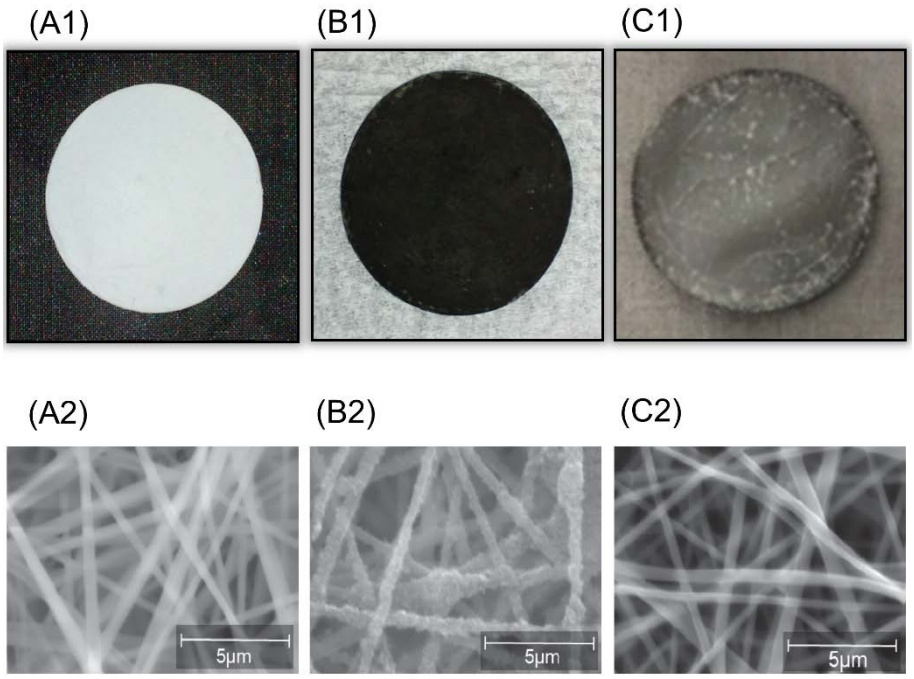

Fig. 1-6 Images of PAN and nanocarbon/PAN composite nanofibers: (A1) PAN nanofiber; (A2) SEM image of PAN nanofiber; (B1) nanocarbon/PAN composite nanofiber; (B2) SEM image of nanocarbon/PAN composite nanofiber; (C1) oxidized nanocarbon/PAN composite nanofiber; (C2) SEM image of oxidized nanocarbon/PAN composite nanofiber [61].

1.3.3 Inorganic nanofibers

Carbon nanofibers [62,63], ceramic nanofibers [64~66], metal nanofibers [67~69] have been successfully prepared previously. Inorganic materials are difficult to be electrospun after melting because of their high melting point. Figure 1-7 shows a typical procedure for preparing inorganic nanofibers. The preparation of inorganic nanofibers is mainly divided into three steps: (1) preparation of an inorganic precursor solution; (2) electrospinning of the precursor solution to obtain polymer/inorganic composite fibers; (3) calcination of the composite fibers at high temperature to remove the organic components form the fibers.

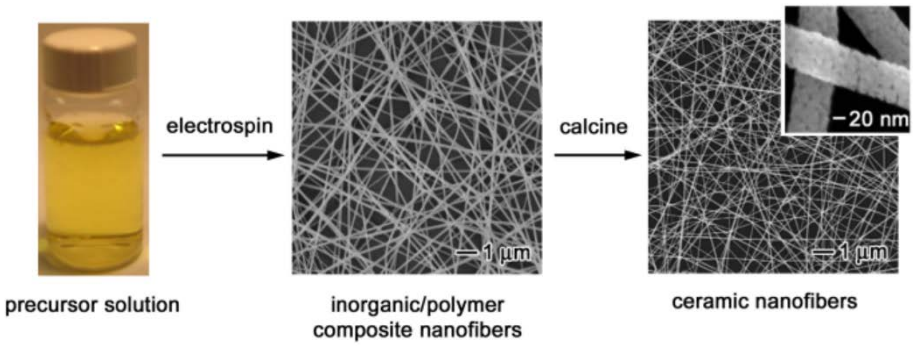

Fig. 1-7 Schematic illustration of a typical procedure for preparing inorganic nanofibers by electrospinning [65].

1.4 Surface modification techniques of nanofiber

Through physical or chemical treatment, the nanofibers can obtain some new surface properties while maintaining the bulk properties. These surface properties include electrical conductivity, hydrophilicity, hydrophobicity, biocompatibility, adsorption and

so on. Surface modification technologies have greatly expanded the application field of nanofibers.

1.4.1 Plasma treatment

Plasma treatment is regarded as an economical, facile, and environmentally benign process. Plasma is described as the fourth state of matter composed of electrons, radicals, photons, and ions positively or negatively charged. Suitable gas sources such as H_2, O_2 and N_2 can be used to functionalize the nanofiber surface [70]. Plasma-induced graft copolymerization treatment is limited to the surface, and the thickness of the modified layer can be controlled down to an ångström level.

Wang et al. investigated the hydrophilic changes of the polyphenylsulfone (PPSU) nanofiber before and after the O_2 plasma treatment [71]. Figure 1-8 shows the contact angle test results of the PPSU nanofibers. The water drop disappeared into the plasma-treated nanofiber surface immediately during the contact angle test, indicating that the nanofiber surface turned to be super hydrophilic.

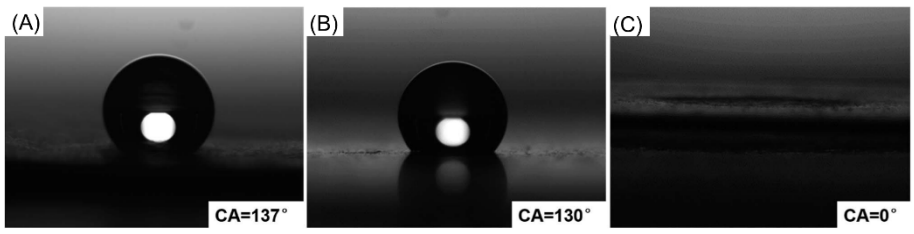

Fig. 1-8 Contact angles of water droplets on the polyphenylsulfone (PPSU) nanofibers: (A) As-spun nanofiber; (B) Heat-treated nanofiber; (C) Heat-treated and plasma-treated nanofiber [71].

1.4.2 Wet chemical method

The wet chemical method is a method to modify the nanofibers by chemical reaction in the liquid phase. The modification of nanofibers using wet chemistry usually uses the oxygen-containing functional groups on the fiber surface, such as carbonyl, hydroxyl, and carboxyl groups, for the reaction [72]. Thien et al. [73] used a wet chemical process to mineralize chitosan nanofiber's surface and obtained a homogeneous hydroxyapatite deposit. The resulting nanofibrous scaffolds have considerable potential in future bone tissue engineering applications.

1.4.3 Surface graft polymerization

The technology of surface graft polymerization is to modify the matrix by grafting macromolecules on the matrix. Especially in biomedicine, the nanofibers can interact with specific biological tissues or cells only after their surfaces are modified by bioactive molecules or cell recognition ligands [74]. Chua et al. [75] grafted galactose ligands on the poly(ε-caprolactone-co-ethyl ethylene phosphate) nanofiber scaffold. The hepatocytes cultured on galactosylated nanofiber scaffold formed smaller aggregates of 20–100 μm that engulfed the functional nanofibers, resulting in an integrated spheroid-nanofiber construct.

1.4.4 Sputtering technology

Sputtering technology refers to the generation of electrons and positively charged ions by ionizing inert gases through direct current or high frequency electric fields, and using these particles to sputter out atoms or molecules by bombarding the target material at high

speed and depositing them on the substrate to form a thin film [76].

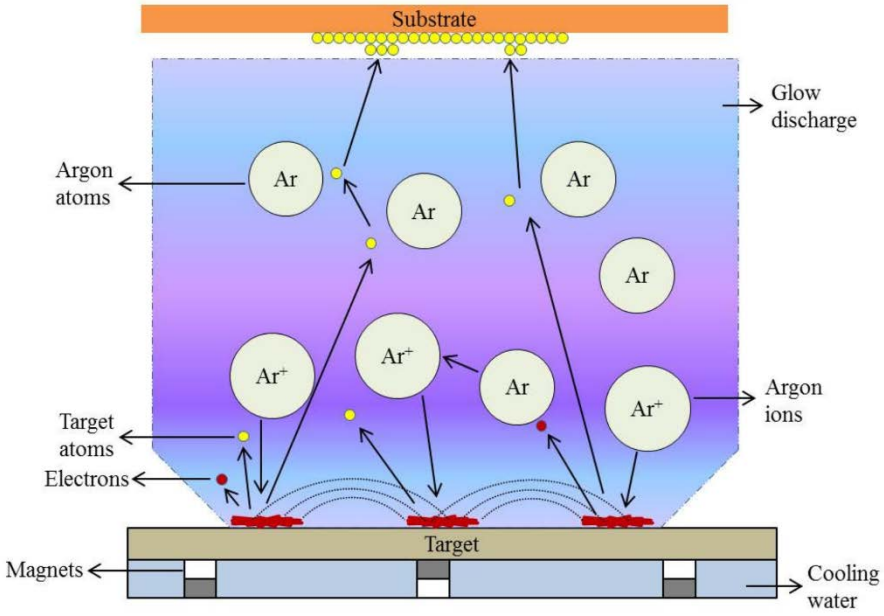

Fig. 1-9 Schematic representation of sputtering technology [76].

Figure 1-9 shows the schematic representation of sputtering technology. Nanoparticles of metals such as silver and copper are deposited on the surface of electrospun fibers by sputtering technology, which allows the nanofibers to acquire antibacterial properties and improve biocompatibility [77, 78].

1.5 Protein isolation and purification

Proteins are biological macromolecules, which maintain the integrity of the cell structure and function [79]. Proteins are abundant in biology and are essential building blocks of life [80]. All metabolic activities of living organisms, including growth, development and reproduction, are related to the activity and metabolism of proteins. The cells of living organisms consist of different kinds of proteins, each of which has a

different structure and function [81~83]. Proteins generally exist in complex mixed forms in tissues and cells, and various types of cells contain thousands of different proteins.

Protein products not only have a broad usage in daily life such as food engineering and daily chemicals [84,85], but also play a vital role in the frontier fields of biomedicine, medical diagnosis and proteomics [86]. Protein products are mainly obtained through two sources, one is the extraction from natural products; the other is the large-scale production using biotechnology and fermentation engineering. Protein extraction, separation and purification processes are necessary for the both sources. To ensure the efficacy and safety of protein products, the fields of food engineering, bioreagents and biopharmaceuticals have high requirements for the purity of protein products, which must meet the requirements of food specifications, reagent standards and pharmacopoeias. In the production process of protein products, the separation and purification steps directly determine the purity and biological activity of the target protein [87]. The tedious process of biological product recovery dramatically impacts the final product cost because separation and purification accounts for 70% to 80% of the total biological process cost [88].

1.5.1 Filtration

Filtration is broadly used processes in protein separation. Filtration separation is based on the variability of the size and shape of protein molecules [89], where the protein solution is driven by pressure difference to flow through porous filter media. Protein molecules whose sizes are smaller than the filter pore size pass through the filter medium, while protein molecules of larger sizes are retained, resulting in the separation and

purification of proteins [90].

Ultrafiltration is most widely used in protein separation and purification. During the ultrafiltration process, pore blockage and fouling usually lead to a gradual decrease in treatment flux [91]. There are still some limitations in the separation of protein with traditional filtration technologies. In particular, protein filtration can only be applied to protein with significant differences in molecular weight. The separation selectivity is hardly controllable for the protein molecules of similar sizes [92].

1.5.2 Precipitation

Precipitation serves to achieve separation by converting solutes to solids, which can subsequently be removed by a liquid-solid separation process [93]. Precipitation is a traditional method to accomplish the purification and concentration of proteins. Protein molecules can be uniformly dissolved / dispersed in the solvent system to form a stable colloidal solution. When changing the properties of the solvent system (ionic strength, pH, type of solvent, addition of high molecular mass polymers), some proteins in the protein colloidal solution aggregate each other and precipitate to form amorphous particles. The proteins are then collected by liquid-solid separation processes, and concentration of proteins can be achieved by redissolving the collected precipitated proteins in a much smaller volume than that in which it was dissolved originally. Depending on the induction mode, the commonly used protein precipitation methods are salting out [94], isoelectric precipitation [95], addition of organic solvents [96], and so on.

1.5.3 Centrifugation

Centrifugation is based on the differential sedimentation coefficients between protein molecules of different molecular weights and sizes, and proteins of solution systems are separated from each other under the powerful centrifugal force generated by the high-speed rotation of the centrifuge. As a common method of protein separation and purification, centrifugation can be divided into differential centrifugation and density gradient centrifugation [97,98]. Differential centrifugation causes particles in a uniform density medium to sediment at different speeds by increasing the centrifugal speed. Particles of different densities or sizes in a suspension sediment at different speeds, with larger and denser particles settling more quickly. Differential centrifugation is suitable for the separation and purification of protein molecules with large differences in sedimentation coefficients or molecular weights. This method has a large processing throughput, but the separation grade is not high, so it is generally employed in the primary separation stage [99].

In the method of density gradient centrifugation, the sample solution is placed on a liquid column with a density gradient formed by a specific medium, and the mixed substances are separated by centrifugation. The separated substances are distributed in different areas of the density gradient column, showing a zonal distribution, so it is also called zonal centrifugation. It is applicable to the separation of biological macromolecules of different densities [100]. Although density gradient centrifugation is an effective method for the separation of biological macromolecules without destroying the activity of proteins, it is mainly applied to experimental scientific research because of the expensive equipment, long operation time, complicated process, and small processing

volume.

1.5.4 Adsorption

Materials with nanoporous surfaces are broadly applied as adsorbents in industry, especially in applications for selective adsorption of specific components in mixtures [101]. Adsorption process is characterized by high efficiency, time-saving, and easy processing. Porous resin beads and gel microspheres are usually used as adsorbents for the separation of proteins. However, large pressure drop, unsatisfactory binding capacity, consumption of huge amounts of solution, and low processing rates are the problems associated with the use of these adsorbents [102,103]. Because of the high specific surface area and nano-size effect, nanofiber fabrics have gained much interest as a matrix for fixing affinity substances having special functional groups in recent years [104].

Nanofiber fabrics with adsorption functional groups have proven to be one of the most promising adsorbents for protein adsorption [105,106]. With the development of nanofiber fabrics technology, affinity ligands are introduced into the surfaces of fabrics to selectively capture target molecules, while letting other molecules pass through [107, 108]. Lu et al. [109] prepared a highly efficient and versatile cellulose nanofiber fabric by immobilizing a dye of CB on the internal surface of the fabric. The produced fabric had a facile lipase loading of approximately 150 mg/g. Duan et al. [110] developed a new type of nanofiber based metal-chelating affinity fabrics by orderly modifying the electrospun regenerated cellulose nanofiber fabric with intermediate bridging agent of cyanuric chloride, chelating agent of iminodiacetic acid and affinity ligand of Fe ions. The resultant fabric exhibited a high lysozyme adsorption amount of 365 mg/g. Wang et

al [111] prepared an amine-functionalized PVA-co-PE nanofiber fabric for bilirubin removal, where the adsorption capacity for bilirubin reached 110 mg/g.

1.6 Research content and significance of the thesis

Electrospun nanofiber fabrics are characterized by large specific surface ratio, high porosity, superior mechanical strength, excellent controllability of the spinning process, and a wide variety of raw materials [112]. These excellent properties make nanofiber fabrics play an important role in filtration [113], personal protection [114~117], biomedicine [118], energy [119] and other fields.

The significant growth of the protein market poses a considerable challenge to industrial production, particularly downstream processing, due to its limited production capacities and high cost. Therefore, it is necessary to develop simple, rapid, scalable, and economically feasible methods for protein separation. Addressing this problem, the development of nanofiber fabrics has provided a direction for the solution of the troubles in protein separation.

In this thesis, PVA nanofiber fabrics were prepared by electrospinning technology and functionalized with CB. The thesis focuses on the preparation process, modification method, structural characterization and application of PVA nanofiber fabrics in protein adsorption and separation.

BSA and BHb were used as model proteins as adsorption objects in the adsorption experiments for the CB modified PVA nanofiber fabrics. Serum albumin maintains the osmotic pressure and pH of the blood, and transports a wide variety of endogenous and exogenous compounds, and BSA displays approximately 76% sequence homology with

human serum albumin [120]. Hemoglobin is a carrier of oxygen and aids the transport of carbon dioxide, and BHb has more than 85% amino acid sequence homology with human hemoglobin [121]. The molecular weights of BSA and BHb are 67000 and 64500, respectively [122,123].

The potential application properties of the resultant fabrics were evaluated by testing their BSA static and dynamic adsorption properties. The Langmuir isotherm model was applied to elucidate the equilibrium adsoiption data. The pseudo-first-order and pseudosecond-order kinetic models were also used to analyze the kinetics adsorption data. Moreover, the efficiency of the static and dynamic adsorption behaviors was examined.

The sizes of BHb and BSA are too close to be effectively separated by conventional filtration operations. The static and dynamic adsorption performances of the PVA nanofiber fabrics for BHb before and after the CB modification were investigated. Then, the effect of pH on the BHb and BSA adsorption performance was examined. Finally, the selective separation experiments of BHb and BSA were carried out at the optimal pH value, with the reusability of the PVA nanofiber fabrics also being studied. This research demonstrated the potential of the CB modified PVA nanofiber fabric in protein adsorption and separation application.

Chapter 2 Fabrication of Cibacron Blue-Modified PVA Nanofiber Fabrics

2.1 Introduction

PVA is a widely used polymer with the chemical formula of $[C_2H_4O]_n$. PVA molecules contain a large number of hydroxyl groups and have good water solubility. Generally, the higher the temperature, the more soluble PVA is in water. PVA has good light transmission and biocompatibility, so it is generally applied in packaging engineering [124], and tissue engineering [125]. Because of its degradable nature, PVA has been also regarded as an eco-friendly material. With the increasing awareness of environmental protection, the demand for green environmental protection is becoming more and more urgent. More and more attention has been paid to the application of PVA materials.

PVA solution is easily electrospun into nanofibers through electrospinning technology. PVA nanofiber fabric with excellent chemical and physical properties can be obtained by adding appropriate bridging agents to the PVA spinning solution or by heat treatment of the raw nanofiber fabrics. PVA nanofiber fabric is characterized by large specific surface area, easy modification, non-toxic and odorless, which is suitable as matrix to provide abundant active sites for protein adsorption.

CB is a monochlorotriazine dye which contains three acidic sulfonate groups and four basic primary and secondary amino groups, which bind with considerable specificity and significant affinity to proteins [126]. For instance, Lu and Hsieh [109] prepared a highly efficient and versatile cellulose nanofiber fabric by a nucleophilic reaction of the cellulose hydroxyl with the triazinyl chloride of the CB ligand. The

resulting fabric had a facile lipase loading of approximately 150.0 mg/g. Zhang et al. [127] immobilized the CB ligand on the chitosan-coated polyacrylonitrile (PAN) nanofiber fabric. The CB-attached PAN nanofiber fabric showed a capturing capacity of 161.6 mg/g towards bromelain. Zhu et al. [128] fabricated the CB functionalized poly(vinyl alcohol-co-ethylene) as affinity materials. The functionalized fabric achieved a BSA capture capacity of 105.5 mg/g. Although the fabrication of modified nanofiber-based mediums has certainly progressed, some bottleneck problems still exist, such as the convoluted modification processes, unsatisfactory adsorption performance, and weak mechanical properties. Therefore, it is highly urgent to exploit a terse approach for fabricating highly effective nanofiber-based adsorption media.

In this study, PVA nanofiber fabrics were prepared by electrospinning method, and then the nanofiber surface was modified by CB, aiming to develop a novel nanofiber fabric as a protein adsorption platform.

2.2 Experimental

2.2.1 Materials

PVA (Mw=66,000-79,000) with a saponification degree of 78-82 mol%, Sodium chloride (NaCl) and sodium carbonate (Na_2CO_3), maleic acid ($C_4H_4O_4$) were purchased from Wako Pure Chemical Industries, Ltd., Japan. CB was purchased from Polysciences, Inc., Japan. The electrospun PVA nanofiber fabrics were supplied by Japan Vilene Company, Ltd., Japan.

2.2.2 Electrospinning

In this study, the electrospinning apparatus of SNAN-10 (MECC CO., LTD., Japan)

was used to fabricate PVA nanofiber fabric, as shown in Fig. 2-1. Table 2-1 shows the operation parameters of the electrospinning apparatus.

Fig. 2-1 Electrospinning apparatus.

Table 2-1 Operation parameters of the electrospinning apparatus.

Parameter	Setting range
HVPS Voltage	0.5～30 kV
Solution Volume	0.1～10.0 mL
Feed Rate	0.1～20.0 mL/h
Syringe Diameter	5.0～18.0 mm
Spinneret Center	-100～100 mm
Spinneret Width	0～200 mm
Spinneret Speed	0～100 mm/s

A schematic layout of the electrospinning process is illustrated in Fig. 2-2. The electrospinning solution was prepared by 10 wt% PVA solution in water [129,130]. Mechanical stirring was applied over 12 h at 90 ℃ in order to obtain a homogeneous PVA solution. Since partially saponified PVA is easily dissolved in water, insolubilization is required. Hence, serving as a crosslinker of the composite through esterification reaction, maleic acid (20 wt% of PVA) was added to the PVA solution before electrospinning [104]. For the preparation of PVA nanofiber fabrics using the electrospinning apparatus, the parameters of the apparatus were set as follows: the high voltage of the power supply was 28 kV; the distance from the needle tip to the collector was 15 cm; and the flow rate of the PVA solution in the syringe was 0.2 mL/h. The electrospinning process was performed at the humidity of 30% under the room temperature. The as-spun fabrics were dried in an oven at 120 ℃ for 1 h.

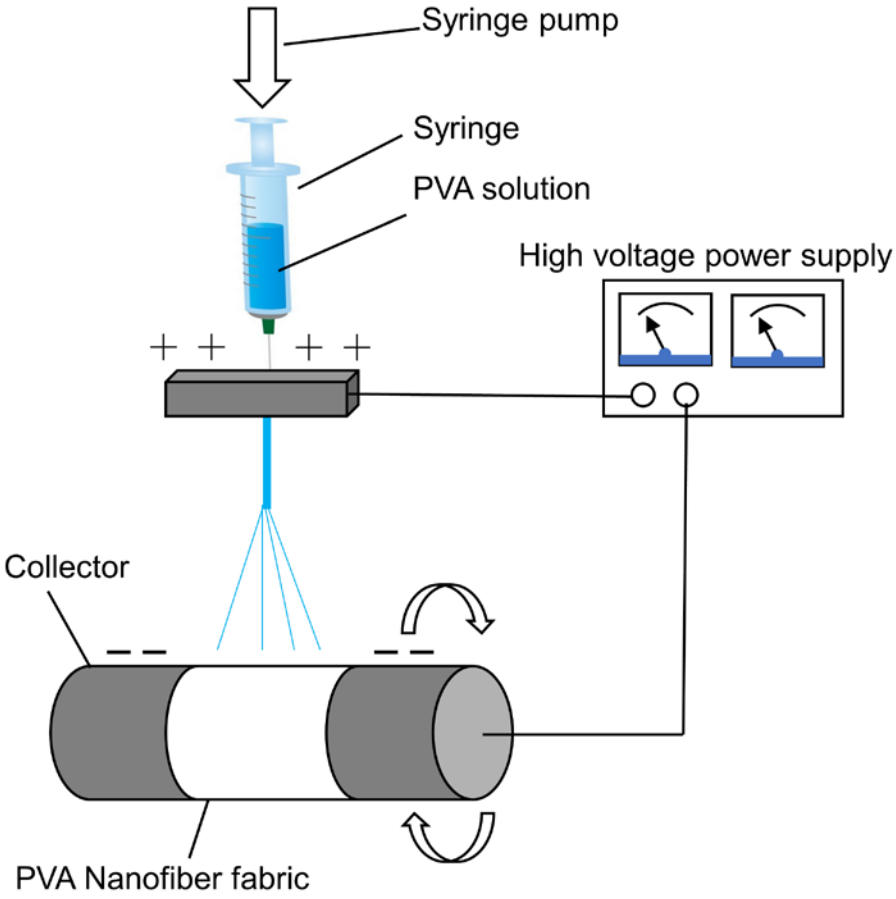

Fig. 2-2 Schematic illustration of PVA electrospinning process.

The cross-linking reaction between PVA and maleic acid is used to improve the water resistance and mechanical properties of PVA nanofiber fabrics. The cross-linking reaction is achieved by the esterification reaction between PVA molecules and maleic acid at high temperature, as shown in Fig 2-3. The esterification cross-linking reaction introduces carbonyl groups between the polymer chains of PVA, but does not affect the main chain structure of PVA molecules.

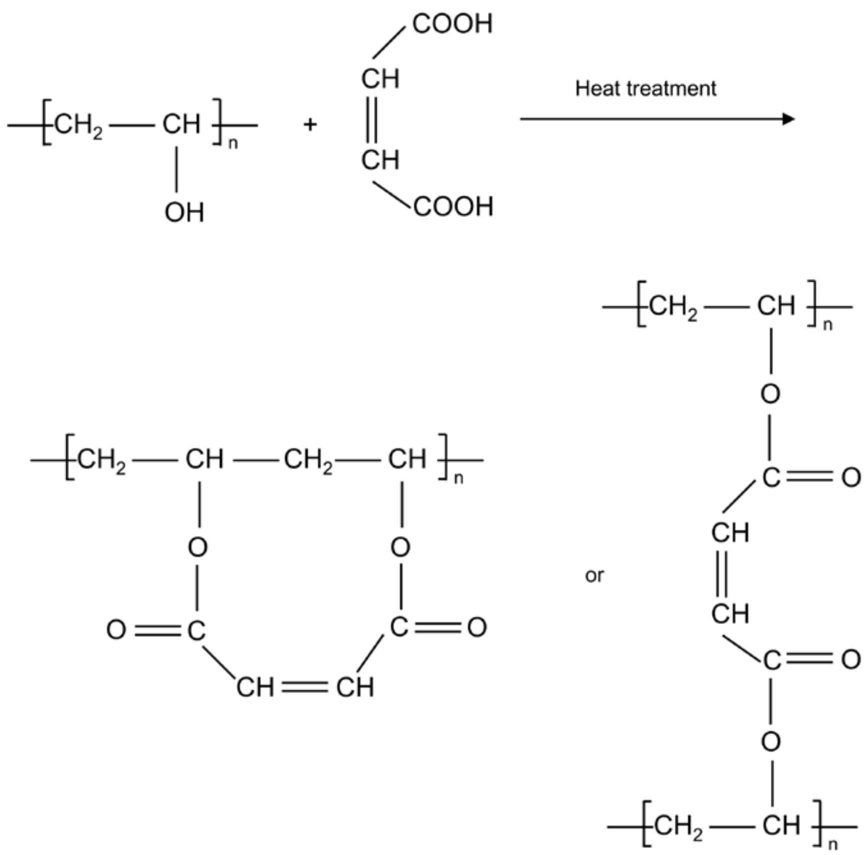

Fig. 2-3 Cross-linking of PVA with maleic acid [129].

2.2.3 Functionalization of nanofiber fabric

The CB-enhanced affinity PVA nanofiber fabrics were prepared by the method described previously [131,132]. The CB molecules were immobilized onto PVA nanofibers by covalent bonding between the hydroxyl group of PVA and chlorinated triazine ring of CB under the alkaline condition. Figure 2-4 shows the mechanism of the CB immobilization on the PVA nanofiber fabrics.

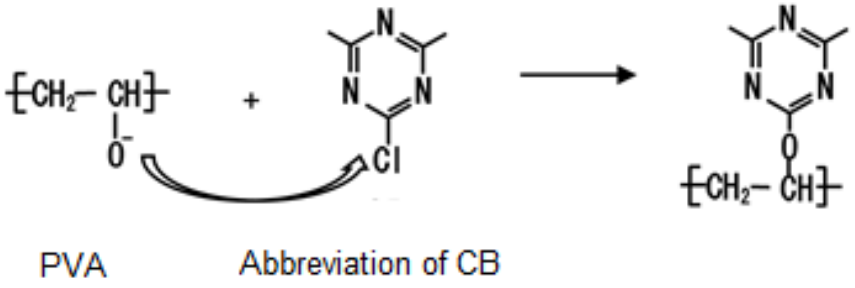

Fig. 2-4 Immobilization of CB on the PVA nanofiber fabrics.

Briefly, 100 mg of CB was dissolved in 10 mL of water to prepare a dyeing solution. Then, the dyeing solution was heated to 60 ℃, and a PVA nanofiber fabric mat was soaked in the solution for 30 min. After that, 2 g of NaCl was added to stimulate the deposition of the dye on the internal surface of the PVA nanofiber fabric mat. After maintaining at 60 ℃ for 1 hour, 0.2 g Na_2CO_3 sodium carbonate was added to adjust the solution's pH value to accelerate the reaction between the dye and the PVA nanofiber fabric mat, which took place at 80 ℃ for 2 hours. Finally, the dyed PVA nanofiber fabric mat was thoroughly washed with deionized water until the absence of CB molecules in the washing was detected by measuring the UV-vis absorbance at 600 nm (the maximum absorption wavelength of CB).

Guo et al. [133] immobilized CB and Active Red K2BP as affinity ligands to a cellulose matrix. They found that by the alkali treatment, the capacity for the immobilization of CB rose from 20 mg/g to 100 mg/g, and the immobilization of Active Red K2BP rose from 39 mg/g to 90 mg/g. After removing from the solution, the nanofiber fabrics were extensively washed with pure water until the washing solution gave no optical absorption at 600 nm (CB's maximum absorption wavelength). Residual CB solutions and the washing solutions were carefully collected together and measured by a UV–vis spectrophotometer to determine the amount of CB that was not incorporated onto the nanofiber fabrics. The initial and final CB concentrations derived

were used to calculate the CB amount immobilized on the nanofiber fabrics.

The resultant CB-enhanced affinity nanofiber fabrics are as shown in Fig. 2-5. The amount of dye ligands immobilized onto the nanofiber fabric constitutes an important parameter in the adsorption process. However, very high dye concentrations do not necessarily mean very high binding capacities because of steric hindrance. The saturated amount of CB immobilized on the PVA fabrics was 91 mg/g. The white PVA nanofiber fabrics were dyed with vivid blue CB.

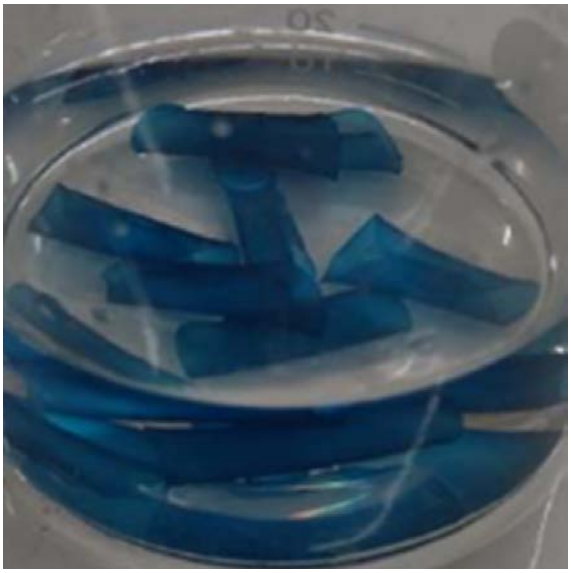

Fig. 2-5 CB-modified PVA nanofiber fabrics.

2.3 Characteristics of the PVA nanofiber fabrics

2.3.1 SEM analysis

Morphologies of the original PVA nanofiber were observed by scanning electron microscopy (SEM, S4300, Hitachi High-Technologies Corporation, Japan). A typical SEM image of the PVA nanofiber fabrics prepared by our lab is shown in Fig. 2-6. As

can be seen, the fabric was bead-free and had a uniform shape. Diameters of the as-spun nanofiber fabrics were measured by the ImageJ software. Figure 2-7 indicates the distribution of the fiber diameter. The fiber diameters ranged from 50 to 250 nm, and the average diameter was around 149 nm.

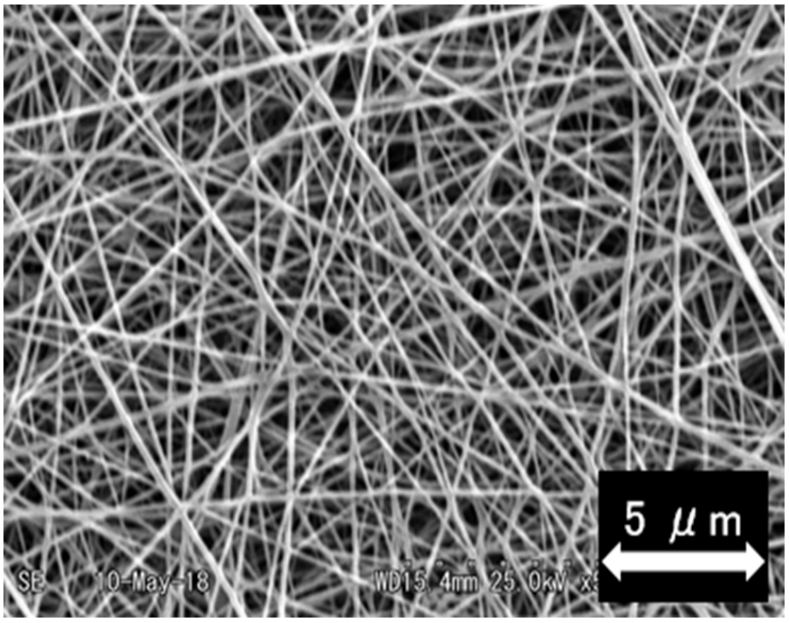

Fig. 2-6 SEM image of the PVA nanofiber fabric prepared by lab.

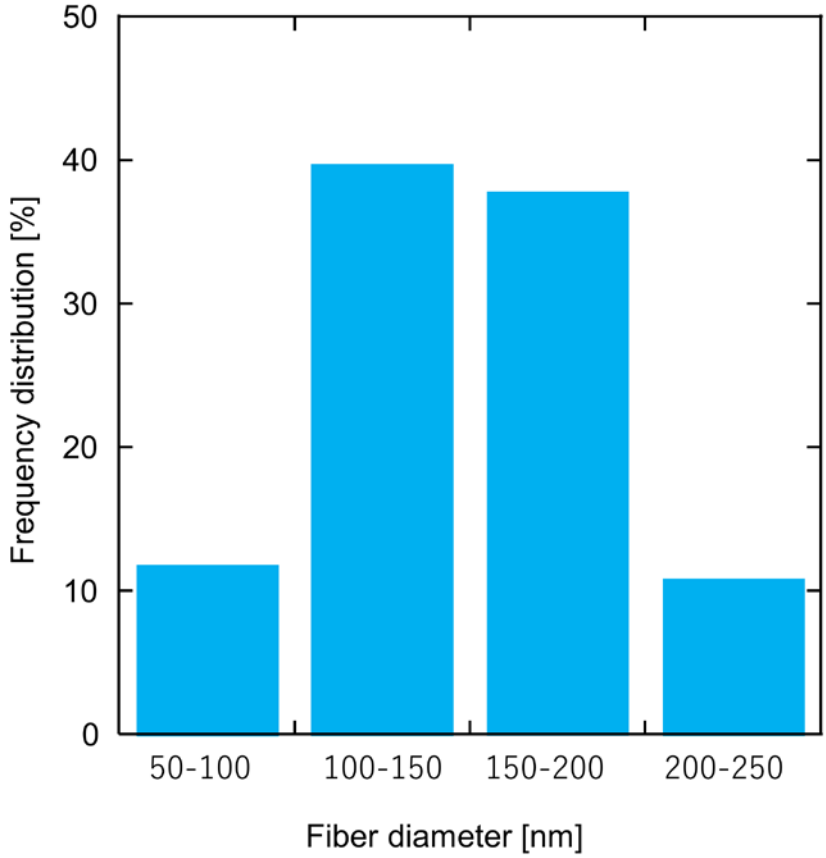

Fig. 2-7 Size distribution of the PVA nanofiber fabric prepared by lab.

Figure 2-8 shows a typical SEM image of the PVA nanofiber fabrics supplied by Vilene Company, and Fig. 2-9 displays the distribution of the fiber diameter (average diameter was approximately 232 nm).

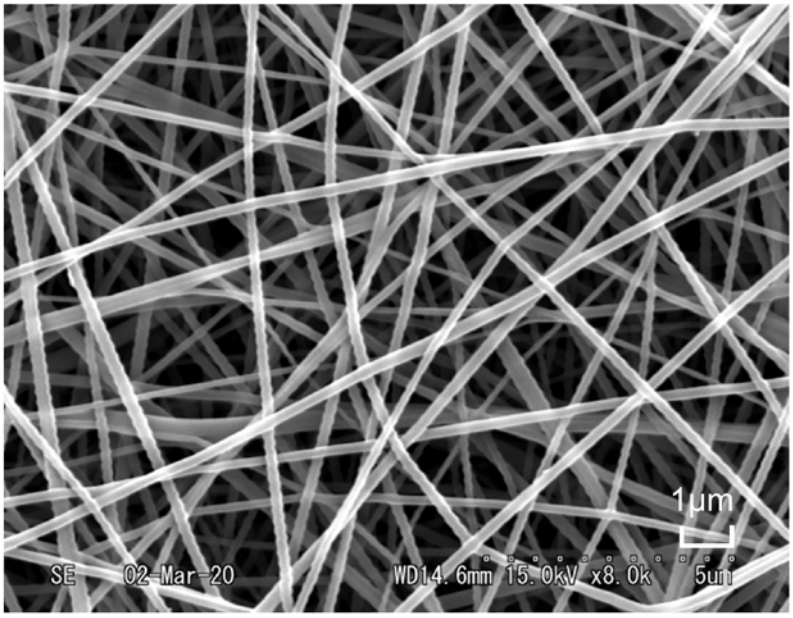

Fig. 2-8 SEM image of the PVA nanofiber fabric supplied by Vilene.

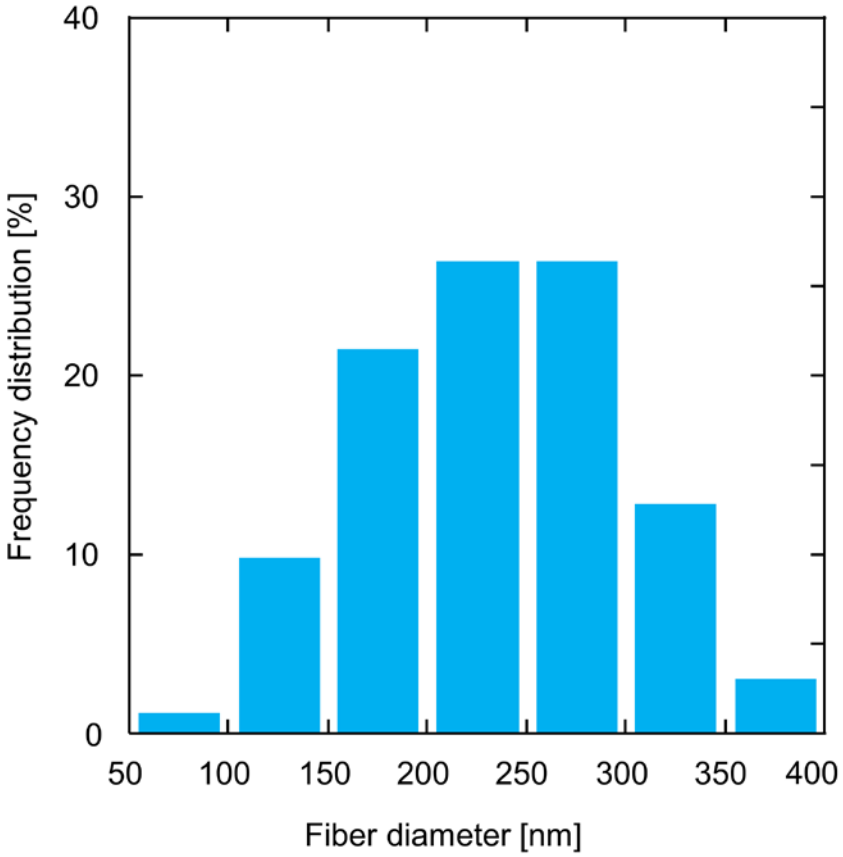

Fig. 2-9 Size distribution of the PVA nanofiber fabric supplied by Vilene.

2.3.2 FTIR analysis

Direct coupling of reactive triazinyl dyes to the matrices bearing hydroxyl groups is a simple, inexpensive and safe method. Coupling is achieved at alkaline conditions by nucleophilic substitution of hydroxyl groups with the reactive chlorine on the dye molecules [134]. CB was attached onto the PVA nanofiber through nucleophilic reaction between the chloride of the triazine ring and the hydroxyl group of PVA. Figure 2-10 shows the structure of CB molecule, the multiple aromatic part and the parts of three acidic sulfonate groups on CB influence the bindings of proteins and CB [126].

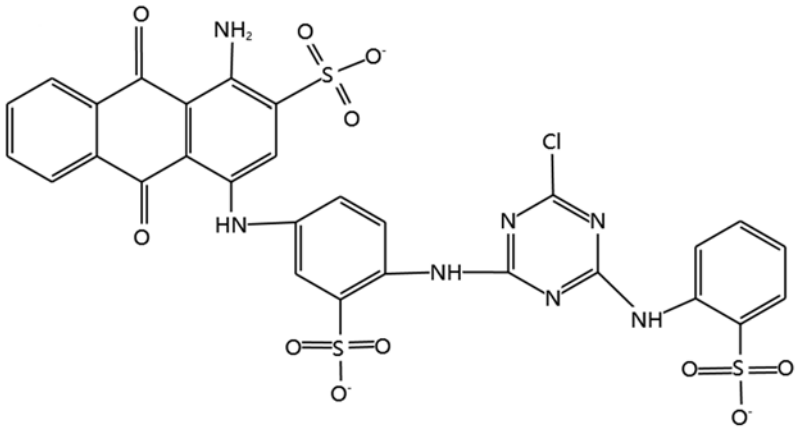

Fig. 2-10 Structure of CB molecule.

The chemical changes in the PVA nanofibers before and after CB modification were confirmed by Fourier transform infrared spectroscopy (FTIR-4100, JASCO, Japan), shown in Fig. 2-11. The Fourier transform infrared spectrums in the range 4000 ~ 400 cm^{-1} were recorded with a scan resolution of 1 cm^{-1} through an average of 16 scans. In the FTIR spectrum of CB-modified PVA nanofiber, the characteristic absorption bands at 1504 cm^{-1}, 1296 cm^{-1} and 1024 cm-1 were observed, which were different from that of the original PVA nanofiber. The peaks at 1504 cm^{-1} characterized the benzene ring

stretching vibrations. The absorption peaks at 1296 cm^{-1} and 1024 cm^{-1} were attributed to the stretching vibrations of C-N, and sulfonic acid groups, respectively [128,135, 136]. The FTIR spectra confirm that CB molecules were thus successfully attached onto the PVA nanofiber.

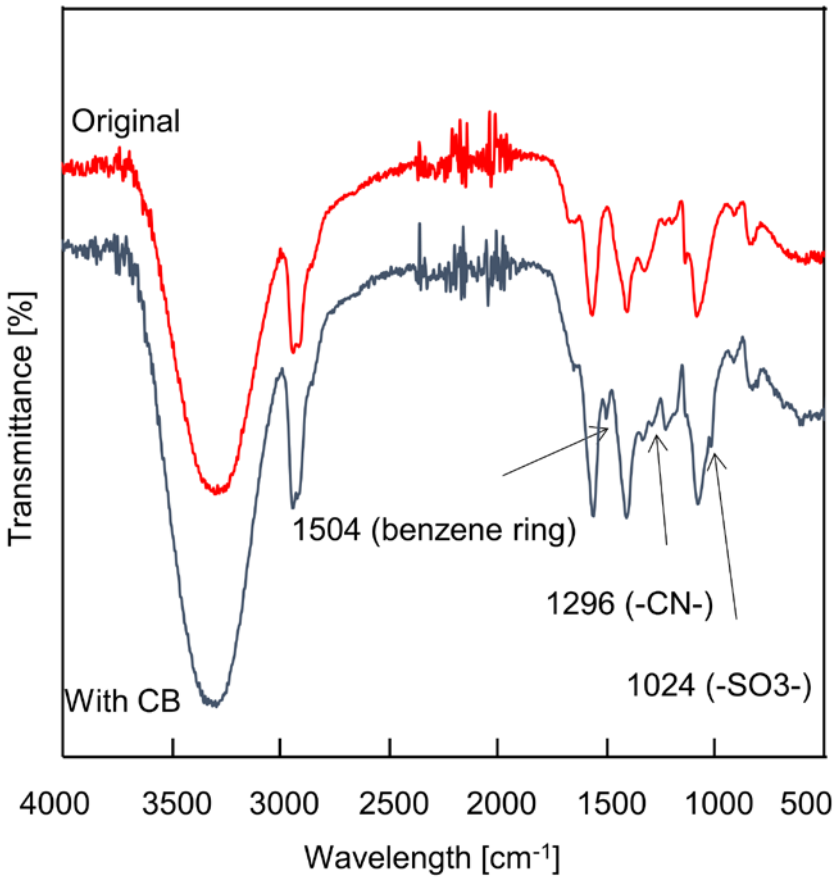

Fig. 2-11 FTIR spectra of the original PVA nanofiber fabric and the CB-modified PVA nanofiber fabric.

2.4 Chapter summary

PVA nanofiber fabrics were fabricated using electrospinning. The surface morphology of the PVA nanofiber fabrics was observed by SEM, the fiber size

distribution was counted, and the average diameter of the fibers was estimated. After covalent immobilization of the CB ligands on the PVA nanofiber surface, the chemical structures of the PVA nanofiber fabrics were characterized by FTIR.

Chapter 3 CB-Modified PVA Nanofiber Fabrics for Protein Adsorption

3.1 Introduction

With the extraordinary interaction to proteins, CB has become the most popular ligand for dye affinity chromatography [134]. In addition to cheapness and ease of purchase, the ability of group-specific interaction against proteins and easy binding onto matrices with hydroxyl functionality is the main reason for the selection of CB.

Although much progress has been made in CB-enhanced matrices for protein adsorption, the problem of low adsorption capacity still exists. The intent of this study was to develop high adsorption efficiency nanofiber fabric as a novel type of protein adsorption media. BSA, which represents structural homology with human serum albumin (HSA), was used as a model protein. BSA adsorption experiments were carried out to investigate the adsorption mechanism of protein on the PVA nanofiber fabrics.

3.2 Experimental

3.2.1 Materials

PVA nanofiber fabrics were prepared by the lab. BSA (MW=67,000) was provided by Sigma-Aldrich Co. LLC., Japan. Sodium acetate (CH_3COONa), 0.1 M hydrochloric acid (HCl), 0.1 M sodium hydroxide solution (NaOH), and phosphate buffer powder (NaH_2PO_4-K_2HPO_4) were purchased from Wako Pure Chemical Industries, Ltd., Japan. Acetic acid (CH_3COOH) was purchased from Kanto Chemical Co., INC., Japan.

3.2.2 Protein adsorption

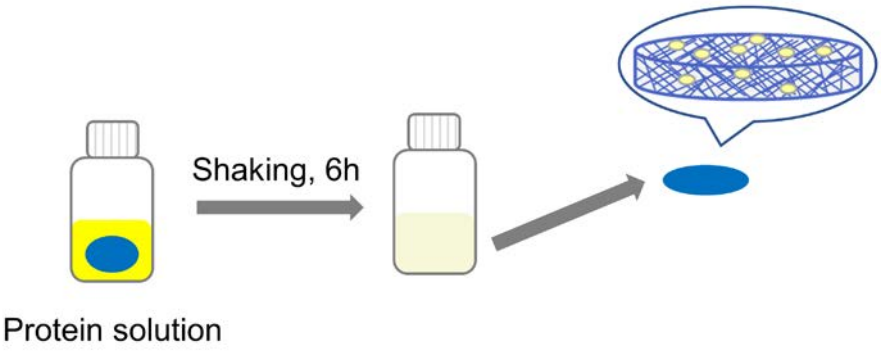

Fig. 3-1 Schematic diagram of protein static adsorption.

Protein solutions were prepared by dispersing a certain amount of BSA in the buffer solution, and the initial concentration of BSA was varied between 0 and 10.0 g/L. The pH of the test solution was varied from 3.2 to 6.8 using different buffer systems (0.1 M CH_3COONa-CH_3COOH for pH 3.2~5.0, 0.1 M NaH_2PO_4-K_2HPO_4 for pH 5.0~6.8). To investigate static adsorption, several milligrams of nanofiber fabrics were immersed in an 8 mL BSA solution at different concentrations and the mixture was shaken at 25 °C for 6 h, as shown in Fig. 3-1. The impact of the test solution's ionic strength (from 0 to 1.0 M NaCl) was also evaluated. The concentration of BSA was determined by using a UV-vis spectrophotometer according to its absorbance at 280 nm. The amount of adsorbed BSA was calculated based on the following formula:

$$q = \frac{(C_0 - C)V}{W} \tag{3-1}$$

where q is the adsorption amount (mg/g), C_0 is the initial concentration of BSA (mg/mL), C is the final concentration of BSA (mg/mL), V is the volume of protein solution (mL), and W is the weight of the nanofiber fabrics (g).

3.2.3 Desorption experiment

The desorption experiment of BSA was carried out in sodium chloride solutions at pH = 10.0. The BSA-adsorbed nanofiber fabrics were placed in the desorption medium and shaken for 6 h at 25 °C. The concentration of the remaining BSA in the elution solution was measured at 280 nm by UV-vis spectrophotometer. The desorption ratio of the protein was calculated according to the following equation:

$$\eta = \frac{q_d}{q} \times 100\% \quad (3\text{-}2)$$

where η is the desorption ratio, q and q_d are the nanofiber fabric adsorption capacity (mg/g) and desorption capacity (mg/g), respectively.

3.3 Results and discussion

3.3.1 Results of BSA adsorption test

The effect of initial concentration on adsorption capacity of the nanofiber fabrics was investigated at different concentrations of BSA from 0 to 10 g/L. The BSA adsorption amount increased with the rise of equilibrium concentration, as shown in Fig. 3-2. Significantly, the adsorption capacity of the CB-supported PVA nanofiber fabrics was higher than that of the untreated PVA nanofiber fabric.

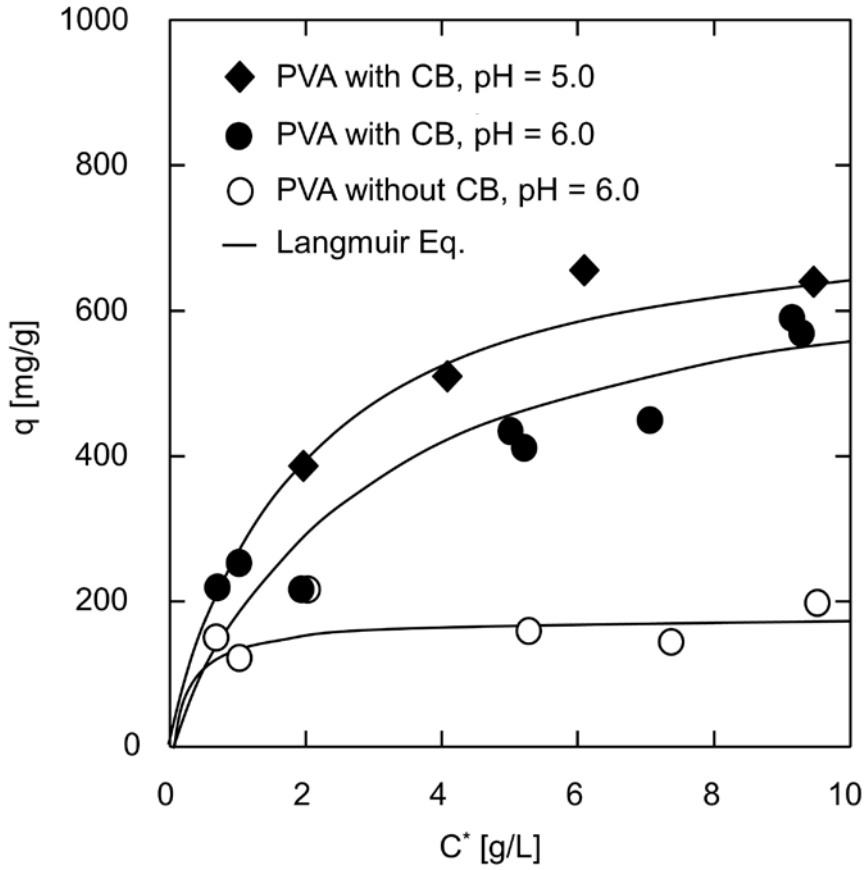

Fig. 3-2 Adsorption isotherms.

The major and minor axes of BSA molecule are 14 nm and 3.8 nm [123]. The PVA nanofiber fabric has a porous structure, and the size of the pores is much greater than that of BSA molecule. BSA molecules can reach the internal space of the fabrics and attach to the fabric surface. The outer surface and the interior vary in adsorption behavior and rate. The outer surface area only accounts for a small proportion of the total surface area of the PVA nanofiber fabric mat. The amount of protein adsorbed in the interior is dominant after the adsorption reaches equilibrium.

Unlike small and rigid gas molecules, proteins exist in a large variety of structural properties, size, and shape. The number of positive and negative charges inside proteins changes with the environmental conditions depending on pH, ionic strength, or

temperature [137]. Although the classical adsorption isotherms may be too simplistic to match the complex behaviour of protein adsorption to nanofiber fabrics, they are still a kind of starting point serving for the development of theoretical descriptions of the adsorption events. In general, the adsorption process is performed according to the arrangement of adsorbate molecules on the surface of adsorbent based on single-layer and multi-layer adsorption. The Langmuir and Freundlich models were applied to clarify the equilibrium isotherms for the adsorption of BSA. Monolayer adsorption of molecules is assumed in Langmuir isotherm, where adsorption occurs onto a surface having a limited number of homogeneous adsorption sites [138]. The linear form of Langmuir equation is depicted as:

$$\frac{C^*}{q} = \frac{C^*}{q_s} + \frac{1}{k_L q_s} \tag{3-3}$$

where q is the equilibrium adsorption capacity of BSA adsorbed on the nanofiber fabric (mg/g), q_s is the maximum adsorption capacity (mg/g), C^* is the equilibrium concentration of BSA in solution (mg/mL), and k_L is the constant of the system (mL/mg).

On the other hand, the Freundlich isotherm presumes that the multilayer of the adsorption process occurs on a heterogeneous surface [139]. The Freundlich equation is described in linear form as:

$$\log q = \log k_F + \frac{1}{n} \log C^* \tag{3-4}$$

where q and C^* values are the same as in the Langmuir equation, while k_F and n are empirical constants that indicate the Freundlich constant (mL/mg) and heterogeneity factor, respectively.

The Langmuir and Freundlich isotherm parameters for BSA adsorption are summarized in Table 3-1. A comparison using the regression coefficient R^2 reveals that

the equilibrium isotherm data fits the Langmuir isotherm model better than the Freundlich isotherm model. The fitting of the data to the Langmuir equation indicates the adsorption process was monolayer adsorption. Furthermore, k_L is the Langmuir constant related to the adsorption of binding sites [140]. The CB-supported PVA fabric at pH = 5.0 has the lowest k_L value, which is a measure of the energy of adsorption.

Table 3-1 Summary of the Langmuir and Freundlich isotherm fitting parameters for the adsorption of BSA.

	Langmuir Parameters			**Freundlich Parameters**		
	q_s (mg/g)	k_L (mL/mg)	R^2	$1/n$	k_F (mL/mg)	R^2
PVA with CB, pH = 5.0	769.23	0.3556	0.9077	2.6099	227.70	0.8891
PVA with CB, pH = 6.0	714.29	0.5244	0.9785	2.8586	313.76	0.9051
PVA without CB, pH = 6.0	178.95	3.4816	0.9407	14.2684	150.85	0.1320

At pH = 6.0 the q_s-values are estimated at 179 mg/g and 714 mg/g before and after immobilizing CB, resulting in 4 times increase. The q_s-value of functionalized nanofiber fabric at pH = 5.0 is 769 mg/g, which is slightly larger than at pH = 6.0. These q_s-values of CB-supported PVA nanofiber fabrics are remarkably larger than that of

CB-supported cellulose nanofiber fabric [141] and CB-supported chitosan particles [142] reported, while the BSA adsorption capacity of the latter two was 13 mg/g and 109 mg/g. The interaction between PVA and BSA mainly involved electrostatic interaction and hydrophobic interaction, while the latter was considered to be the primary interaction. The experimental results of the untreated PVA nanofiber fabric show that under the hydrophobic interaction, BSA overcame the electrostatic repulsion from the fabric surface and was adsorbed on it. Moreover, the BSA adsorption amount on CB itself at C^* of 10 g/L at pH = 6.0 is estimated at 2.50 g/g, which indicates an extremely high BSA adsorption ability of CB. The numerous CB affinity ligands contributed to the rise of BSA adsorption capacity on the CB-supported PVA nanofiber fabrics.

3.3.2 Effect of pH on BSA adsorption

The pH values of the buffer solution affects the surface charge of protein, which in turn is closely related to protein adsorption performance on the nanofiber fabrics. Figure 3-3 shows the adsorption capacity of the nanofiber fabrics at a protein concentration of 5.0 g/L. As can be seen, the adsorption capacity increased and reached the maximum at pH = 5.0, and then decreased. The isoelectric point of BSA is at pH = 5.0, where the net charge of BSA molecule became zero, and electrostatic repulsion between BSA and CB was minimized. Otherwise, BSA has several isomeric forms at different pH media and correspondingly has different α-helix contents, with the maximum α-helix content at its isoelectric point [123,143]. This means that BSA molecules were in most compact states at pH = 5.0 and resulted in a minimum intermolecular repulsion, which led to a higher adsorption amount.

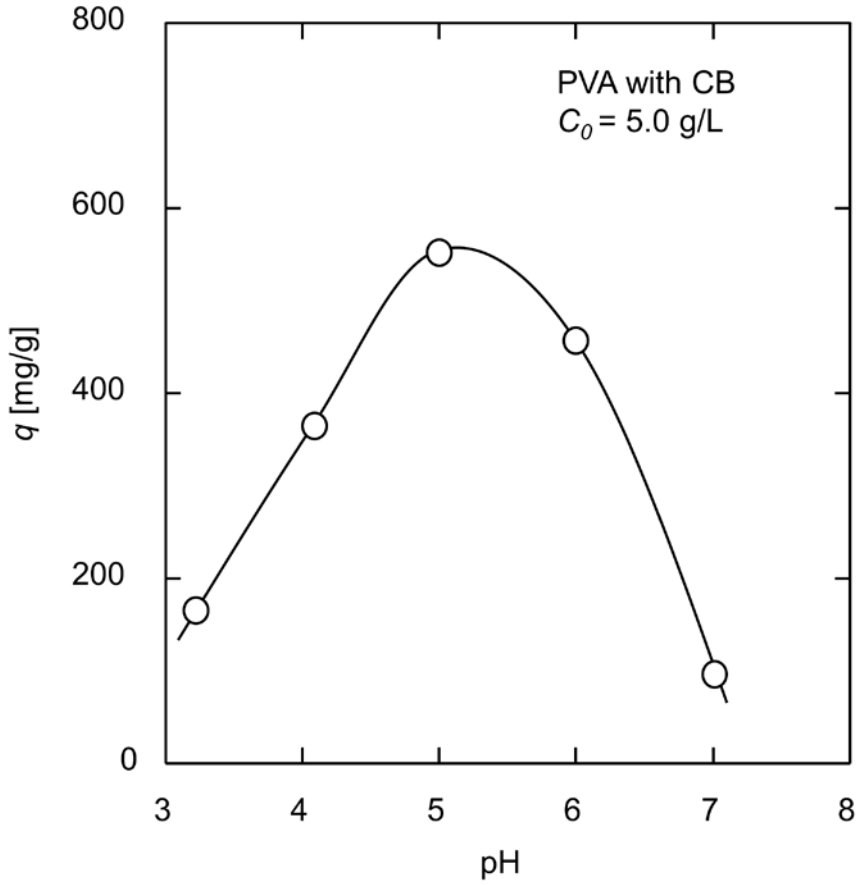

Fig. 3-3 Effect of pH on adsorption amount.

In some previous studies reported, highest adsorption capacities for BSA were also observed at pH = 5.0 [142,143,144,145]. CB is a monochlorotriazine dye and includes three acidic sulfonate groups and four basic primary and secondary amino groups. CB has a particular chemical structure, so that the binding mechanism of CB and protein molecules is complicated. The part of triazine is used for CB immobilization to PVA fabric. The multiple aromatic part and the parts of three acidic sulfonate groups influence the bindings of BSA and CB [126]. Within the range of pH from 3.0 to 7.0, the surface of CB supported PVA nanofiber fabric had a negative charge due to the

three negatively charged sulfonate groups on CB. Thus, hydrophobic interaction and electrostatic attraction are the main binding force below pH = 5.0. Higher pH increased the electrostatic repulsion between BSA and CB, resulting in a decrease in the BSA adsorption capacity.

3.3.3 Effect of ionic strength

The effect of the ionic strength (NaCl concentration) on BSA adsorption capacity is presented in Fig. 3-4. As is known, the enthalpy of adsorption would be affected by the salt concentration on the electrostatic and hydrophobic interaction between BSA and the affinity ligands [111]. Figure 3-4 shows that the adsorption capacity decreased with increasing the NaCl concentration in the BSA solution. This result is in agreement with the previous reports [136,142,144,146]. Increasing ionic strength could intense the binding of CB molecules to the PVA fabric surface by hydrophobic interaction, which results in the decrease of CB coupling density accessible to BSA molecules. Moreover, as the salt concentration increased, it can lead to coordination of the deprotonated sulfonic acid groups of CB with sodium ions of the salt (NaCl), which leads to low protein adsorption [132,147].

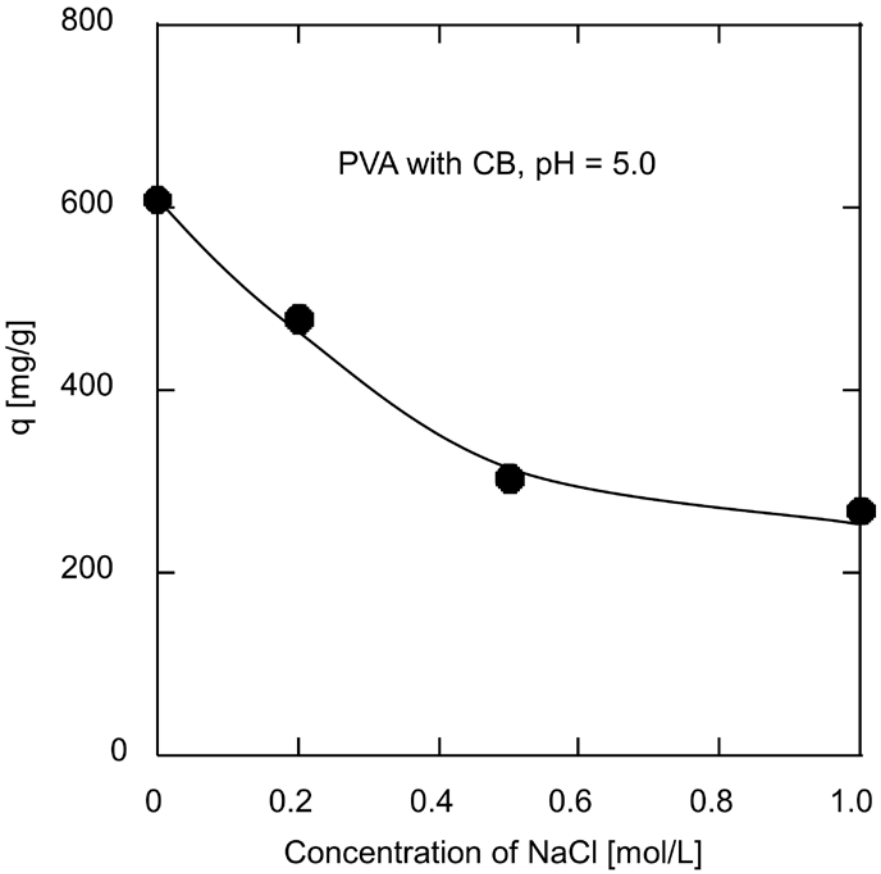

Fig. 3-4 Effect of concentration of NaCI on adsorption amount.

3.3.4 Desorption and reusability

To recover BSA molecules from the BSA-adsorbed nanofiber fabrics, desorption test was carried out with a salt solution at pH = 10.0. Figure 3-5 displays the desorption ratio at different concentrations of NaCl solution. The results showed that 97.3% of the BSA molecules were desorbed into the 1.0 M NaCl solution from the surface of the nanofiber fabrics successfully. Firstly, at pH = 10.0, which is well above the isoelectric point of BSA, electrostatic repulsion between BSA and CB is enhanced to a great extent. Secondly, as discussed above, BSA molecules lose their most compact states away from pH = 5.0. Thirdly, the increasing ionic strength affects the hydrophobic interaction of

CB and its electrostatic interaction with BSA. In order to evaluate the reusability of the CB-supported PVA nanofiber fabrics, the adsorption-desorption cycle was repeated five times. Some decrease was observed in the adsorption capacity, as shown in Fig. 3-6. However, in the fifth cycle of the adsorption experiment, the BSA adsorption capacity was still remaining a high level of 447 mg/g, indicating that the affinity fabrics developed in this study can be recycled and reused.

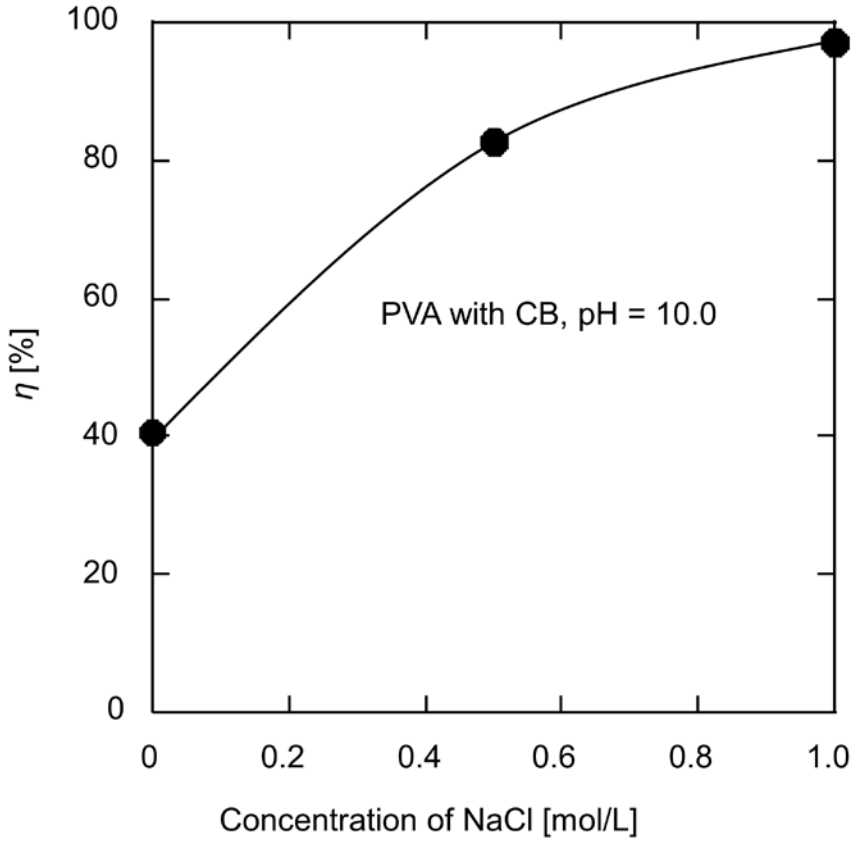

Fig. 3-5 Effect of concentration of NaCl on desorption ratio.

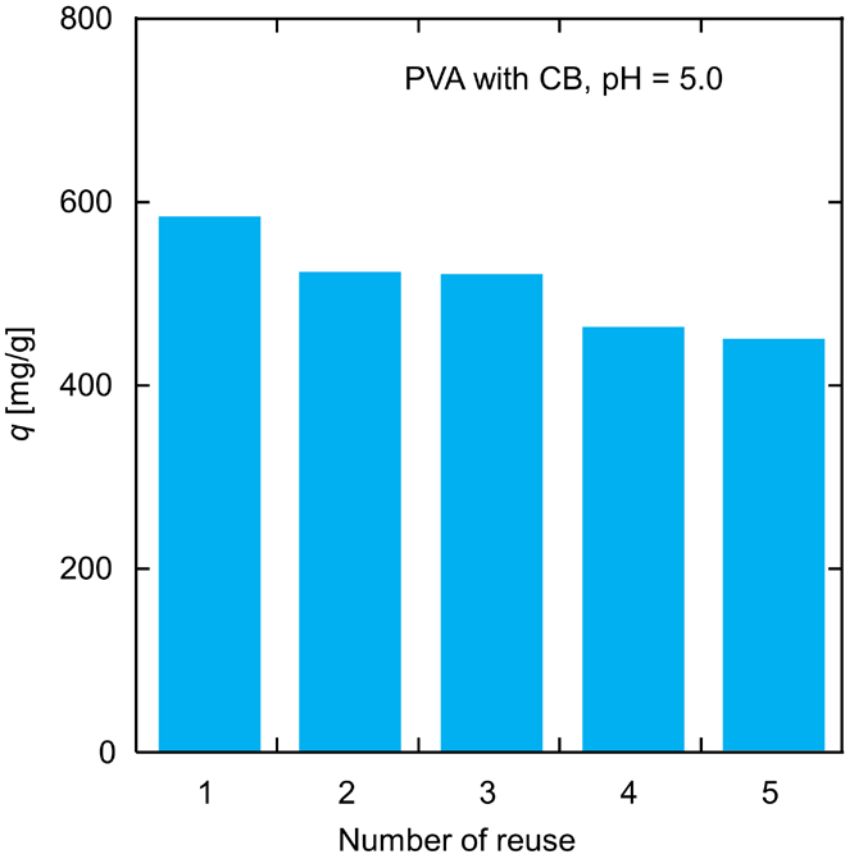

Fig. 3-6 Reusability of the CB-supported PVA nanofiber fabric.

3.4. Chapter summary

In this chapter, CB-enhanced affinity PVA nanofiber fabrics were used as a platform for the adsorption of protein. The BSA adsorption amounts on the PVA nanofiber fabric were greatly improved after CB modification. The effects of different parameters such as protein concentration, buffer pH, and ionic strength to the BSA adsorption performance on the nanofiber fabric were examined. The experimental data clearly demonstrated that the BSA adsorption and desorption characteristics were heavily dependent on the solution environment. A large adsorption capability of approximately

769 mg/L was achieved for the PVA nanofiber fabric in a buffer at pH = 5.0 (Table 3.1). The desorption ratio reached to 97.3% at the elution test performed by using 1 M NaCl (Fig. 3-5) as an elution medium, and the affinity nanofiber fabrics indicated superior durability and reusability in the repeated adsorption-desorption cycles (Fig 3-6). In view of the integrate characteristics including high protein adsorption capability as well as the facile and low-cost fabrication process, the obtained Cibacron Blue-enhanced affinity nanofiber fabric has the potential to be developed for the separation and purification of proteins [148].

Chapter 4 Dynamic Adsorption Behaviors of Protein on CB-Modified PVA Nanofiber Fabrics

4.1 Introduction

The CB-modified PVA nanofiber fabric has high affinity for protein adsorption. In the static adsorption, the PVA nanofiber fabrics were immersed in the protein solution and reached equilibrium after a long contact time. The dynamic adsorption is a flow adsorption mode, and commonly applicated in industrial separations. In the dynamic adsorption experiments, a certain mass of PVA nanofiber fabrics were packed in the filter holder, and protein solution permeated through the fabrics at a constant flow rate.

Kinetic studies of adsorption processes are used to describe the rate of solute adsorption by the adsorbent and to fit the data by kinetic models in order to investigate the adsorption mechanism. Adsorption process is usually affected by solute diffusion and chemical interaction between adsorbent and adsorbate, which is one of the focuses of kinetic research. The potential application properties of the CB-modified PVA nanofiber fabrics for protein adsorption were evaluated by testing their static and dynamic adsorption properties. The Langmuir isotherm model was applied to elucidate the equilibrium adsorption data. The pseudo-first-order and pseudo-second-order kinetic models were also used to analyze the kinetics adsorption data. Moreover, the efficiency of the static and dynamic adsorption behaviors was examined.

4.2 Experimental

4.2.1 Materials

The electrospun PVA nanofiber fabrics were supplied by Japan Vilene Company, Ltd.,

Japan. Sodium acetate (CH_3COONa), 0.1 M hydrochloric acid (HCl), 0.1 M sodium hydroxide solution (NaOH), and phosphate buffer powder (NaH_2PO_4-K_2HPO_4) were purchased from Wako Pure Chemical Industries, Ltd., Japan. Acetic acid (CH_3COOH) was purchased from Kanto Chemical Co., INC., Japan.

4.2.2 Modification of PVA nanofiber fabrics

The mass per unit area of the PVA nanofiber fabrics is 40 g/m^2. The CB molecules were immobilized onto the PVA nanofiber fabrics by the method described in section 2.2.3. Four types of PVA nanofibers with the heat treatment time of 30 minutes were supplied by Japan Vilene Company, Ltd., with varying heat treatment temperatures of 180, 150, 120, and 80 ℃, respectively.

4.2.3 Adsorption experiments

BSA was used as a model protein. BSA solutions were prepared by dispersing a certain amount of BSA in the 0.1 M CH_3COONa-CH_3COOH buffer solution with pH 5.0, since BSA molecules are in most compact states and have a minimum electrostatic repulsion with CB at pH = 5.0. The concentration of BSA was measured by a UV-1800 spectrophotometer (Shimadzu Corporation, Japan) with the UV absorption band at 280 nm. In order to obtain the optimal BSA affinity material, the adsorption performances of the four types of PVA nanofibers were compared. The four nanofibers were immersed in 8 mL solutions of various BSA concentrations and shaken at 25 ℃ for 6 hours to reach equilibrium. Adsorption isotherms were conducted with initial concentrations ranging from 1.0 to 6.0 g/L. The concentration of BSA was determined from the difference between the absorbance before and after adsorption. The amount of adsorbed BSA was calculated in accordance with the following equation:

$$q = \frac{(C_0 - C)V}{W} \tag{4-1}$$

where q (mg/g) is the adsorption amount, C_0 and C (g/L) are the initial and the final concentrations of BSA, respectively, V (mL) is the volume of protein solution, and W (g) is the mass of the adsorbent.

The permeation experiments were investigated only for the CB-modified PVA nanofiber with the heat treatment temperature of 80 ℃, since the static adsorption experiments demonstrated that it was the most efficient adsorption platform of the four nanofibers. The experimental setup is shown in Fig. 4-1.

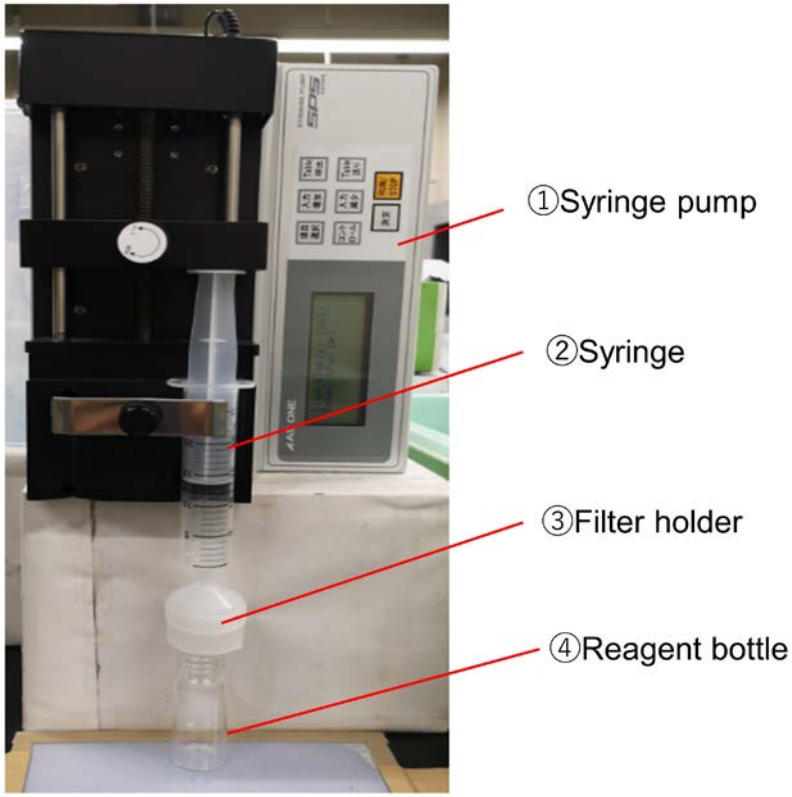

Fig. 4-1 Experimental apparatus of the dynamic adsorption.

A fabric mat with a weight of 19.6 mg was packed in the Millipore filter holder (SX0002500) with an effective diameter of 2.2 cm and a permeation area of 3.8 cm^2. BSA solution was injected into the filter holder by the syringe pump (SRS-2, AS ONE Co., Japan). The study in details was carried out at 25 ℃ under various initial BSA

concentrations (from 0.3 to 1.2 g/L), and permeation rates (from 2 to 10 mL/h). The BSA rejection *R* was calculated according to Eq. (4-2):

$$R = 1 - \frac{C_p}{C_0} \tag{4-2}$$

where C_0 (g/L) is the BSA concentration of feed solution, and C_p (g/L) is the BSA concentration of permeate solution.

In order to test the reusability of the CB-modified PVA nanofiber, the BSA-adsorbed nanofiber mats were eluted using buffer solutions (0.1 M NaH_2PO_4-K_2HPO_4, pH = 10.0) containing 1.0 M NaCl. The concentration of the remaining BSA in the eluent was measured at 280 nm by the UV-1800 spectrophotometer. Desorption efficiency η was calculated according to the following equation:

$$\eta = \frac{q_d}{q} \times 100\% \tag{4-3}$$

where q_d (mg/g) and q (mg/g) are the nanofiber fabric desorption and adsorption capacities, respectively.

The effects of eluent volume were conducted at eluent flowrates of 5 mL/h and 10 mL/h. After obtaining the optimal eluent parameters, the nanofiber mats were used for the next cycle of the dynamic test. Desorption and adsorption processes were repeated three times.

4.3 Results and discussion

4.3.1 Static adsorption for BSA

4.3.1.1 Effect of initial BSA concentration

The four modified nanofibers with the heat treatment temperatures of 180, 150, 120 and 80 ℃ are shown in Fig. 4-2. An important parameter to evaluate different adsorbents is their maximum uptake ability. The effects of initial protein concentration on the adsorption are shown in Fig. 4-3.

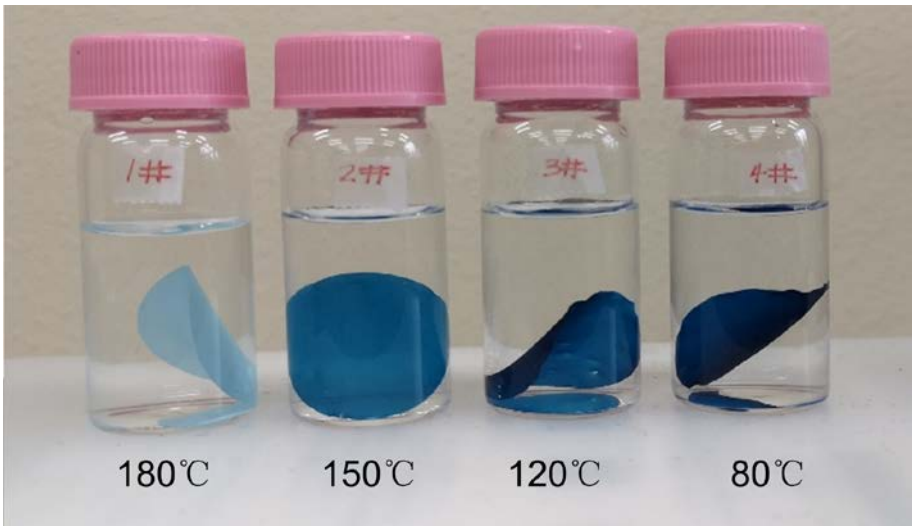

Fig. 4-2 Photos of different CB-modified PVA nanofiber fabric mats.

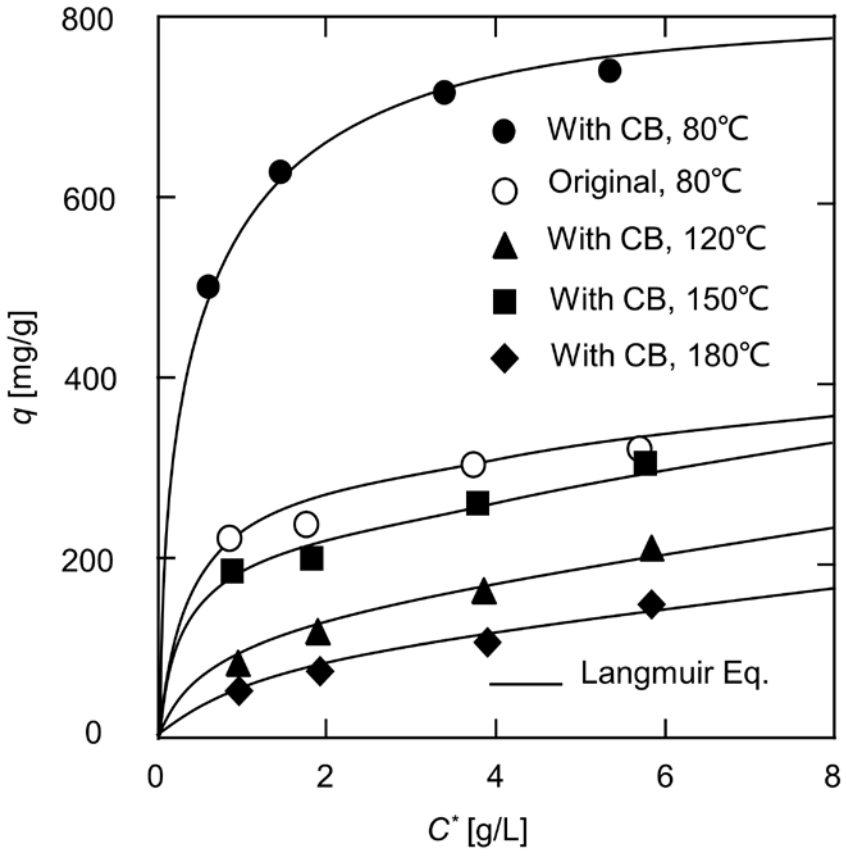

Fig. 4-3 Adsorption isotherms of BSA onto different PVA nanofiber fabrics.

For all types of the nanofibers, the adsorbed BSA amount raised with an increase in the protein equilibrium concentration. Increase in the initial concentration of BSA provides a potent driving force to overcome the mass transfer resistance between the aqueous and solid phases. The adsorption capacity of the PVA nanofiber with the heat treatment temperature of 80 ℃ is noticeably greater than the other three types of nanofibers. The nanofiber with the lowest heat treatment temperature showed the deepest blue colour, which is due to more fixed CB molecules. Compared to the original nanofiber, the adsorption ability of the CB-modified nanofiber was improved significantly. The adsorption isotherm is the relationship between the amounts of a substance adsorbed per unit mass of adsorbent at constant temperature and its concentration in the equilibrium solutions. The experimental results fitted well with the Langmuir isothermal adsorption equation, where the model assumes adsorption to be the monolayer type and describes the adsorbent surface as homogeneous having identical surface sites [140]. The adsorption process can be expressed by the following equation:

$$q_e = \frac{q_s K C^*}{1 + K C^*} \tag{4-4}$$

where q_e and q_s (mg/g) are the equilibrium adsorption capacity and the saturated adsorption capacity of BSA, respectively, K (L/g) is a constant of adsorption associated with free energy, and C^* (g/L) denotes the equilibrium concentrations of BSA in solution. The saturated adsorption capacity of q_s can be predicted by the linear form of the Langmuir equation:

$$\frac{C^*}{q_e} = \frac{C^*}{q_s} + \frac{1}{K q_s} \tag{4-5}$$

The BSA adsorption capacities for the PVA nanofiber with the heat treatment temperature of 80 ℃ are 355.9 and 793.7 mg/g before and after immobilizing CB, resulting in a 2.2 times increase. However, without CB modification, the BSA adsorption capacity of the original PVA nanofiber is much greater than that of the two nanofibers with heat treatment temperatures of 180 and 150 ℃. Xiao et al. [149]

functionalized PVA nanofiber fabrics by incorporating poly(methyl vinyl ether-alt-maleic anhydride) (PMA) and invested the effect of heat treatment on the fabric properties. The maleic anhydride on PMA has chemically crosslinked with the hydroxyl groups on PVA through an esterification reaction. They pointed out that increased crystallinity of PVA and densely crosslinked structure due to high temperature will limit the accessibility of charged moieties to the internal binding sites of PVA. They chose the PVA fabrics with the heat treatment temperature of 120 ℃ in the range of 120 to 160 ℃ for the dye capturing study. The crosslinking agent of the PVA nanofibers we used is also PMA. Gohil et al. [150] used maleic acid (MA) as a crosslinking agent to crosslinking PVA with varying heat treatment temperature from 120 to 160 ℃. It is demonstrated that the interaction between PVA and maleic acid is inferior at a lower temperature and the heat treatment results in the elimination of water, which in turn enhances the alignment order of the polymeric chains through the formation of polyene. The hydroxyl groups are consumed by the reaction between PVA the crosslinking agent. A decrease in the hydroxyl groups reduces the affinity of PVA polymer with water.

The abundant presence of hydroxyl groups in PVA results in a hydrophilic nanofiber surface. The crosslinking reaction makes the polymer stable in water. On the other hand, the residual uncrosslinked fraction of hydroxyl groups of PVA provided the hydrophilic properties for the modified nanofiber surface [151]. Xie et al. [152] analyzed the water contact angle for the PVA hybrid membrane at different heat treatment temperatures. The water contact angle remained almost unchanged at about 45° at heating temperatures less than 140 °C, but increased significantly at higher temperatures, indicating that the hybrid membrane became less hydrophilic at the higher heating temperature. It can be attributed to the fact that the crosslinking reaction is incomplete at lower heating temperatures and more complete at higher temperatures. What is really needed is a network that provides a tight restraining without serious loss of hydrophilic behavior. When the heating temperature increased higher than 120 °C, more hydrophilic groups were consumed, consequently increased the hydrophobicity of the PVA

nanofibers. As displayed in Fig. 4-2, a lighter color of the modified nanofibers reflects less CB fixed amount, which is caused by insufficient hydroxyl groups. The better adsorption performance of the PVA nanofiber heat-treated at 80 °C is due to the excellent affinity of the matrix materials and the abundant hydroxyl groups to participate in the nucleophilic substitution reaction with CB.

4.3.1.2 Effect of contact time

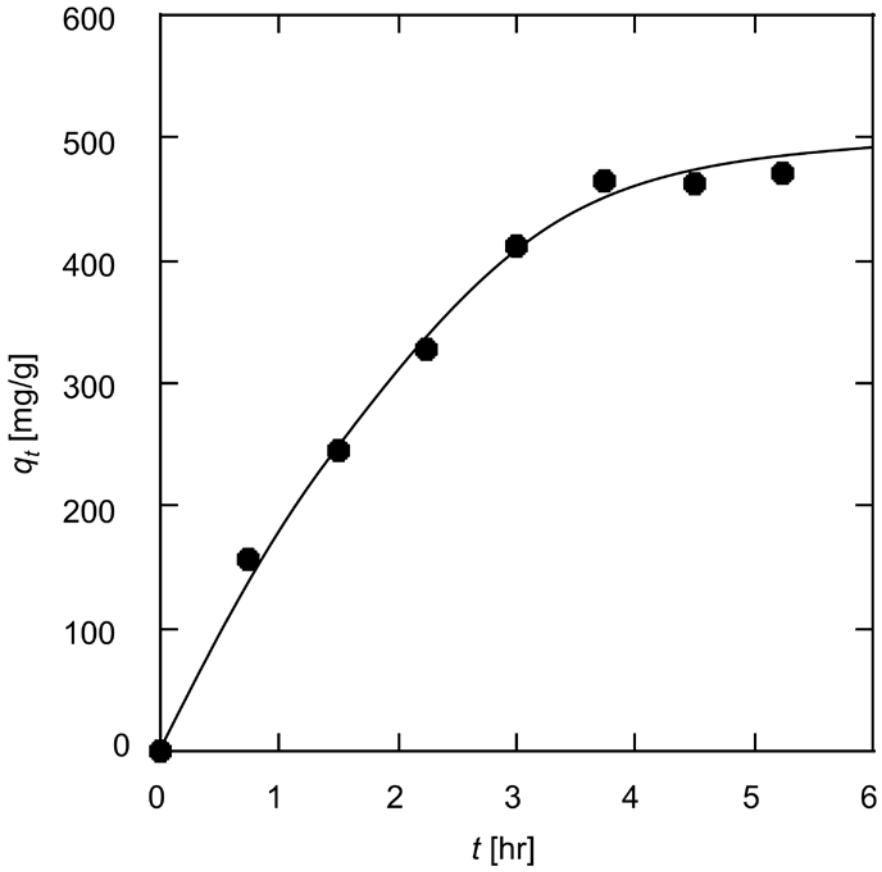

Fig. 4-4 Function of contact time on BSA adsorption amount for the CB-modified PVA nanofiber fabric.

To investigate the static adsorption kinetics, the CB-modified PVA nanofiber with the heat treatment temperature of 80 ℃ was immersed in 20 mL BSA solution (0.6 g/L) under shaking for 6 hours. As shown in Fig. 4-4, the BSA adsorption amount onto the

nanofiber mats increased rapidly in the first 4 hours. Then, the adsorption gradually slowed down, eventually reaching equilibrium. At the initial stage of adsorption, since there were sufficient adsorption sites on the surface of the modified nanofiber, the BSA concentration was conducive to the rapid adsorption of BSA onto the nanofiber. During the adsorption process, the adsorption sites of the nanofiber surface declined, thus decreasing the adsorption rate as time elapsed. At the end of adsorption, the adsorption sites were depleted, and the adsorption reached saturation.

The kinetic data was modeled using the pseudo-first-order kinetic and the pseudo-second-order kinetic. As the pseudo-first-order kinetics assumes that the rate of change of the adsorption capacity is proportional to the concentration of available active sites per unit mass of adsorbent material [61,153], the following formula can be expressed:

$$\frac{dq_t}{dt} = k_1(q_\infty - q_t) \tag{4-6}$$

where q_t (mg/g) is the adsorption amount at time t (h), q_∞ (mg/g) is the adsorption amount at $t = \infty$, and k_1 (h^{-1}) is the pseudo-first-order rate constant. Integrating Eq. (4-6), q_t can be expressed as:

$$q_t = q_\infty\{1 - \exp(-k_1 t)\} \tag{4-7}$$

and its linear form is given as:

$$\ln(q_\infty - q_t) = \ln q_\infty - k_1 t \tag{4-8}$$

The pseudo-second-order kinetic assumes that the rate of change of the concentration of occupied active sites per unit mass of the adsorbent material is proportional to the square of the concentration of free active sites per unit mass of sorbent [154, 155]. In terms of adsorption capacity, the pseudo-second-order rate equation can be written as:

$$\frac{dq_t}{dt} = k_2(q_\infty - q_t)^2 \tag{4-9}$$

where q_t (mg/g) is the adsorption amount at time t (h), q_∞ (mg/g) is the adsorption amount at $t = \infty$, and k_2 ($g \cdot mg^{-1}h^{-1}$) is the pseudo-second-order rate constant. Integrating Eq. (4-6), q_t can be expressed as:

$$q_t = \frac{{q_\infty}^2 k_2 t}{1 + q_\infty k_2 t} \tag{4-10}$$

and its linear form is given as:

$$\frac{t}{q_t} = \frac{1}{k_2 q_\infty{}^2} + \frac{1}{q_\infty} t \quad (4\text{-}11)$$

Fitting was carried on plots $\ln(q_\infty - q_t)$ against t for the pseudo-first-order model, and t/q_t against t for the pseudo-second-order model. The correlation coefficients (R^2) for the pseudo-first-order model and the pseudo-second-order model were 0.944 and 0.974, respectively. This implies that the pseudo-second-order model is more suitable to describe the BSA adsorption behavior. The fitting of experimental data on the pseudo-second-order model depicts that the adsorption rate of BSA onto the modified PVA nanofiber depends on the availability of the adsorption sites.

4.3.2 Dynamic adsorption and desorption performance studies

4.3.2.1 Mathematical models for BSA dynamic adsorption

The PVA nanofibers have the advantages of large specific surface area, high porosity, and large pores. The thickness of the fabric mats was 151 μm. Assuming that the nanofibers have a uniform diameter, the outer surface area of the fabric can be calculated from the average diameter of 232 nm. As a result, the ideal specific surface area of the fabric mats was around 13.2~14.5 m^2/g, and the ideal porosity was about 0.78~0.80. The mass transfer resistance is tremendously reduced and the binding kinetics dominates the adsorption process. It results a rapid processing, which greatly improves the adsorption, regeneration steps. Mathematical models were derived to analyze the dynamic adsorption results in accordance with the pseudo-first-order kinetic and the pseudo-second-order kinetic. Rejection can be defined as the ratio of BSA adsorption rate W_f (dq_t/dt) to BSA inflow rate C_0Q [61], given by:

$$R = \frac{W_f}{C_0 Q} \frac{dq_t}{dt} \quad (4\text{-}12)$$

where W_f is the weight of the PVA nanofiber mat (g), C_0 (g/L) is the BSA concentration of feed solution, Q is the permeation rate (mL/h), and q_t (mg/g) is the adsorption amount

at time t (h).

Permeate time is defined as:

$$t = \frac{V}{Q} \tag{4-13}$$

where V (mL) is the permeate volume of BSA solution.

Substituting Eqs. (4-6), (4-7) and (4-13) into Eq. (4-12), results in the following equation:

$$R = \frac{W_f k_1 q_\infty}{C_0 Q} \exp\left(-\frac{k_1}{Q} V\right) \tag{4-14}$$

Because the value of rejection cannot be greater than 1,

$$R = 1 \text{ at } 0 \le V \le \frac{Q}{k_1} \ln \frac{W_f k_1 q_\infty}{C_0 V} \tag{4-15}$$

$$R = \frac{W_f k_1 q_\infty}{C_0 Q} \exp\left(-\frac{k_1}{Q} V\right) \text{ at } V > \frac{Q}{k_1} \ln \frac{W_f k_1 q_\infty}{C_0 Q} \tag{4-16}$$

Equations (4-15) and (4-16) are rejection equations obtained for the dynamic adsorption model based on the pseudo-first-order kinetic model. According to the two equations, the establishment condition of the dynamic adsorption period of R = 1 is as follows:

$$\frac{W_f k_1 q_\infty}{C_0 Q} > 1 \tag{4-17}$$

where the left side of Eq. (4-17) is R at V = 0 in Eq. (14). Taking the logarithm on both sides of Eq. (4-14),

$$-\ln R = \frac{k_1}{Q} V - \ln \frac{W_f k_1 q_\infty}{C_0 Q} \tag{4-18}$$

The values of k_1 and q_∞ can be calculated by plotting a straight line with ln$R$ and V from the slope and the intercept.

By substituting Eqs. (4-9), (4-10) and (4-13) into Eq. (4-12), rejection equation for the dynamic adsorption model based on the pseudo-second-order kinetic model is given below:

$$R = \frac{k_2 W_f Q {q_\infty}^2}{C_0 (Q + k_2 V q_\infty)^2} \tag{4-19}$$

Similarly, since the value of rejection cannot be greater than 1,

$$R = 1 \text{ at } 0 \leq V \leq \sqrt{\frac{W_f Q}{k_2 C_0}} - \frac{Q}{k_2 q_\infty} \tag{4-20}$$

$$R = \frac{k_2 W_f Q {q_\infty}^2}{C_0 (Q + k_2 V q_\infty)^2} \text{ at } V > \sqrt{\frac{W_f Q}{k_2 C_0}} - \frac{Q}{k_2 q_\infty} \tag{4-21}$$

The establishment condition of the dynamic adsorption period of $R = 1$ is as follows:

$$\frac{k_2 W_f {q_\infty}^2}{C_0 Q} > 1 \tag{4-22}$$

where the left side of Eq. (4-22) is R at $V = 0$ in Eq. (4-19). The linear form of Eq. (4-19) is given as:

$$\frac{1}{\sqrt{R}} = \sqrt{\frac{C_0 k_2}{W_f Q}} V + \frac{1}{q_\infty} \sqrt{\frac{C_0 Q}{k_2 W_f}} \tag{4-23}$$

The values of k_2 and q_∞ can be calculated by plotting a straight line with $1/\sqrt{R}$ and V from the slope and the intercept.

4.3.2.2 Discussion of dynamic adsorption

In this study, the effects of adsorption conditions on the BSA dynamic adsorption process, such as modification of CB, concentration of BSA in permeate solution, and permeation rate, were examined in a continuous system. Adsorption results were fitted using the adsorption kinetics of the pseudo-first-order kinetic and the pseudo-second-order kinetic.

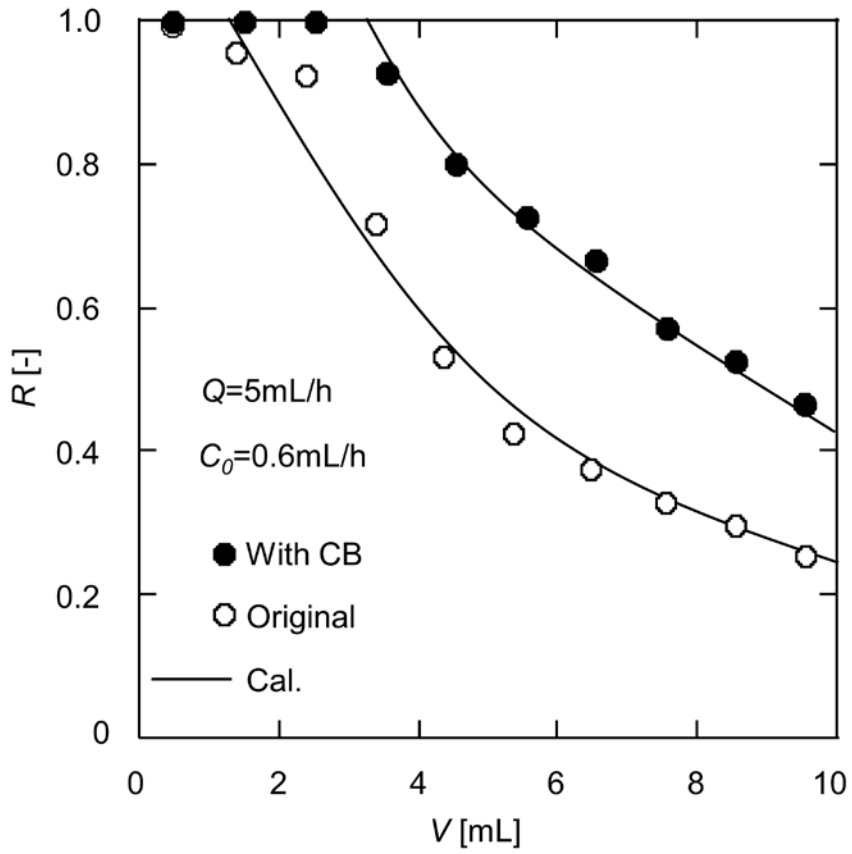

Fig. 4-5 Dynamic adsorption test results and calculated rejection curves for the original PVA nanofiber fabric and the CB-modified PVA nanofiber fabric.

Figure 4-5 shows the permeate volume evolution of the BSA rejection for both of the original PVA nanofiber mat and the CB-modified PVA nanofiber mat. The BSA rejection for the original PVA nanofiber mat decreased from the initial 2 mL of the process to 0.254 after permeating 10 mL BSA solution. In comparison, a significant increase in dead volume area can be observed in the process using the CB-modified PVA nanofiber mat, and the rejection still remained 0.465 by permeating the same volume of BSA solution. The CB modification effectively improves the binding efficiency of the PVA nanofiber to the protein and avoids the rapid decline of rejection during the permeate process.

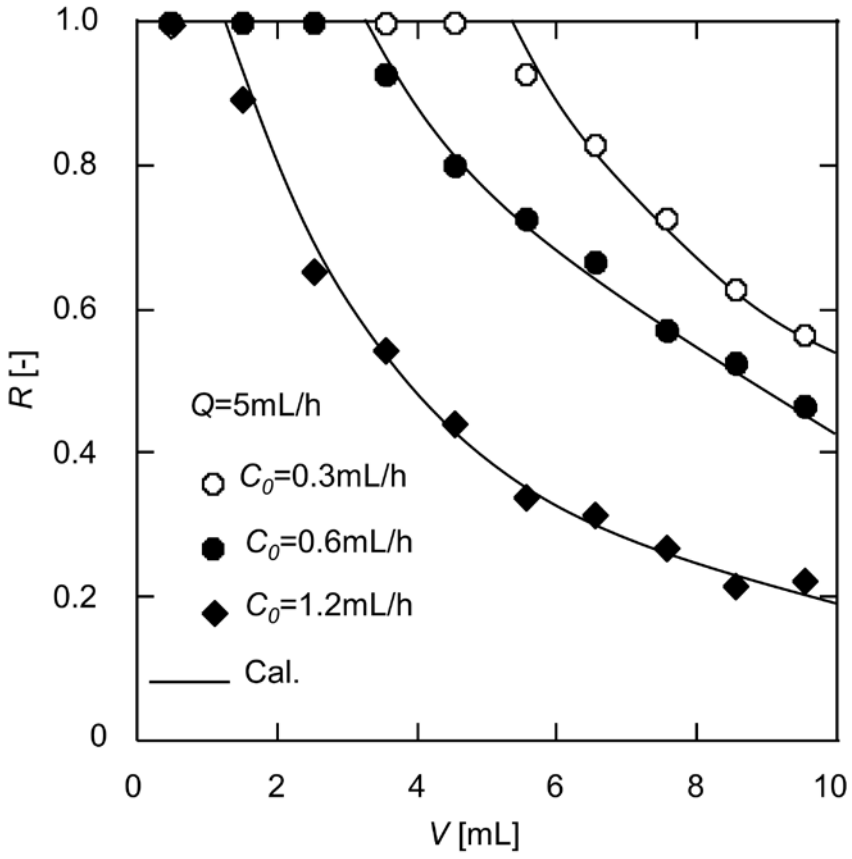

Fig. 4-6 Dynamic adsorption test results and calculated rejection curves at different initial concentrations for the CB-modified PVA nanofiber fabric.

Figure 4-6 shows the change of BSA rejection with permeate volume under different initial concentrations. With the increase of permeate volume, the rejection revealed a similar downward trend though the margins of decline varied. As the rise of initial concentration, BSA molecules in the mobile phase have more chances to interact with the nanofiber surface, and the driving force also increases. There were the same number of adsorption sites for BSA capture for the PVA nanofiber mats of the same mass; as a result, the rejection reduced fastest for the largest permeate concentration.

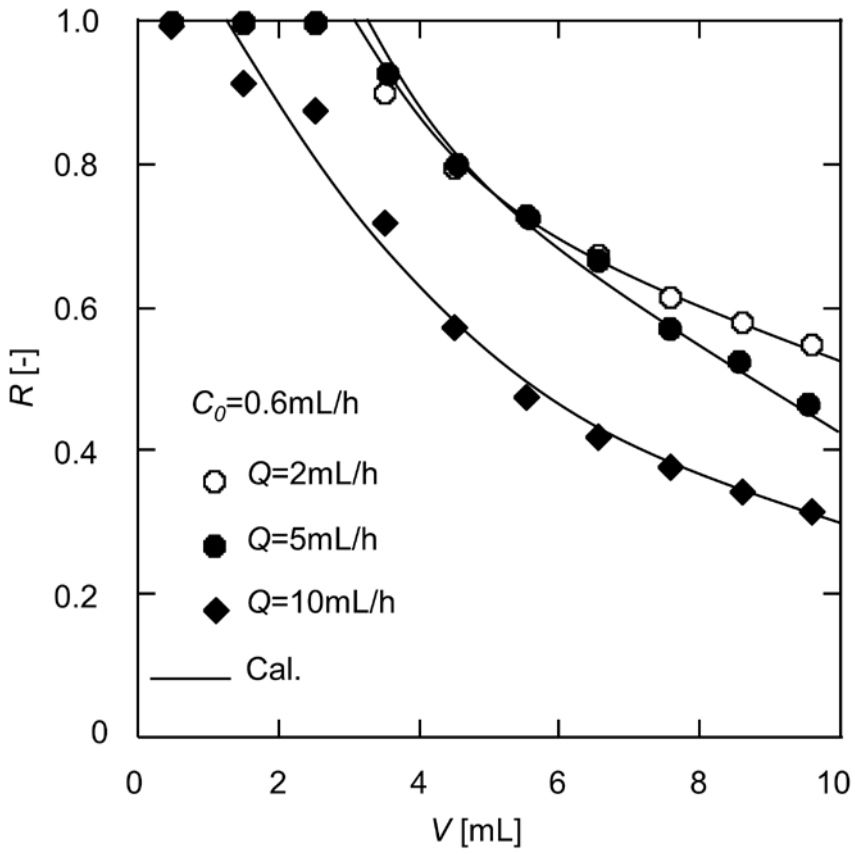

Fig. 4-7 Dynamic adsorption test results and calculated rejection curves at different permeation rates for the CB-modified PVA nanofiber fabric.

The effect of permeation rate on BSA rejection was investigated by permeating the 10 mL BSA solutions, with the results shown in Fig. 4-7. The BSA rejections showed a

very similar downward trend under the permeation rates of 2 and 5 mL/h, but it was slightly higher in the former at the end of the permeate process. It can be seen from Table 4-1 that the maximum adsorption capacity of the former is higher than that of the latter, since a slower permeation rate allows enough time for the BSA molecules to be captured. However, a noticeable decrease in rejection occurred under the permeation rate of 10 mL/h, due to insufficient residence time of BSA molecules in the pores of the PVA nanofiber mat.

Table 4-1 Kinetic model parameters for the dynamic adsorption of BSA.

Models	Pseudo-first order kinetic			Pseudo-second order kinetic		
Parameters	q_∞ [mg/g]	k_1 [h^{-1}]	R^2	q_∞ [mg/g]	k_2 [$g \cdot mg^{-1}h^{-1}$]	R^2
Q=5mL/h, C_0=0.6, original	301.9	0.8259	0.972	422.5	1.727×10^{-3}	0.986
Q=5mL/h, C_0=0.6, with CB	518.8	0.5539	0.988	768.8	0.591×10^{-3}	0.991
Q=5mL/h, C_0=0.3, with CB	322.7	0.3916	0.959	453.9	1.408×10^{-3}	0.997
Q=5mL/h, C_0=1.2, with CB	458.3	0.9056	0.967	710.8	1.389×10^{-3}	0.976
Q=2mL/h, C_0=0.6, with CB	573.9	0.1731	0.986	920.1	1.239×10^{-4}	0.992
Q=10mL/h, C_0=0.6, with CB	490.9	1.4507	0.975	486.3	2.552×10^{-3}	0.987

All kinetic parameters and correlation coefficient (R^2) values obtained at different adsorption conditions are listed and compared in Table 4-1. The higher R^2 values in all these results suggest that the pseudo-second-order kinetic model fits the data better than the pseudo-first-order kinetic model. This is consistent with the conclusion obtained in

the static experiment by using the two kinetic models to study the effect of time on the adsorption amount. As shown in Fig. 4-5, Fig. 4-6, and Fig. 4-7, the BSA rejection curves calculated by the pseudo-second-order model are in good agreement with the experimental results.

4.3.2.3 Desorption and reusability

The dynamic desorption experiments were performed to evaluate the reusability of the CB-modified PVA nanofibers. Phosphate buffer at pH = 10.0 containing 1.0 M NaCl was used as the eluent, because the adsorption capacity of BSA on adsorbent was low at pH far from its isoelectric point, and ionic strength affects electrostatic and hydrophobic interaction between BSA and the affinity ligands [148, 136]. As presented in Fig. 4-8, under the eluent rate of 10 mL/h, the desorption ratios at the eluent volumes of 10, 15, and 20 mL were 47.1%, 52.6%, and 56.6%, respectively. However, under the eluent rate of 5 mL/h, the desorption ratios raised to 92.4%, 95.9%, and 97.3%. Hence, sufficient residence time and volume of eluent are necessary for the efficient desorption of the adsorbed BSA molecules.

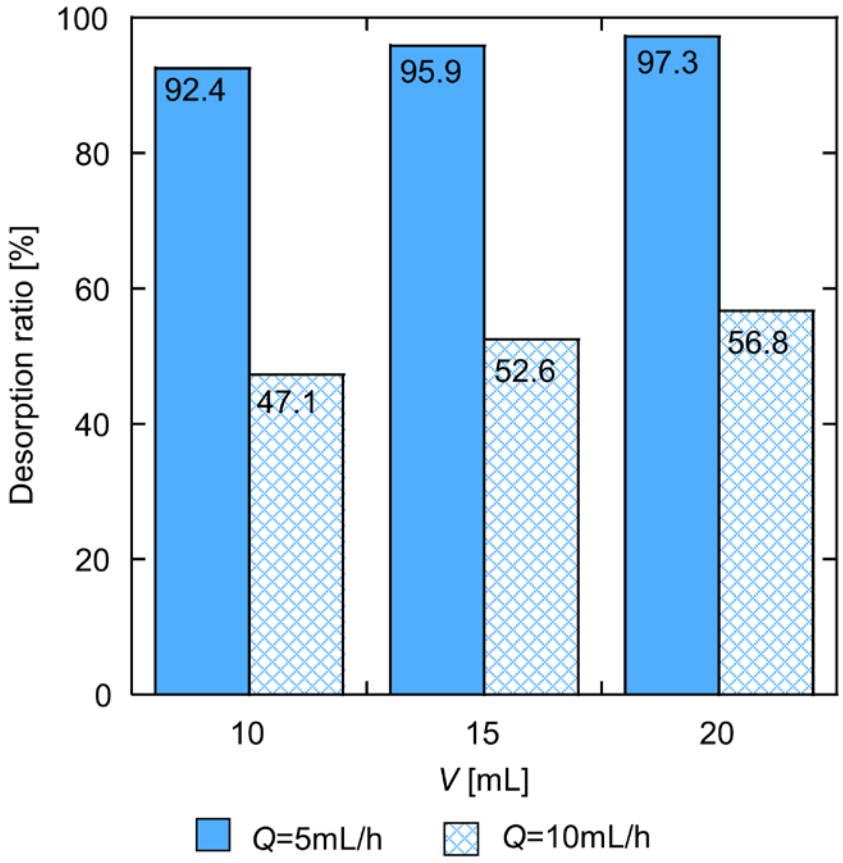

Fig. 4-8 Effect of volume and flowrate of eluent on desorption ratios for the CB-modified PVA nanofiber fabric.

The adsorption-desorption cycle experiments were carried out under the eluent rate of 5 mL/h by 20 mL eluent solution. The adsorption-desorption cycle was repeated three times, where the permeation concentration of BSA was 0.6 g/L. As shown in Fig. 4-9, the adsorption ratio decreased gradually in the three cycles. In the three adsorptions processes, the BSA instantaneous rejection at the end of permeating 10 mL BSA solution was 0.494, 0.326, and 0.269, respectively. Total rejection can be calculated as:

$$R_{\text{total}} = \frac{1}{V}\int_0^V R\, dV \tag{4-24}$$

According to Eq. (4-24), the total rejections for the three cycles were 0.765, 0.663, and 0.576, which remained in a high range.

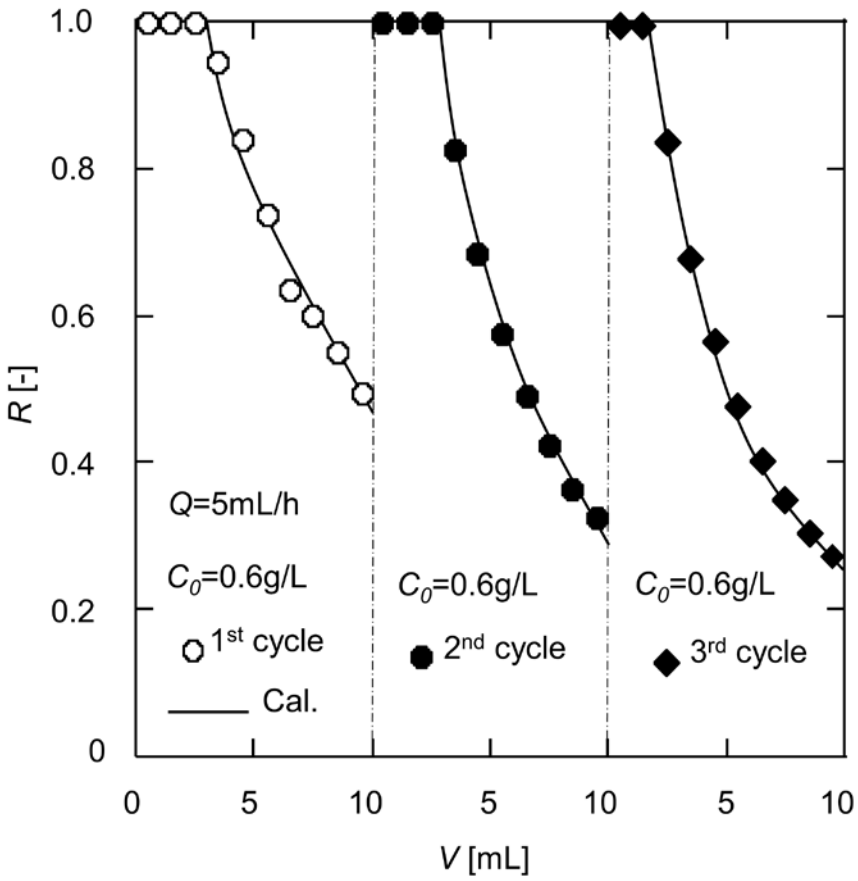

Fig. 4-9 Cycle dynamic adsorption test results and calculated rejection curves for the CB-modified PVA nanofiber fabric.

Table 4-2 Adsorption results of the reused PVA nanofiber fabric.

Cycle	**1st**	**2nd**	**3rd**
R_{total}	0.749	0.919	0.992

In the other set of adsorption-desorption experiments, 10 mL BSA solution was permeated at the permeation rate of 5 mL/h, where the initial BSA concentration was 0.6 g/L. The concentration of the permeated solution was measured, and the BSA-adsorbed nanofiber mat was eluted. Then the collected permeation from the previous

adsorption process continued to be permeated through the regenerated nanofiber mat again. After three rounds of dynamic adsorption, the BSA total rejection increased from 0.749 to 0.992, as shown in Table 4-2. Thus, the CB-modified PVA nanofibers can be recycled and reused.

4.3.2.4 Comparison between static and dynamic adsorption

In order to provide a design basis for adsorption operation, the static and dynamic adsorption efficiencies were compared by the fitting curves according to the experimental data.

When the static adsorption reached equilibrium, the BSA adsorption amount calculation Eq. (4-1) is rewritten by:

$$q_e = \frac{(C_0 - C^*)V}{W} \tag{4-25}$$

where C^* (g/L) is the equilibrium concentrations of BSA in solution.

Substituting Eq. (4-25) into Eq. (4-4) to obtain a quadratic equation with respect to C^*. Solving the quadratic equation, then C^* can be expressed through the following equation:

$$C^* = \frac{-(q_s KW - C_0 VK + V) + \sqrt{(q_s KW - C_0 VK + V)^2 + 4KC_0 V^2}}{2KV} \tag{4-26}$$

Substituting Eq. (4-26) for C_p into Eq. (4-2), the rejection R in the static adsorption at equilibrium can be expressed by:

$$R = 1 - \frac{-(q_s KW - C_0 VK + V) + \sqrt{(q_s KW - C_0 VK + V)^2 + 4KC_0 V^2}}{2KVC_0} \tag{4-27}$$

According to the study of 3.1.2, it is assumed that after 5 hours of PVA nanofiber mat being immersed into BSA solution of various volumes, the static adsorption has reached equilibrium. At the concentrations of 0.3, 0.6, and 1.2 g/L, through varying the volume from 0 to 25 mL, the static rejection values can be calculated according to Eq. (4-27). The total dynamic rejection values can be calculated by substituting Eqs. (4-20), (4-21)

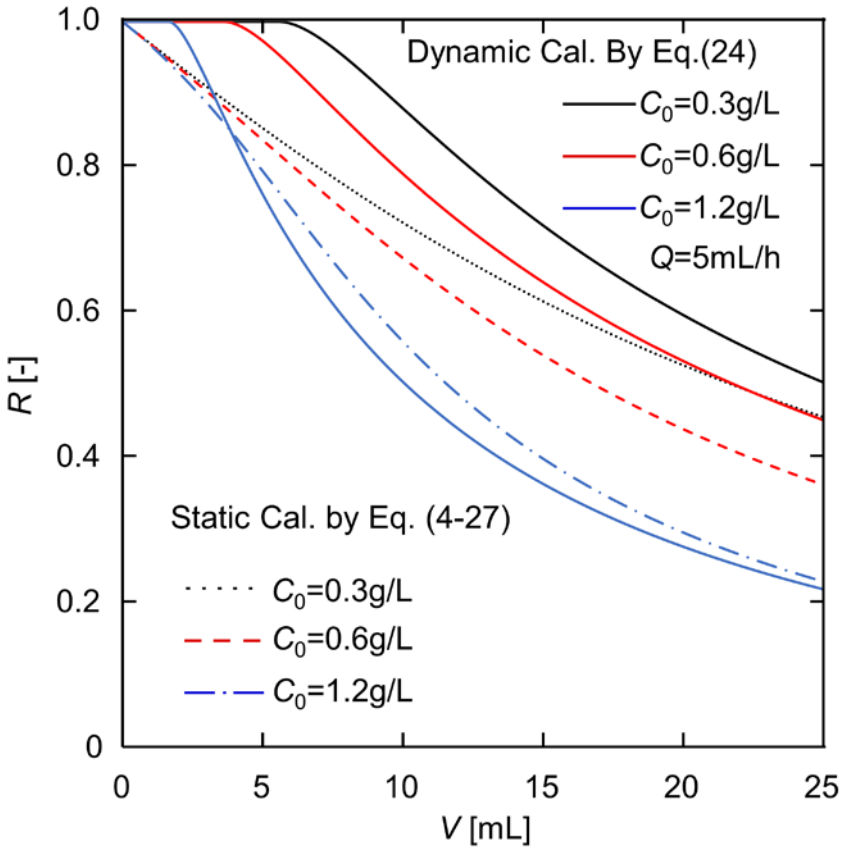

Fig. 4-10 Calculated rejection curves for static adsorption and dynamic adsorption for the CB-modified PVA nanofiber fabric.

into Eq. (4-24). The theoretical rejection curves of static and dynamic conditions are shown in Fig. 4-10. For the initial concentrations of 0.3 and 0.6 g/L, all the rejections of the dynamic adsorption are greater than that of the static adsorption. It is worth noting that the dynamic adsorption takes the same 5 hours as the static adsorption only at the permeate volume of 25 mL. Under the other volume conditions of less than 25 mL, the dynamic adsorption takes a shorter time. For example, the operating time with 12.5 mL BSA solution of the static adsorption and the dynamic adsorption is 12 and 6 hours; the latter provides higher rejection while saving half the time. For the initial concentration of 1.2 g/L, rejection of the dynamic adsorption is higher than the static adsorption at the beginning but reverses at the volume of 3.8 mL. Under high-concentration conditions, both of the rejections decrease rapidly. From the perspective of design

optimization, very low rejection is meaningless for protein purification process. Taking 0.5 as the rejection design requirement, the disposable treatment volume of the static adsorption and the dynamic adsorption is 12.6 and 11.5 mL. The two treatment volumes for the 1.2 g/L solution are distinctly close, but the operating time of the static adsorption and the dynamic adsorption time is 5 and 2.3 hours. It can be concluded that dynamic adsorption is highly efficient and time-saving at the test concentrations. Furthermore, continuous operation of dynamic adsorption presents advantages for automated control, labor saving and integration with other continuous processes.

4.4 Chapter summary

In this chapter, the electrospun PVA nanofiber fabrics were functionalized by CB as an affinity ligand. The PVA nanofibers under four different heat treatment temperatures were modified, and their adsorption behaviors for BSA were examined. The adsorption ability of the PVA nanofibers under the optimal heat treatment temperature before and after CB modification was analyzed by the Langmuir equation. Then, dynamic experiments were conducted to determine the effects of initial concentration and permeation rate. The pseudo-second-order model better fitted the experimental data than the pseudo-first-order model in both static and dynamic adsorption performance. Furthermore, the CB-modified PVA nanofibers possessed excellent regeneration ability and cycle performance. Finally, the adsorption efficiency by the static and dynamic methods was compared, and the results can provide a reference for process scale-up design. Considering the simple fabrication process, large binding capacity, and high adsorption efficiency, the CB-modified PVA nanofiber has great potential for the affinity adsorption and isolation of proteins [156].

Chapter 5 Selective Adsorption and Separation of Proteins by CB-Modified Nanofiber Fabrics

5.1 Introduction

Proteins exist in complex biological systems, and separation of proteins is a challenging task. Proteins are easily denatured and inactivated by heat or certain solvents, so they have strict requirements for separation conditions. Although chromatography has the advantage of high resolution in the separation and purification of proteins, it is not conducive to large-scale industrial production because of its tedious operation, difficult scale-up and high cost. Ultrafiltration is the most commonly used protein separation technology, which has the characteristics of high efficiency, low energy consumption and simple operation. Ultrafiltration is a process of separating proteins based on molecular size, governed by transmembrane pressure driving force [90]. Ultrafiltration is usually recommended for the separation of molecules with more than 10-fold difference in molecular weight [157], and is hardly effective for the separation of proteins of similar size. Mukai et al. [158] successfully separated BSA with a molecular weight of 67000 and lysozyme with a molecular weight of 14300 using ultrafiltration membranes with a molecular weight cut-off (MWCO) of 30000 by properly controlling the solution environment and operating conditions.

BHb and BSA were used as model proteins for selective separation. The molecular weights of BHb and BSA are 64500 and 67000, respectively, which are very close to each other. In the previous chapters, the static and dynamic adsorption behaviors of CB modified PVA nanofiber fabric for BSA were investigated. In this chapter, batch experiments were performed to study the nanofiber fabric's BHb adsorption capacity

of at different protein concentrations before and after modification. After that, the effect of feed concentration and permeation rate on the dynamic adsorption behaviors for BHb of the nanofiber fabric was investigated. The pH impact on BHb and BSA adsorption was examined by static adsorption experiments of single protein solutions. The selective separation experiments of the BHb-BSA binary solution were carried out at the optimal pH value, with the reusability of the PVA nanofiber fabrics also being studied. This research demonstrated the potential of the CB modified PVA nanofiber fabric in protein adsorption and selective separation.

5.2 Experimental

5.2.1 Materials

The electrospun PVA nanofiber fabrics were supplied by Japan Vilene Company, Ltd., with a heat treatment temperature of 80 ℃. BHb were purchased from Sigma-Aldrich Co. LLC., Japan. The other chemicals were the same described in section 4.2.1.

5.2.2 Preparation of CB modified PVA nanofiber fabrics

The CB-modified PVA nanofiber fabrics were prepared according to the method described in section 2.2.3.

5.2.3 BHb adsorption studies

BHb adsorption capacities of the original and CB-modified PVA nanofiber fabrics were measured under different initial BHb concentrations at pH = 6.8 (BHb's isoelectric point). The two types of fabrics were immersed into an 8 mL BHb solution with concentrations varing from 1 g/L to 6 g/L. The static adsorption experiments were carried out at 25 °C for 6 hours. The BHb solution concentrations were detected by a UV–vis spectrophotometer at 406 nm before and after adsorption. To analyze the

adsorption results, the amount of adsorbed protein per unit mass of fabric was determined with the following equation:

$$q = \frac{(C_0 - C)V}{W} \quad (5\text{-}1)$$

where q is the adsorption capacity (mg/g); C_0 and C are the initial and the final BHb concentrations (g/L), respectively; V is the volume of the solution (mL), and W is the fiber mass (g). The BHb adsorption capacities were plotted against the final concentrations to obtain an adsorption curve.

The dynamic adsorption performance of BHb on the PVA nanofiber fabrics was studied by permeation tests. Figure 5-1 depicts the experimental setup. The PVA nanofiber fabric mat with a weight of 19.6 mg was placed in the Millipore filter holder (SX0002500) with an effective diameter of 2.2 cm and a permeation area of 3.8 cm^2. Then, the inlet of the filter holder was mounted to the outlet of the syringe by a threaded connection. Subsequently, a syringe pump (SRS-2, AS ONE Co., Japan) was used to inject the BHb solution into the filter holder. After setting of the flow rate, the permeation experiment was started by collecting the permeate from the outlet below the filter holder and monitoring the concentration of BHb. Detailed studies were conducted at 25 °C, BHb feed concentration of 0.3 ~ 1.2 g/L, and permeation rates of 2 ~ 10 mL/h. The momentary rejection ratio R_m for protein was determined according to the following equation:

$$R_m = 1 - \frac{C_p}{C_0} \quad (5\text{-}2)$$

where C_0 (g/L) and C_p (g/L) are the protein concentrations in the feed solution and the permeate, respectively.

At a cumulative permeate volume of V (mL), the rejection ratio R_c for protein of the CB modified PVA nanofiber fabric is given by

$$R_c = \frac{1}{V}\int_0^V R_m dV \quad (5\text{-}3)$$

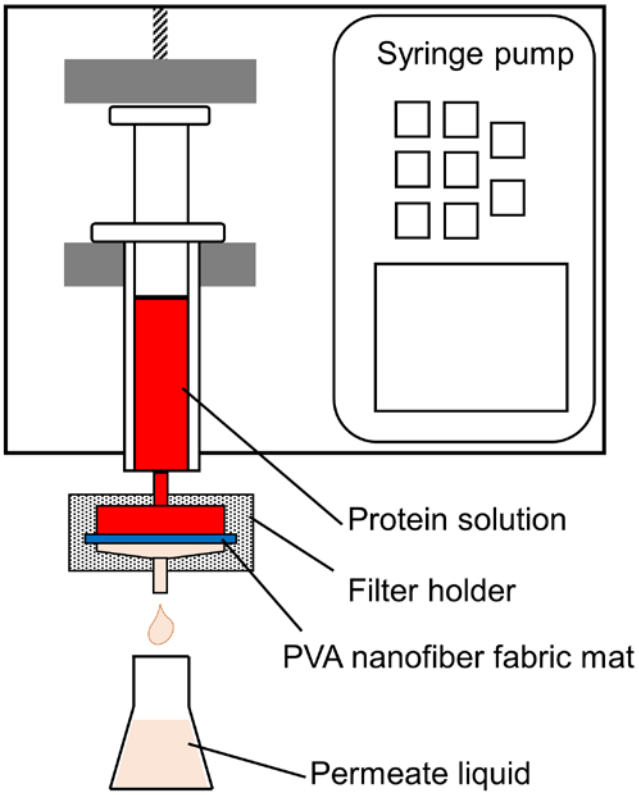

Fig. 5-1 Schematic diagram of the dynamic adsorption apparatus.

5.2.4 Selective separation of binary BHb-BSA solution

The single protein adsorption experiments were carried out at 25 °C for 6 hours. The single component concentrations of BHb or BSA solution was 3 g/L. The effect of pH on the adsorption capacity was investigated using different pH values ranging from 4 to 9. The protein concentrations before and after adsorption were measured using a UV–vis spectrometer, referring to the absorption band at 406 nm for BHb and 280 nm for BSA.

Selective experiments were carried out with the permeation apparatus at the optimum pH of 6.8. The initial concentrations of both proteins were 0.6 g/L in the BHb-BSA binary solution. The BHb solution exhibits two characteristic absorbance peaks at

280 nm and 406 nm, while the absorbance of the BSA solution exhibits a maximum around 280 nm and can be negligible around 406 nm. Accordingly, the BHb concentration was determined directly from the absorbance at 406 nm. The BSA concentration was determined at 280 nm by subtracting the contribution of BHb from the concentration detected at 406 nm. The rejection ratio for BHb or BSA is calculated according to equation (3), and the selectivity factor (*S*) of protein is defined as the following equation:

$$S = \frac{R_{c,BHb}}{R_{c,BSA}} \tag{5-4}$$

Finally, the reusability tests for BHB-BSA binary protein dynamic adsorption were repeated for three cycles to examine the stability of the CB modified PVA nanofiber fabrics.

5.3 Results and discussion

5.3.1 Static adsorption isotherm of BHb

In order to evaluate the BHb adsorption capacity of the PVA nanofiber fabrics before and after CB modification, the effect of the initial concentration on the adsorption capacity of the nanofiber fabrics was studied, with the results shown in Fig. 5-2.

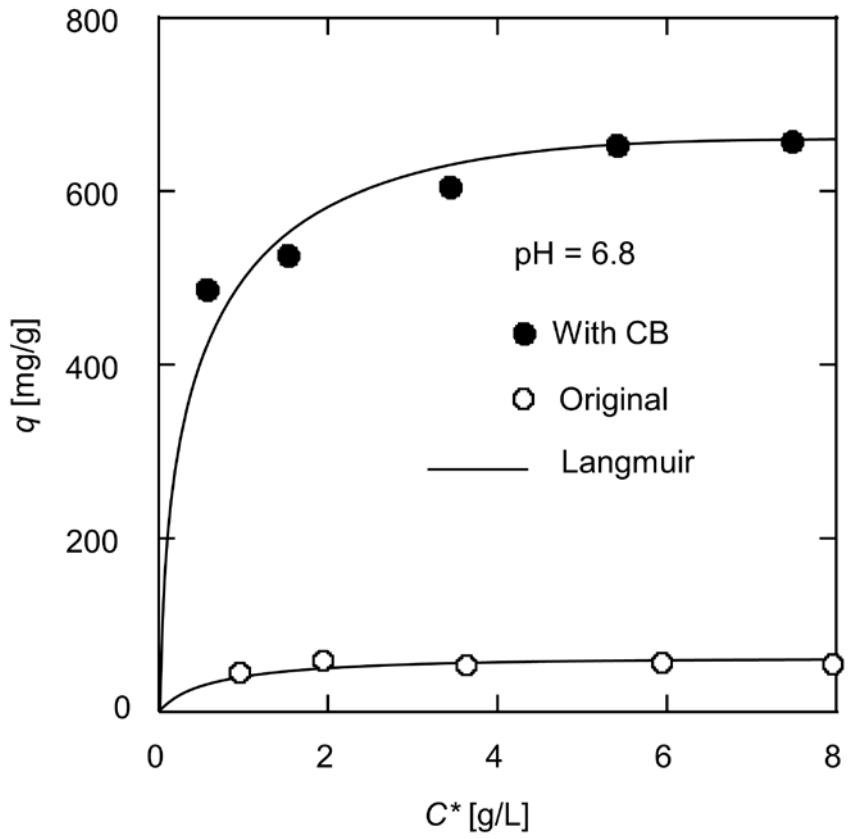

Fig. 5-2 Effect of the BHb initial concentration on adsorption capacities of the original and CB-modified PVA nanofiber fabrics.

The BHb adsorption on the PVA nanofiber fabrics increased with the increase of the BHb concentration. The adsorption capacity of the CB modified PVA nanofiber fabrics was markedly greater than that of the original fabrics. The adsorption amount of BHb on the original PVA nanofiber fabrics was at a low level in all experimental concentrations, while the adsorption amount of the modified nanofiber fabrics was around 655 mg/g when the BHb concentration exceeded 6.0 g/L. The excellent adsorption capacity of the modified nanofiber fabrics is attributed to the affinity of CB molecules. The interaction between the CB molecule and BHb is a consequence of the combined effects of electrostatic, hydrophobic interactions and hydrogen bonding. As a monochlorotriazine dye, the CB molecule contains three sulfonic acid groups and four basic primary and secondary amino groups. The triazine part of CB is used to fix onto

the PVA matrix, while the three sulfonic acid groups and the multiple aromatic parts are mainly responsible for the CB-BHb binding [126].

The Langmuir adsorption isotherm is one of the most widely used adsorption isotherms, which is used to fit adsorption equilibrium data. It is assumed that adsorption is a monolayer type occurring on the homogeneous surface of the adsorbent [140,159]. The linear form of the Langmuir equation is expressed as:

$$\frac{C^*}{q_e} = \frac{C^*}{q_s} + \frac{1}{Kq_s} \tag{5-5}$$

where q_s (mg/g) is the maximum adsorption capacity, q_e (mg/g) is the equilibrium adsorption capacity, C^* (g/L) is the equilibrium BHb concentration, and K (L/g) is the dissociation constant of the system.

By fitting the experimental data to the Langmuir linear equation, the maximum adsorption capacities of BHb on the PVA nanofiber fabrics before and after CB modification were calculated to be 58 mg/g and 686 mg/g, respectively. Zhang et al. [160] prepared magnetic carbon nanotubes with a hierarchical copper silicate nanostructure for BHb adsorption, with the maximum BHb adsorption capacity being 302 mg/g. Wang et al. [161] reported that magnetic mesoporous ytterbium silicate microspheres achieved a BHb adsorption capacity of 304 mg/g. Compared to these materials, the CB modified PVA nanofiber fabric has a distinct advantage in adsorption capacity.

5.3.2 BHb dynamic adsorption performance

Dynamic adsorption operation offers the benefits of automatic control, labor-savings and easy integration with other continuous processes. Thus, we tested the BHb dynamic adsorption behavior of the CB modified PVA nanofiber fabrics.

Figure 5-3 shows the changes in the BHb rejection ratio over the permeation volume from 0 to 10 mL for both the original and CB modified PVA nanofiber fabrics. The BHb rejection ratio by both nanofiber fabrics showed a downward trend with the increase of the permeation volume. Whereas the BHb rejection ratio of the CB PVA

nanofiber modified nanofiber fabric remained at a high level, reducing from 1.0 to 0.62, the BHb rejection ratio of the original nanofiber fabric was meagre, being 0.23 at the beginning and only 0.10 at the end of the experiment. The enhancement in protein rejection ratio of the CB modified PVA nanofiber fabric comes from the affinity effect of CB molecules.

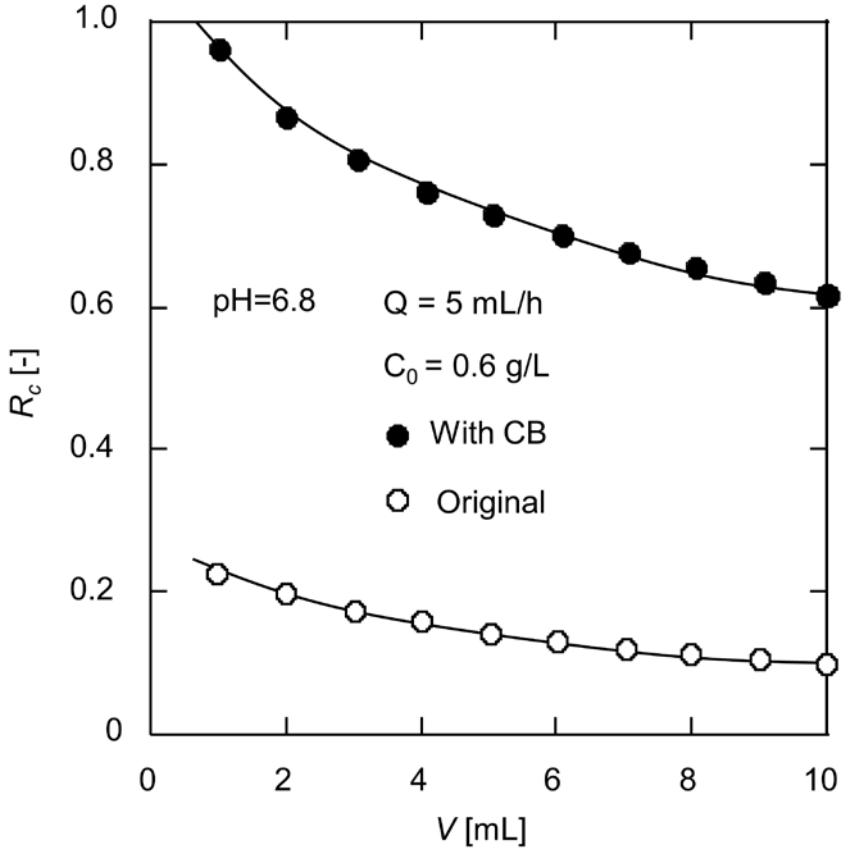

Fig. 5-3 Dynamic adsorption test results for the original and CB-modified PVA nanofiber fabrics.

Figure 5-4 shows the BHb rejection ratio of the CB modified PVA nanofiber fabrics varied with permeation volume at different feed concentrations. For the highest feed concentration of 1.2 g/L, the contact probability for interaction between BHb molecules in the mobile phase and nanofiber surface was the highest, and the driving force was the largest. As a result, the BHb adsorption sites on the nanofiber surface were occupied sooner, and the rejection ratio was markedly lower than that of the other two dilute

solutions. For the solutions with concentrations of 0.3 and 0.6 g/L, the changes in the BHb rejection ratio were similar, but the rejection ratio values were higher at 0.3 g/L.

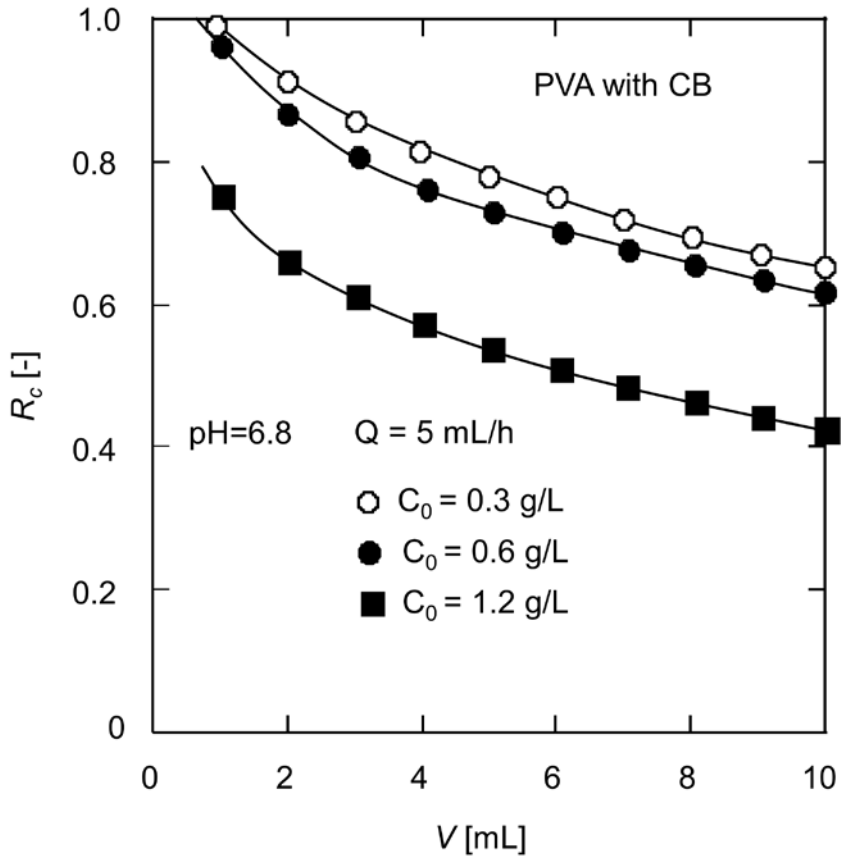

Fig. 5-4 Dynamic adsorption test results for the CB modified PVA nanofiber fabrics at different feed concentrations.

The influence of permeation rate on the BHb rejection ratio was examined, and the results are shown in Fig. 5-5. When the permeation rate was 10 mL/h, the BHb rejection ratio dramatically reduced due to the insufficient retention time of BHb molecules in the pores of the nanofiber fabric. In contrast, the BHb rejection ratio decreased more slowly in the permeation experiments with the permeation rate of 2 and 5 mL/h. Therefore, it is necessary to allow sufficient residence time in order to obtain the protein rejection effect. Additionally, attention needs to be paid to the balance between the productivity and rejection ratio during the dynamic adsorption operation.

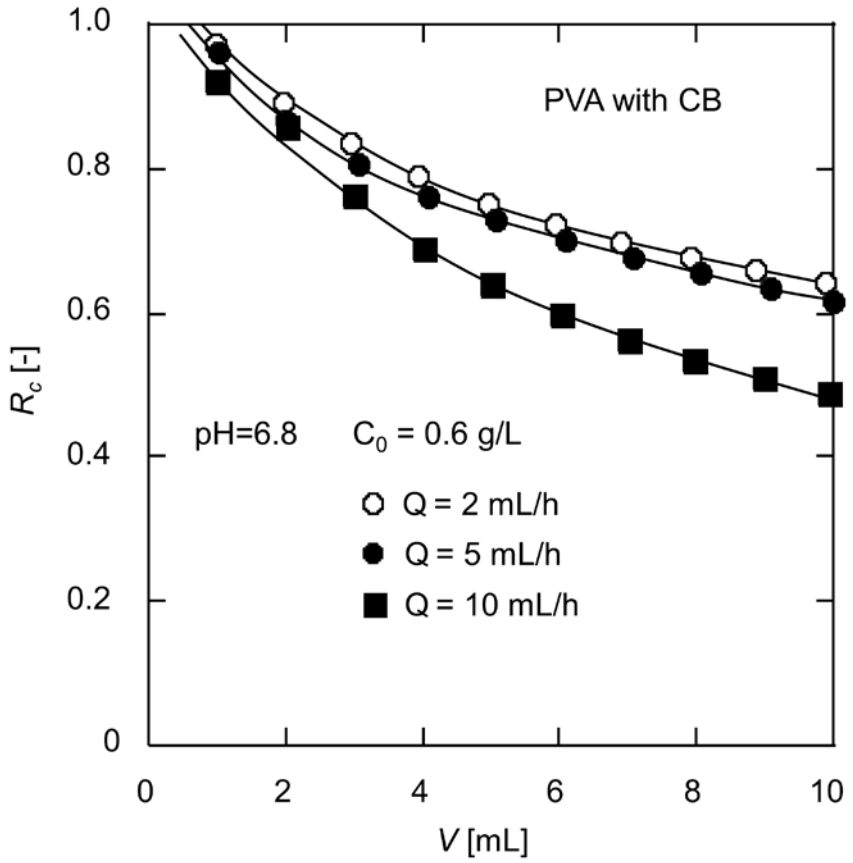

Fig. 5-5 Dynamic adsorption test results for the CB modified PVA nanofiber fabrics at different permeation rates.

5.3.3 Effect of pH on BHb and BSA adsorption

Both BHb and BSA are homologous proteins derived from bovine blood, and their molecular weights are so close that they are difficult to separate with conventional filtration methods. Nevertheless, it is worth noting that the two proteins have different isoelectric points, 5.0 and 6.8, respectively. Proteins are amphoteric biomolecules because the amino acids that make up proteins contain both basic and acidic functional groups [123]. The protein surface charge depends on the pH value of the protein solution. At the isoelectric point, the electric charge of protein becomes zero. When the pH value of the protein solution is lower than the isoelectric point, the protein surface

has positive charge; in the contrary situation, the protein is negatively charged. Therefore, pH has a considerable influence on the adsorption capacity.

The pH effect on the adsorption capacity in a single component solution of BHb or BSA was studied by the static adsorption experiments. As BSA undergoes irreversible structural transitions in the range of pH < 4 [162], so the experiments were performed at pH = 4 ~ 9. Figure 5-6 displays the adsorption amounts of the CB modified PVA nanofiber fabrics towards BHb and BSA. Under different pH values, the adsorption capacities of BHb and BSA were different. The greater the difference between the adsorption amounts, the more likely it is to realize selective separation. The adsorption capacity of BHb was the maximum at its corresponding isoelectric point of 6.8. The BHb adsorption capacity decreased in varying degrees at other pH values. Similarly, the BSA adsorption capacity showed the maximum at its isoelectric point of 5.0. At the isoelectric point, the repulsive force between protein molecules was minimal because the protein charge was zero. As a result, more protein molecules arranged on the nanofiber surface during the affinity interaction with the CB molecules immobilized on the nanofiber fabrics. At pH = 6.8, the adsorption amounts of the CB modified PVA nanofiber fabrics were 594 mg/g for BHb and 244 mg/g for BSA. The difference in the adsorption amounts was more extensive than that of other pH values, about 350 mg/g. In this case, pH = 6.8 was taken as the condition of the binary protein separation.

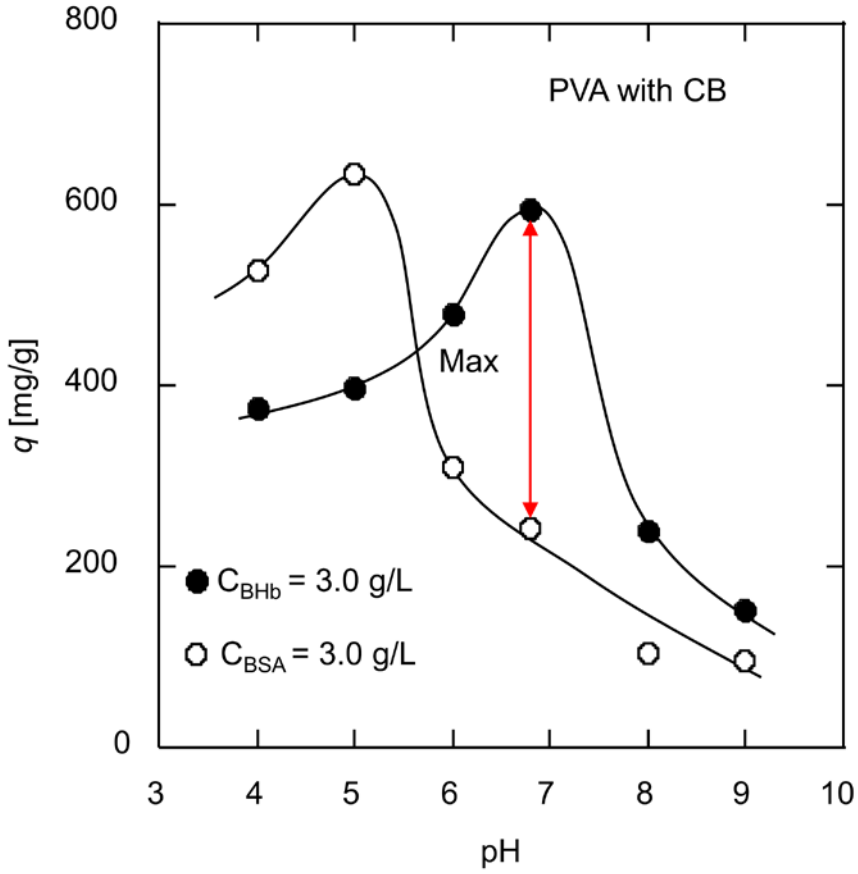

Fig. 5-6 Effect of pH on BHb and BSA adsorption performance.

5.3.4 Selective separation of binary BHb-BSA solution

Dynamic adsorption experiments of the CB modified PVA nanofiber fabrics were conducted with binary BHb-BSA solutions. Figure 5-7 shows the variation of rejection ratios for BHb and BSA versus the permeation volume. From the beginning of the permeation experiment, the rejection ratio for BHb was much higher than BSA, and the rejection ratios decreased gradually as the permeation volume increased. The selectivity factor *S* of BHb for the initial 1 mL of the permeate was about 3.01. The initial *S* seemed unsatisfactory due to a large number of vacant active sites on the nanofiber surface where BHb and BSA molecules were both able to attach at the beginning of the

experiment. However, at the end permeation volume of 10 mL, the rejection ratios for BHb and BSA were 0.60 and 0.11, respectively, and *S* rose to 5.45.

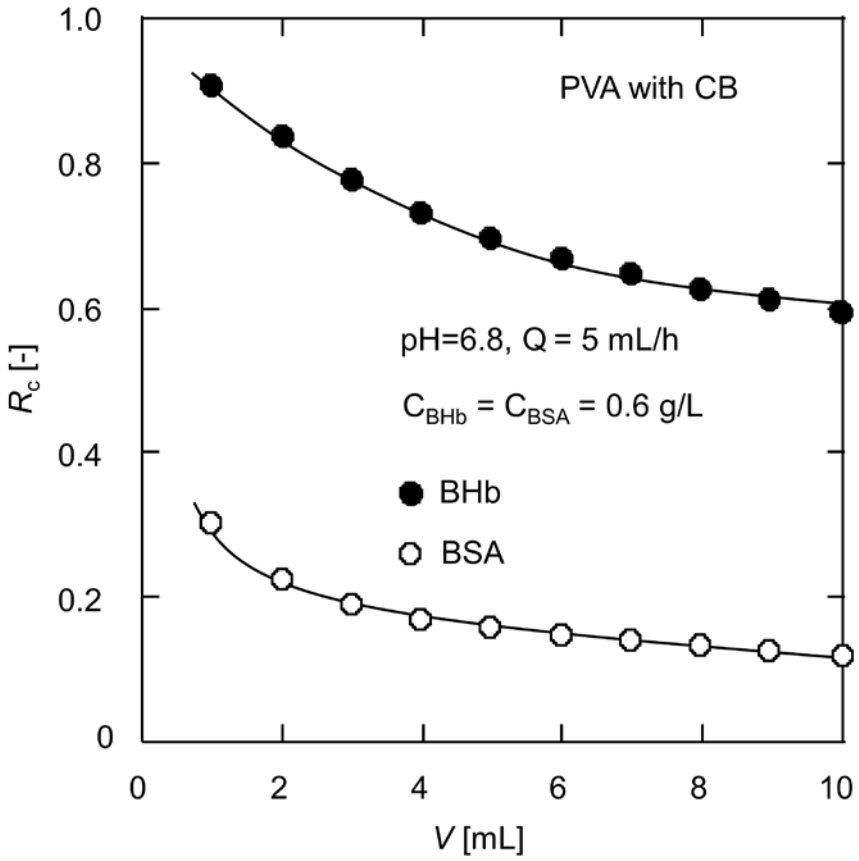

Fig. 5-7 Selective separation results for BHb-BSA binary solution.

The BHb molecules with zero charge occupied more active sites on the nanofiber surface. On the contrary, at pH = 6.8, BSA was negatively charged and had difficulty in close arrangement on the nanofiber surface due to the electrostatic repulsion between molecules resulting in weaker competition for active sites on the nanofiber surface compared to BHb. In addition, the size of the BHb molecule is 6.4 nm × 5.5 nm × 5 nm, with a spherical shape, while the size of the BSA molecule is 14 nm × 3.8 nm × 3.8 nm, with a shape similar to a prolate ellipsoid [163]. When BSA molecules flowed through the intricate pores inside the nanofiber fabrics, in order to obtain minimal interaction with the nanofiber surface, the ellipsoidal molecules might align their long axis parallel

to the centerline of the nanofiber, resulting in a lower hydrodynamic hindrance than that of BHb molecules. In contrast, spherical BHb molecules were more easily attracted by the CB molecules immobilized on the nanofiber surface when passing through the internal pores of the nanofiber fabric.

5.3.5 Desorption and reusability

It has been reported that increasing the solution ionic strength leads to a decrease in protein adsorption amount [146, 156]. Salts in the adsorption medium can lead to coordination of the deprotonated sulfonic acid groups of CB molecule with sodium ions; on the other hand, the distortion of existing salt bridges contributes to low protein adsorption at high ionic strength [132]. In addition, moving the pH of the adsorption medium away from the protein's isoelectric point is also detrimental to adsorption. Thus, a phosphate buffer at pH = 10.0 containing 1.0 M NaCl was used as the eluent to desorb BHb and BSA from the protein adsorbed CB- modified PVA nanofiber fabrics. The protein-adsorbed nanofiber fabric was eluted with 20 mL eluent at a rate of 5 mL/h using the permeation apparatus, and above 96% of the protein molecules were eluted off. The adsorption-desorption was repeated for three cycles to evaluate the reusability of the CB modified PVA nanofiber fabrics.

Figure 5-8 displays the changes in rejection ratios for BHb and BSA with the permeation volume during the three adsorption cycles. The rejection ratios for both proteins declined slightly. However, the selectivity factor *S* maintained above 5 at the end permeate volume of 10 mL in all three cycles with 5.36, 5.07 and 5.13, respectively. It is demonstrated that the CB-modified PVA nanofiber fabrics can be reused without losing activity easily.

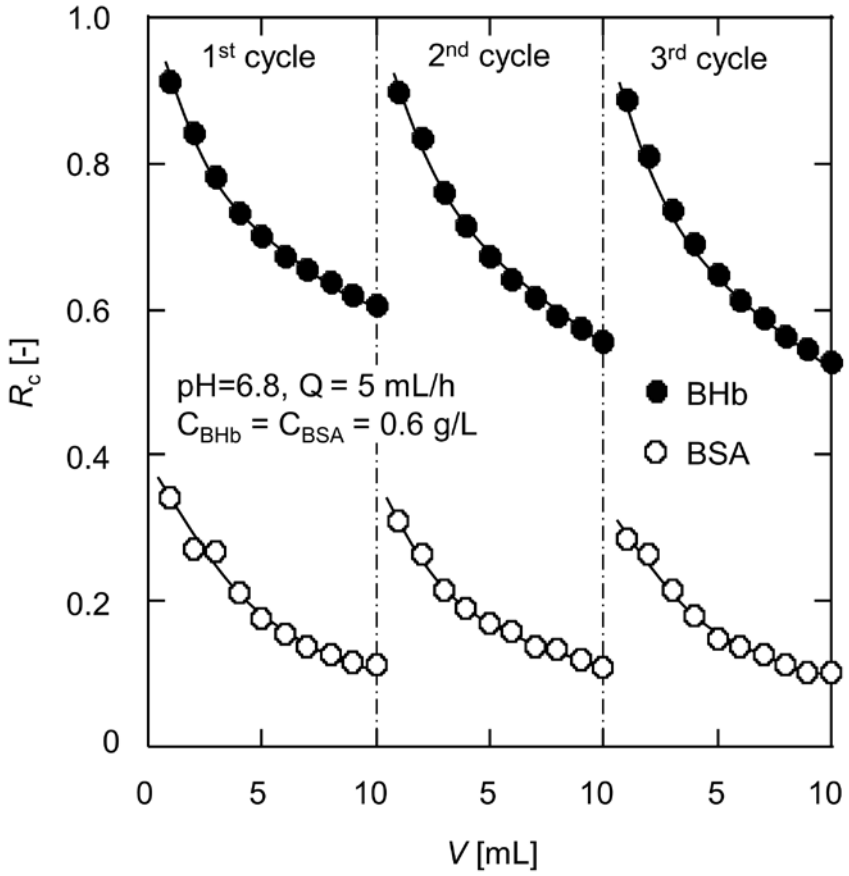

Fig. 5-8 Reusability test of the CB-modified PVA nanofiber fabrics for selective separation.

5.4 Chapter summary

In this chapter, the CB-modified PVA nanofiber fabrics were fabricated via immobilization of CB molecules on the nanofiber surface. The batch experiments showed that the modified nanofiber fabrics have a high adsorption capacity for BHb. The Langmuir isotherm was used to fit the experimental data, and the maximum adsorption capacity of the nanofiber fabric was calculated to be 686 mg/g. Then, dynamic experiments were performed to determine the effect of feed concentration and permeation rate on the BHb rejection ratio. In the single protein static adsorption experiments, the pH impact on the adsorption of BHb and BSA was investigated

separately, where the pH value with the largest difference in the adsorption amount was explored. Finally, a high selectivity factor of 5.45 for BHb was achieved during the dynamic adsorption of the BHb-BSA binary solution at pH=6.8, corresponding to the isoelectric point of BHb. The selectivity factors for BHb maintained above 5 in the three adsorption-elution cycles, indicating the reusability of the nanofiber fabric. This work demonstrated the potential of the CB-modified PVA nanofiber fabric in the selective separation for proteins with similar sizes [164].

Chapter 6 Conclusions

In recent years, with the rapid development of life science, biotechnology and pharmaceutical industry, the requirements for the separation and purification of proteins have been increasing. Proteins usually come from natural products or fermentation broth, and their initial concentrations are generally low. Proteins are easily inactivated or degraded due to their great sensitivity to temperature, pH, and organic solvents. The efficient separation and purification of proteins are one of the key issues in downstream technology of bioengineering. It is desirable to achieve high production efficiency and high product quality while reducing the cost of the isolation process.

The separation and purification of proteins are primarily based on differences in the characteristics of proteins, including molecular size and shape, acid-base properties, solubility, adsorption properties, and biological affinity for other molecules. The ultrafiltration process, which is the most widely applied in protein separation, is difficult to control the selectivity for proteins with similar sizes. Although chromatography is characterized by high precision in protein separation, it has the disadvantages of high cost, slow flow rate, large pressure drop, and not easy for large-scale industrial production.

The development of nanotechnology has brought a bright prospect for protein separation. In this thesis, PVA nanofiber fabrics with high affinity for proteins were prepared, and their applications in protein adsorption and separation were investigated. The effects of the physical and chemical structure of nanofiber fabrics and adsorption environmental conditions on the adsorption properties of proteins were clarified. Also, the adsorption mechanism of proteins on the surface of PVA nanofiber fabrics was examined. The research results and main conclusions are as follows:

(1) Electrospinning polymer solution was prepared by dissolving PVA in water, and maleic acid was added as a cross-linking agent. Then PVA nanofibers were prepared using the electrospinning method. The PVA nanofiber fabric surface was observed by SEM, and the resultant nanofiber fabric showed a distinctive highly porous structure with micro-scale interstitial spaces. The diameter distribution of the fibers was counted, and the average diameter was calculated. The PVA nanofiber fabric surface was subsequently modified with the reactive dye of CB through a series of surface modification steps. CB molecule contains electrophilic triazine chloride groups capable of reacting with the nucleophilic group -OH of PVA molecule. The chemical structures of the original and CB modified PVA nanofiber fabrics were detected via FTIR. The characteristic spectra of the CB molecules, such as benzene ring, C-N, and sulfonic acid groups, were observed on the CB-modified PVA nanofiber fabrics, which confirms that CB molecules were successfully fixed onto the PVA nanofiber fabrics.

(2) The static adsorption performance of CB-modified PVA nanofiber fabrics on BSA was investigated. The adsorption amount increased with the increase of the initial concentration of BSA, and the saturation adsorption amount of CB-modified PVA nanofiber fabrics was increased by 4 times compared with the original PVA nanofibers. The equilibrium isotherm data was analyzed by the Langmuir and Freundlich isotherms, respectively. The Langmuir isotherm fitted the results better than the Freundlich isotherm, which shows that the BSA adsorption on the nanofiber surface is a monolayer adsorption. The effects of pH value and ionic strength on the adsorption capacity were studied. In the desorption test with 1.0 M NaCl at pH 10, the desorption ratio of BSA-adsorbed PVA nanofiber fabrics reached 97.3%. The affinity PVA nanofiber fabrics showed no significant decrease in adsorption performance during repeated adsorption-desorption cycles and exhibited excellent reusability. These results reveal that CB-

modified PVA nanofiber fabrics are superior candidates for affinity adsorption of proteins.

(3) The usage of nanofiber fabrics for dynamic adsorption is more prevalent in the industrial production process. The effects of adsorption conditions on the BSA dynamic adsorption process, such as modification of CB, BSA concentration of the permeate solution, and permeation rate, were examined in a continuous system. Adsorption results were fitted using the adsorption kinetics of the pseudo-first-order kinetic and the pseudo-second-order kinetic. All kinetic parameters and correlation coefficient values were compared between the pseudo-first-order kinetic and the pseudo-second-order kinetic. The higher correlation coefficient values of the pseudo-second-order kinetic model demonstrated that the adsorption rate of BSA on the nanofiber surface is not proportional to the concentration driving force but proportional to the square of the driving force, and the adsorption rate is controlled by the chemical adsorption mechanism. In order to provide a design basis for adsorption operation, the static and dynamic adsorption efficiencies were compared by the fitting curves according to the experimental data. The dynamic adsorption was more efficient and time-saving than the static adsorption in the concentration range of the experiment. These results can provide a reference for process scale-up design.

(4) To tackle the challenge of separating proteins of similar sizes, selective adsorption studies were performed using the CB-modified PVA nanofibers with BHb and BSA as model proteins. The molecular weights of BHb and BSA are 64500 and 67000, respectively, and the sizes of BHb and BSA are too close to be effectively separated by conventional filtration operations. The static and dynamic adsorption behaviors of the PVA nanofiber fabrics on BHb before and after CB modification were investigated. Then, the effect of pH on the adsorption properties of BHb and BSA was investigated.

The positive and negative charges of protein molecule are equal at a specific pH value, which means that the surface charge of protein molecule is zero at the isoelectric point. The maximum adsorption amounts for BHb and BSA on the CB-modified PVA nanofiber fabrics appeared at pH = 6.8 and pH = 5.0, respectively. However, the maximum difference of the adsorption amounts for the two protein was observed at pH 6.8, which is corresponding to the isoelectric point of BHb. The selective separation experiments of the BHb-BSA binary solution were carried out at pH 6.8, and a high selectivity factor of 5.45 for BHb was achieved. Finally, the reusability of the nanofiber fabric was examined by three adsorption-elution cycle tests. This research demonstrated the potential of the CB modified PVA nanofiber fabric in protein adsorption and selective separation.

The application of modified electrospun nanofiber fabrics in protein adsorption and separation was explored in this thesis. The static and dynamic adsorption mechanisms of protein molecules on nanofiber fabrics were elucidated, providing a design basis for the scale-up industrial applications. The study of selective separation of binary protein solutions made a meaningful exploration for the application of nanofiber fabrics in the purification and separation of protein mixtures.

References

[1] Vajtai R. Springer Handbook of Nanomaterials. Springer-Verlag Berlin Heidelberg, 2013.

[2] Feynman RP. There's plenty of room at the bottom. Journal of Microelectromechanical Systems, 1992, 1, 60–66.

[3] Kolahalam LA, Viswanath IVK, Diwakar BS, Govindh B, Reddy V, Murthy YLN. Review on nanomaterials: Synthesis and applications. Materials Today: Proceedings,2019, 18, 2182–2190.

[4] Hulla JE, Sahu SC, Hayes AW. Nanotechnology: history and future. Human and Experimental Toxicology, 2015, 34(12), 1318–1321.

[5] Khan FA. Applications of Nanomaterials in Human Health. Springer Nature Singapore Pte Ltd., 2020.

[6] Terrones M. Science and technology of the twenty-first century: synthesis, properties, and applications of carbon nanotubes. Annual Review of Materials Research, 2003, 33, 419–501.

[7] Niu W, Zheng S, Wang D, Liu X, Li H, Han S, Chen J, Tang Z, Xu G. Selective synthesis of single-crystalline rhombic dodecahedral, octahedral, and cubic gold nanocrystals. Journal of the American Chemical Society, 2009, 131, 697–703.

[8] Najafi M, Frey MW. Electrospun nanofibers for chemical separation. Nanomaterials, 2020, 10(5), 982.

[9] Ruiz R, Kang H, Detcheverry FA, Dobisz E, Kercher DS, Albrecht TR, Pablo JJ, Nealey PF. Density multiplication and improved lithography by directed block copolymer assembly. Science, 2008, 321, 936–939.

[10] Ko FK, Wang Y. Introduction to Nanofiber Materials. Cambridge University Press, 2014.

[11] Yoo HS, Kim TG, Park TG. Surface-functionalized electrospun nanofibers for tissue engineering and drug delivery. Advanced Drug Delivery Reviews, 2009, 61, 1033–1042.

[12] Cooley JF. Improved methods of and apparatus for electrically separating the relatively volatile liquid component from the component of relatively fixed substances of composite fluids. United Kingdom Patent 6385, 1900.

[13] Tucker N, Stanger JJ, Staiger MP, Razzaq H, Hofman K. The history of the science and technology of electrospinning from 1600 to 1995. Journal of Engineered Fibers and Fabrics, 2012, 7, 63–73.

[14] Taylor G. Disintegration of water drops in an electric field. Proceedings of the Royal Society A: Mathematical, Physical and Engineering Sciences, 1964, 280, 383–397.

[15] Taylor G. The force exerted by an electric field on a long cylindrical conductor. Proceedings of the Royal Society A: Mathematical, Physical and Engineering Sciences, 1966, 291, 145–158.

[16] Taylor G. Electrically driven jets. Proceedings of the Royal Society A: Mathematical, Physical and Engineering Sciences, 1969, 313, 453–475.

[17] Larrondo L, St John Manley R. Electrostatic fiber spinning from polymer melts. I. Experimental observations on fiber formation and properties. Journal of Polymer Science: Polymer Physics Edition, 1981, 19, 909–920.

[18] Nascimento MLF, Araújo ES, Cordeiro ER, Oliveira AHP, Oliveira HP. A literature investigation about electrospinning and nanofibers: historical trends, current status and future challenges. Recent

Patents on Nanotechnology, 2015, 9(2), 76–85.

[19] Koenig K, Beukenberg K, Langensiepen F, Seide G. A new prototype melt-electrospinning device for the production of biobased thermoplastic sub-microfibers and nanofibers. Biomaterials Research, 2019, 23, 10.

[20] Abdel-Hady F, Alzahrany A, Hamed M. Experimental validation of upward electrospinning process. ISRN Nanotechnology, 2011, 851317.

[21] Islam MS, Ang BC, Andriyana A, Afifi AM. A review on fabrication of nanofibers via electrospinning and their applications. SN Applied Sciences, 2019, 1, 1248.

[22] Haghi AK, Akbari M. Trends in electrospinning of natural nanofibers. Physica Status Solidi (a), 2007, 204(6), 1830–1834.

[23] Zong X, Kim K, Fang D, Ran S, Hsiao BS, Chu B. Structure and process relationship of electrospun bioabsorbable nanofiber membranes. Polymer, 2002, 43, 4403–4412.

[24] Thompson CJ, Chase GG, Yarin AL, Reneker DH. Effects of parameters on nanofiber diameter determined from electrospinning model. Polymer, 2007, 48, 6913–6922.

[25] Reneker DH, Yarin AL. Electrospinning jets and polymer nanofibers. Polymer, 2008, 49, 2387–2425.

[26] Jarusuwannapoom T, Hongrojjanawiwat W, Jitjaicham S, Wannatong L, Nithitanakul M, Pattamaprom C, Koombhongse P, Rangkupan R, Supaphol P. Effect of solvents on electrospinnability of polystyrene solutions and morphological appearance of resulting electrospun polystyrene fibers. European Polymer Journal, 2005, 41, 409–421.

[27] Amiraliyan N, Nouri M, Kish MH. Effects of some electrospinning parameters on morphology of natural silk-based nanofibers. Journal of Applied Polymer Science, 2009, 113, 226–234.

[28] De Vrieze S, Van Camp T, Nelvig A, Hagström B, Westbroek P, De Clerck K. The effect of temperature and humidity on electrospinning. Journal of Materials Science, 2008, 44, 1357–1362.

[29] Basu S, Agrawal AK, Jassal M. Concept of minimum electrospinning voltage in electrospinning of polyacrylonitrile N,N-dimethylformamide system. Journal of Applied Polymer Science, 2011, 122, 856–866.

[30] Prabu GTV, Dhurai B, Ayush Saxena A. Influence of high voltage polarity in multi-pin upward electrospinning system on the Fiber morphology of poly (vinyl alcohol). Journal of Polymer Research, 2020, 27, 47.

[31] Zhao S, Wu X, Wang L, Huang Y. Electrospinning of ethyl-cyanoethyl cellulose/tetrahydrofuran solutions. Journal of Applied Polymer Science, 2003, 91, 242–246.

[32] Yuan X, Zhang Y, Dong C, Sheng J. Morphology of ultrafine polysulfone fibers prepared by electrospinning. Polymer International, 2004, 53, 1704–1710.

[33] Ki CS, Kim JW, Hyun JH, Lee KH, Hattori M, Rah DK, Park YH. Electrospun three-dimensional silk fibroin nanofibrous scaffold. Journal of Applied Polymer Science, 2007 106, 3922–3928.

[34] Kilic A, Oruc F, Demir A. Effects of polarity on electrospinning process. Textile Research Journal, 2008, 78, 532–539.

[35] Aulova A, Bek M, Kossovich L, Emri I. Needleless electrospinning of PA6 fibers: the effect of

solution concentration and electrospinning voltage on fiber diameter. Journal of Mechanical Engineering, 2020, 66, 421–430.

[36] Mo XM, Xu C, Kotaki M, Ramakrishna S. Electrospun P(LLA-CL) nanofiber: a biomimetic extracellular matrix for smooth muscle cell and endothelial cell proliferation. Biomaterials, 2004, 25, 1883–1890.

[37] Persano L, Camposeo A, Tekmen C, Pisignano D. Industrial upscaling of electrospinning and applications of polymer nanofibers: A review. Macromolecular Materials and Engineering, 2013, 298, 504–520.

[38] Partheniadis I, Nikolakakis I, Laidmäe I, Heinämäki J. A Mini-Review: Needleless Electrospinning of nanofibers for pharmaceutical and biomedical applications. Processes, 2020, 8, 673.

[39] Wang G, Yu D, Kelkar AD, Zhang L. Electrospun nanofiber: Emerging reinforcing filler in polymer matrix composite materials. Progress in Polymer Science, 2017, 75, 73–107.

[40] Santos JPF, Arjmand M, Melo GHF, Chizari K, Bretas RES, Sundararaj U. Electrical conductivity of electrospun nanofiber mats of polyamide 6/polyaniline coated with nitrogen-doped carbon nanotubes. Materials & Design, 2018, 141, 333–341.

[41] Uppal R, Ramaswamy GN, Arnold C, Goodband R, Wang Y. Hyaluronic acid nanofiber wound dressing-production, characterization, and in vivo behavior. Journal of Biomedical Materials Research Part B: Applied Biomaterials, 2011, 97B, 20–29.

[42] Sehaqui H, Ezekiel Mushi N, Morimune S, Salajkova M, Nishino T, Berglund LA. Cellulose nanofiber orientation in nanopaper and nanocomposites by cold drawing. ACS Applied Materials & Interfaces, 2012, 4, 1043–1049.

[43] Maleknia L, Majdi Z. Electrospinning of gelatin nanofiber for biomedical application. Oriental Journal of Chemistry, 2014, 30, 2043–2048.

[44] Barber PS, Griggs CS, Bonner JR, Rogers RD. Electrospinning of chitin nanofibers directly from an ionic liquid extract of shrimp shells. Green Chemistry, 2013, 15, 601–607.

[45] Kaya M, Akyuz B, Bulut E, Sargin I, Eroglu F, Tan G. Chitosan nanofiber production from Drosophila by electrospinning. International Journal of Biological Macromolecules, 2016, 92, 49–55.

[46] Gökbulut B, Yartaşı E, Sunar E, Kalaoglu-Altan OI, Gevrek TN, Sanyal A, Incı MN. Humidity induced inhibition and enhancement of spontaneous emission of dye molecules in a single PEG nanofiber. Optical Materials Express, 2018, 8, 568–580.

[47] Rianjanu A, Kusumaatmaja A, Suyono EA, Triyana K. Solvent vapor treatment improves mechanical strength of electrospun polyvinyl alcohol nanofibers. Heliyon, 2018, 4, e00592.

[48] Nasouri K, Shoushtari AM, Mojtahedi MRM. Effects of polymer/solvent systems on electrospun polyvinylpyrrolidone nanofiber morphology and diameter. Polymer Science Series A, 2015, 57, 747–755.

[49] Sabantina L, Klöcker M, Wortmann M, Mirasol JR, Cordero T, Moritzer E, Finsterbusch K, Ehrmann, A. Stabilization of polyacrylonitrile nanofiber mats obtained by needleless electrospinning using dimethyl sulfoxide as solvent. Journal of Industrial Textiles, 2020, 50, 224–239.

[50] Lee MW, An S, Latthe SS, Lee C, Hong S, Yoon SS. Electrospun polystyrene nanofiber membrane with superhydrophobicity and superoleophilicity for selective separation of water and low viscous oil. ACS Applied Materials & Interfaces, 2013, 5(21), 10597–10604.

[51] Watanabe K, Kim BS, Kim IS. Development of polypropylene nanofiber production system. Polymer Reviews, 2011, 51, 288–308.

[52] Sambaer W, Zatloukal M, Kimmer D. 3D modeling of filtration process via polyurethane nanofiber based nonwoven filters prepared by electrospinning process. Chemical Engineering Science, 2011, 66, 613–623.

[53] Bakr ZH, Wali Q, Ismail J, Elumalai NK, Uddin A, Jose R. Synergistic combination of electronic and electrical properties of SnO_2 and TiO_2 in a single SnO_2-TiO_2 composite nanofiber for dye-sensitized solar cells. Electrochimica Acta, 2018, 263, 524–532.

[54] Diltemiz SE, Ecevit K. High-performance formaldehyde adsorption on CuO/ZnO composite nanofiber coated QCM sensors. Journal of Alloys and Compounds, 2019, 783, 608–616.

[55] Moreno-Cortez IE, Alvarado-Castañeda A, Garcia-Gutierrez DF, Garcia-Gomez NA, Sepulveda-Guzman S, Garcia-Gutierrez DI. Core–shell PEDOT: PSS—PVP nanofibers containing PbS nanoparticles through coaxial electrospinning. Synthetic Metals, 2016, 220, 255–262.

[56] Nie G, Li Z, Lu X, Lei J, Zhang C, Wang C. Fabrication of polyacrylonitrile/CuS composite nanofibers and their recycled application in catalysis for dye degradation. Applied Surface Science, 2013, 284, 595–600.

[57] Mahapatra A, Garg N, Nayak BP, Mishra BG, Hota G. Studies on the synthesis of electrospun PAN-Ag composite nanofibers for antibacterial application. Journal of Applied Polymer Science, 2011, 124(2), 1178–1185.

[58] Zhang Z, Jiang Y, Chi M, Yang Z, Wang C, Lu X. Electrospun polyacrylonitrile nanofibers supported alloyed Pd–Pt nanoparticles as recyclable catalysts for hydrogen generation from the hydrolysis of ammonia borane. RSC Advances, 2015, 5, 94456–94461.

[59] Yeo LY, Friend JR. Electrospinning carbon nanotube polymer composite nanofibers. Journal of Experimental Nanoscience, 2006, 1, 177–209.

[60] Shi Z, Chong C, Wang J, Wang C, Yu X. Electrospun pitch/polyacrylonitrile composite carbon nanofibers as high performance anodes for lithium-ion batteries. Materials Letters, 2015, 159, 341–344.

[61] Mukai Y, Liu S, Amano E. Preparation of nanocarbon-supported nanofiber fabric for purification of contaminated water. Journal of Textile Engineering, 2020, 66, 7–15.

[62] Inagaki M, Yang Y, Kang F. Carbon nanofibers prepared via electrospinning. Advanced Materials, 2012, 24, 2547–2566.

[63] Sharma, CS, Katepalli, H, Sharma, A, Madou M. Fabrication and electrical conductivity of suspended carbon nanofiber arrays. Carbon, 2011, 49, 1727–1732.

[64] Esfahani H, Jose R, Ramakrishna S. Electrospun ceramic nanofiber mats today: Synthesis, properties, and applications. Materials, 2017, 10(11), 1238.

[65] Li D, McCann JT, Xia Y, Marquez M. Electrospinning: A simple and versatile technique for

producing ceramic nanofibers and nanotubes. Journal of the American Ceramic Society, 2006, 89(6), 1861–1869.

[66] Ramaseshan R, Sundarrajan S, Jose R, Ramakrishna S. Nanostructured ceramics by electrospinning. Journal of Applied Physics, 2007, 102(11), 111101.

[67] Wu H, Hu L, Rowell MW, Kong D, Cha JJ, McDonough JR, Zhu J, Yang Y, McGehee MD, Cui Y. Electrospun metal nanofiber webs as high-performance transparent electrode. Nano Letters, 2010 10, 4242–4248.

[68] Wu H, Zhang R, Liu X, Lin D, Pan W. Electrospinning of Fe, Co, and Ni nanofibers: Synthesis, assembly, and magnetic properties. Chemistry of Materials, 2007, 19, 3506–3511.

[69] Barakat NAM, Kim B, Kim, HY. Production of smooth and pure nickel metal nanofibers by the electrospinning technique: nanofibers possess splendid magnetic properties. The Journal of Physical Chemistry C, 2009, 113, 531–536.

[70] Kang YH, Ahn K, Jeong SY, Bae JS, Jin JS, Kim HG, Hong SW, Cho CR. Effect of plasma treatment on surface chemical-bonding states and electrical properties of polyacrylonitrile nanofibers Thin Solid Films, 2011, 519, 7090–7094.

[71] Wang Y, Górecki RP, Stamate E, Norrman K, Aili D, Zuo M, Guo W, Hélix-Nielsen C, Zhang, W. (2019). Preparation of super-hydrophilic polyphenylsulfone nanofiber membranes for water treatment. RSC Advances, 9(1), 278–286.

[72] Ifuku S. (2014). Chitin and chitosan nanofibers: Preparation and chemical modifications. Molecules, 2014, 19(11), 18367–18380.

[73] Thien DVH, Ho MH, Hsiao SW, Li CH. Wet chemical process to enhance osteoconductivity of electrospun chitosan nanofibers. Journal of Materials Science, 2014, 50, 1575–1585.

[74] Yoo HS, Kim TG, Park TG. Surface-functionalized electrospun nanofibers for tissue engineering and drug delivery. Advanced Drug Delivery Reviews, 2009, 61, 1033–1042.

[75] Chua KN, Lim, WS, Zhang P, Lu H, Wen J, Ramakrishna S, Leong KW, Mao HQ. Stable immobilization of rat hepatocyte spheroids on galactosylated nanofiber scaffold. Biomaterials, 2005, 26, 2537–2547.

[76] Maurya D, Sardarinejad A, Alameh K. Recent developments in R.F. magnetron sputtered thin films for pH sensing applications—An overview. Coatings, 2014, 4, 756–771.

[77] Wei QF, Ye H, Hou DY, Wang HB, Gao WD. Surface functionalization of polymer nanofibers by silver sputter coating. Journal of Applied Polymer Science, 2005, 99, 2384–2388.

[78] Kadavil H, Zagho M, Elzatahry A, Altahtamouni T. Sputtering of electrospun polymer-based nanofibers for biomedical applications: A perspective. Nanomaterials, 2019, 9(1), 77.

[79] Watson H. Biological membranes. Essays In Biochemistry, 2015, 59, 43–69.

[80] Buehler MJ, Yung YC. Deformation and failure of protein materials in physiologically extreme conditions and disease. Nature Materials, 2009, 8, 175–188.

[81] Kuhlman B, Bradley P. Advances in protein structure prediction and design. Nature Reviews Molecular Cell Biology, 2019, 20, 681–697.

[82] Stefani M, Dobson CM. Protein aggregation and aggregate toxicity: New insights into protein

folding, misfolding diseases and biological evolution. Journal of Molecular Medicine, 2003, 81, 678–699.

[83] Cournia Z, Allen TW, Andricioaei I, Antonny B, Baum D. Brannigan G, Buchete N-V, Deckman JT, Delemotte L, Val C, Friedman R, Gkeka P, Hege H-C, Hénin J, Kasimova MA, Kolocouris A, Klein ML, Khalid S, Lemieux MJ, Lindow N, Roy M, Selent J, Tarek M, Tofoleanu F, Vanni S, Urban S, Wales DJ, Smith JC, Bondar A-N. Membrane protein structure, function, and dynamics: A perspective from experiments and theory. The Journal of Membrane Biology, 2015, 248, 611–640.

[84] Kumar P, Sharma N, Ranjan R, Kumar S, Bhat Z F, Jeong D K. Perspective of membrane technology in dairy industry: A review. Asian-Australasian Journal of Animal Sciences, 2013, 26(9), 1347–1358.

[85] Aluko RE (2018) Proteins in Food Processing (Second Edition), Woodhead Publishing, 389–412.

[86] Navarro A, Wu HS, Wang SS. Engineering problems in protein crystallization. Separation and Purification Technology, 2009, 68(2), 129–137.

[87] Bonner PLR. Protein Purification. Taylor & Francis Group, 2007.

[88] Nadar SS, Pawar RG, Rathod VK. Recent advances in enzyme extraction strategies: A comprehensive review. International Journal of Biological Macromolecules, 2017, 101, 931–957.

[89] Iritani E, Mukai Y, Tanaka Y, Murase T. Flux decline behavior in dead-end microfiltration of protein solutions. Journal of Membrane Science, 1995, 103, 181–191.

[90] Iritani E, Mukai Y, Murase T. Upward dead-end ultrafiltration of binary protein mixtures. Separation Science and Technology, 1995, 30(3), 369-382.

[91] Casey C, Gallos T, Alekseev Y, Ayturk E, Pearl S. Protein concentration with single-pass tangential flow filtration (SPTFF). Journal of Membrane Science, 2011, 384, 82–88.

[92] Huang L, Ye H, Yu T, Zhang X, Zhang Y, Zhao L, Xin Q, Wang S, Ding X, Li H. Similarly sized protein separation of charge-selective ethylene-vinyl alcohol copolymer membrane by grafting dimethylaminoethyl methacrylate. Journal of Applied Polymer Science, 2018, 135(25), 46374.

[93] Asenjo JA. Separation processes in biotechnology. Taylor & Francis Group, 2020.

[94] Arakawa T, Timasheff SN. Mechanism of protein salting in and salting out by divalent cation salts: balance between hydration and salt binding. Biochemistry, 1984, 23, 5912–5923.

[95] Vilg JV, Undeland I. pH-driven solubilization and isoelectric precipitation of proteins from the brown seaweed Saccharina latissima—effects of osmotic shock, water volume and temperature. Journal of Applied Phycology, 2016, 29, 585–593.

[96] Arakawa T, Kita, Y, Timasheff SN. Protein precipitation and denaturation by dimethyl sulfoxide. Biophysical Chemistry, 2007, 131, 62–70.

[97] Tauro BJ, Greening DW, Mathias RA, Ji H, Mathivanan S, Scott AM, Simpson RJ. Comparison of ultracentrifugation, density gradient separation, and immunoaffinity capture methods for isolating human colon cancer cell line LIM1863-derived exosomes. Methods, 2012, 56, 293–304.

[98] Majekodunmi SO. A review on centrifugation in the pharmaceutical industry. American Journal of Biomedical Engineering 2015, 5(2), 67–78.

[99] Cvjetkovic A, Lötvall J, Lässer C. The influence of rotor type and centrifugation time on the yield and purity of extracellular vesicles. Journal of Extracellular Vesicles, 2014, 3(1), 23111.

[100] Yuana Y, Levels J, Grootemaat A, Sturk A, Nieuwland R. Co-isolation of extracellular vesicles and high-density lipoproteins using density gradient ultracentrifugation. Journal of Extracellular Vesicles, 2014, 3(1), 23262.

[101] Quirke N. Adsorption and Transport at the Nanoscale. Taylor & Francis Group, 2006.

[102] Zhu M, Carta G. Protein adsorption equilibrium and kinetics in multimodal cation exchange resins. Adsorption, 2016, 22, 165–179.

[103] Kanazawa R, Sasaki A, Tokuyama H. Preparation of dual temperature/pH-sensitive polyampholyte gels and investigation of their protein adsorption behaviors. Separation and Purification Technology, 2012, 96, 26–32.

[104] Liu S, Sumi T, Mukai Y. Development of Cibacron Blue-enhanced affinity nanofiber fabric for protein separation. 47th Textile Research symposium (Liberec, Czech Republic), 2019, 83–84.

[105] Shi D, Wang F, Lan T, Zhang Y, Shao Z. Convenient fabrication of carboxymethyl cellulose electrospun nanofibers functionalized with silver nanoparticles. Cellulose, 2016, 23, 1899–1909.

[106] Regis S, Youssefian S, Jassal M, Phaneuf MD, Rahbar N, Bhowmick S. Fibronectin adsorption on functionalized electrospun polycaprolactone scaffolds: Experimental and molecular dynamics studies. Journal of Biomedical Materials Research Part A, 2013, 102, 1697–1706.

[107] Zhu J, Sun G. Facile Fabrication of Hydrophilic Nanofibrous Membranes with an immobilized metal–chelate affinity complex for selective protein separation. ACS Applied Materials & Interfaces, 2014, 6, 925–932.

[108] Zhang H, Wang W, Li M, Lu Z, Liu K, Wang Y, Wang D. Affinity functionalization of PVA-co-PE nanofibrous membrane with Ni(ii)-chelated ligand for bovine hemoglobin adsorption. New Journal of Chemistry, 2018, 42, 3990–3994.

[109] Lu P, Hsieh YL. Lipase bound cellulose nanofibrous membrane via Cibacron Blue F3GA affinity ligand. Journal of Membrane Science, 2009, 330, 288–296.

[110] Duan C, Fu Q, Si Y, Liu L, Yin X, Ji F, Yu J, Ding B. Electrospun regenerated cellulose nanofiber based metal-chelating affinity membranes for protein adsorption. Composites Communications, 2018, 10, 168–174.

[111] Wang W, Zhang H, Zhang Z, Luo M, Wang Y, Liu Q, Chen Y, Li M, Wang D. Amine-functionalized PVA- co -PE nanofibrous membrane as affinity membrane with high adsorption capacity for bilirubin. Colloids and Surfaces B: Biointerfaces, 2017, 150, 271–278.

[112] Yoon K, Hsiao BS, Chu B. Functional nanofibers for environmental applications. Journal of Materials Chemistry, 2008, 18(44), 5326.

[113] Qin XH, Wang SY. Filtration properties of electrospinning nanofibers. Journal of Applied Polymer Science, 2006, 102, 1285–1290.

[114] Srikrishnarka P, Kumar V, Ahuja T, Subramanian V, Selvam AK, Bose P, Jenifer SK, Mahendranath A, Ganayee MA, Nagarajan R, Pradeep, T. Enhanced capture of particulate matter by molecularly charged electrospun nanofibers. ACS Sustainable Chemistry & Engineering, 2020, 8, 7762–7773.

[115] Hathout RM, Kassem DH. Positively charged electroceutical spun chitosan nanofibers can protect health care providers from COVID-19 infection: An opinion. Frontiers in Bioengineering and

Biotechnology, 2020, 8, 885.

[116] Essa WK, Yasin SA, Saeed IA, Ali GAM. Nanofiber-based face masks and respirators as COVID-19 protection: A Review. Membranes, 2021, 11, 250.

[117] Das O, Neisiany RE, Capezza AJ, Hedenqvist MS, Försth M, Xu Q, Jiang L, Ji D, Ramakrishna S. The need for fully bio-based facemasks to counter coronavirus outbreaks: A perspective. Science of The Total Environment, 2020, 736, 139611.

[118] Venugopal J, Ramakrishna S. Applications of polymer nanofibers in biomedicine and biotechnology. Applied Biochemistry and Biotechnology, 2005, 125, 147–158.

[119] Anis SF, Khalil A, Saepurahman, Singaravel G, Hashaikeh R. A review on the fabrication of zeolite and mesoporous inorganic nanofibers formation for catalytic applications. Microporous and Mesoporous Materials, 2016, 236, 176–192.

[120] Carter DC, Ho JX. Structure of serum albumin. Advances in Protein Chemistry, 1994, 45, 153–203.

[121] Das S, Bora N, Rohman MA, Sharma R, Jha AN, Roy AS. Molecular recognition of bio-active flavonoids quercetin and rutin by bovine hemoglobin: an overview of the binding mechanism, thermodynamics and structural aspects through multi-spectroscopic and molecular dynamics simulation studies. Physical Chemistry Chemical Physics, 2018, 20, 21668–21684.

[122] Reddy SM, Sette G, Phan Q. Electrochemical probing of selective haemoglobin binding in hydrogel-based molecularly imprinted polymers. Electrochimica Acta, 2011, 56, 9203–9208.

[123] S T. Serum albumin. Advances in Protein Chemistry, 1985, 37, 161–245.

[124] Abdullah ZW, Dong Y, Davies IJ, Barbhuiya S. PVA, PVA blends, and their nanocomposites for biodegradable packaging application. Polymer-Plastics Technology and Engineering, 2017, 56, 1307–1344.

[125] Karimi A, Navidbakhsh M. Mechanical properties of PVA material for tissue engineering applications. Materials Technology, 2014, 29, 90–100.

[126] Liang-Schenkelberg J, Fieg G, Waluga T. Molecular insight into affinity interaction between Cibacron Blue and proteins. Industrial & Engineering Chemistry Research, 2017, 56, 9691–9697.

[127] Zhang H, Nie H, Yu D, Wu C, Zhang Y, White CJB, Zhu L. Surface modification of electrospun polyacrylonitrile nanofiber towards developing an affinity membrane for bromelain adsorption. Desalination, 2010, 256, 141–147.

[128] Zhu J, Yang J, Sun G. Cibacron Blue F3GA functionalized poly(vinyl alcohol-co-ethylene) (PVA-co-PE) nanofibrous membranes as high efficient affinity adsorption materials. Journal of Membrane Science, 385, 269–276.

[129] Yang, E., Qin, X., & Wang, S. (2008). Electrospun crosslinked polyvinyl alcohol membrane. Materials Letters, 62(20), 3555–3557.

[130] Riyajan, SA, Chaiponban S, Tanbumrung K. Investigation of the preparation and physical properties of a novel semi-interpenetrating polymer network based on epoxised NR and PVA using maleic acid as the crosslinking agent. Chemical Engineering Journal, 2009, 153, 199–205.

[131] Ruckenstein E, Zeng X. Albumin separation with Cibacron Blue carrying macroporous chitosan

and chitin affinity membranes. Journal of Membrane Science, 1998, 142, 13–26.

[132] Yavuz H, Duru E, Genç Ö, Denizli A. Cibacron Blue F3GA incorporated poly(methylmethacrylate) beads for albumin adsorption in batch system. Colloids and Surfaces A: Physicochemical and Engineering Aspects, 2003, 223, 185–193.

[133] Guo, W., Shang, Z., Yu, Y., & Zhou, L. (1994). Membrane affinity chromatography of alkaline phosphatase. Journal of Chromatography A, 685(2), 344–348.

[134] Denizli, A, Pişkin E. Dye-ligand affinity systems. Journal of Biochemical and Biophysical Methods, 2001, 49, 391–416.

[135] Zhang H, Wu C, Zhang Y, White CJB, Xue Y, Nie H, Zhu L. Elaboration, characterization and study of a novel affinity membrane made from electrospun hybrid chitosan/nylon-6 nanofibers for papain purification. Journal of Materials Science, 2010, 45, 2296–2304.

[136] Zhang DH, Chen N, Yang MN, Dou YF, Sun J, Liu YD, Zhi GY. Effects of different spacer arms on Cibacron Blue modification and protein affinity adsorption on magnetic microspheres. Journal of Molecular Catalysis B: Enzymatic, 2016, 133, 136–143.

[137] Rabe M, Verdes D, Seeger S. Understanding protein adsorption phenomena at solid surfaces. Advances in Colloid and Interface Science, 2011, 162, 87–106.

[138] Langmuir I. The adsorption of gases on plane surfaces of glass, mica and platinum. Journal of the American Chemical Society, 1918, 40, 1361–1403.

[139] Freundlich HMF. Over the adsorption in solution. Journal of Physical Chemistry, 1906, 57, 385–471.

[140] Lan T, Shao Z, Gu M, Zhou Z, Wang Y, Wang W, Wang F, Wang J. Electrospun nanofibrous cellulose diacetate nitrate membrane for protein separation. Journal of Membrane Science, 2015, 489, 204–211.

[141] Ma Z, Kotaki M, Ramakrishna S. Electrospun cellulose nanofiber as affinity membrane. Journal of Membrane Science, 2005, 265, 115–123.

[142] Zhang J, Zhang Z, Song Y, Cai H. Bovine serum albumin (BSA) adsorption with Cibacron Blue F3GA attached chitosan microspheres. Reactive and Functional Polymers, 2006, 66, 916–923.

[143] Fukuzaki S, Urano H, Nagata K. Adsorption of bovine serum albumin onto metal oxide surfaces. Journal of Fermentation and Bioengineering, 1996, 81, 163–167.

[144] Ma ZY, Guan YP, Liu HZ. Affinity adsorption of albumin on Cibacron Blue F3GA-coupled non-porous micrometer-sized magnetic polymer microspheres. Reactive and Functional Polymers, 2006, 66, 618–624.

[145] Fukuzaki S, Urano H, Nagata K. Adsorption of protein onto stainless-steel surfaces. Journal of Fermentation and Bioengineering, 1995, 80, 6–11.

[146] Tuzmen N, Kalburcu T, Uygun DA, Akgol S, Denizli A. A novel affinity disks for bovine serum albumin purification. Applied Biochemistry and Biotechnology, 2014, 175, 454–468.

[147] Dou YF, Zhang DH, Liu H, Xia YP, Zhi GY. Polyethyleneimine grafting and Cibacron Blue F3GA modifying poly(methylmethacrylate) magnetic microspheres for protein adsorption. Journal of Chemical Technology & Biotechnology, 2017, 93, 994–1002.

[148] Liu S, Sumi T, Mukai Y. Development of Cibacron Blue-enhanced affinity nanofiber fabric for protein adsorption. Journal of Fiber Science and Technology, 2020, 76, 327–334.

[149] Xiao M, Chery J, Frey MW. Functionalization of electrospun poly(vinyl alcohol) (PVA) nanofiber membranes for selective chemical capture. ACS Applied Nano Materials, 2018, 1, 722–729.

[150] Gohil JM, Bhattacharya A, Ray P. Studies on the crosslinking of poly (vinyl alcohol). Journal of Polymer Research, 2006, 13, 161–169.

[151] Park M J, Gonzales RR, Abdel-Wahab A, Phuntsho S, Shon HK. Hydrophilic polyvinyl alcohol coating on hydrophobic electrospun nanofiber membrane for high performance thin film composite forward osmosis membrane. Desalination, 2018, 426, 50–59.

[152] Xie Z, Hoang M, Ng D, Doherty C, Hill A, Gray S. Effect of heat treatment on pervaporation separation of aqueous salt solution using hybrid PVA/MA/TEOS membrane. Separation and Purification Technology, 2014, 127, 10–17.

[153] Simonin JP. On the comparison of pseudo-first order and pseudo-second order rate laws in the modeling of adsorption kinetics. Chemical Engineering Journal, 2016, 300, 254–263.

[154] Ho Y, McKay G. Pseudo-second order model for sorption processes. Process Biochemistry, 1999, 34, 451–465.

[155] Arias FEA, Beneduci A, Chidichimo F, Furia E, Straface S. Study of the adsorption of mercury (II) on lignocellulosic materials under static and dynamic conditions. Chemosphere, 2017, 180, 11–23.

[156] Liu S, Mukai Y. Dynamic adsorption behaviors of protein on Cibacron Blue-modified PVA nanofiber fabrics. Journal of Textile Engineering, 2021, 67, 1–11.

[157] Emin C, Kurnia E, Katalia I, Ulbricht M. Polyarylsulfone-based blend ultrafiltration membranes with combined size and charge selectivity for protein separation. Separation and Purification Technology, 2018, 193, 127–138.

[158] Mukai Y, Iritani E, Murase T. Fractionation characteristics of binary protein mixtures by ultrafiltration. Separation Science and Technology, 1998, 33(2), 169-185.

[159] Sharma S, Agarwal GP. Interactions of proteins with immobilized metal ions: A comparative analysis using various isotherm models. Analytical Biochemistry, 2001, 288, 126–140.

[160] Zhang M, Wang Y, Zhang Y, Ding L, Zheng J, Xu J. Preparation of magnetic carbon nanotubes with hierarchical copper silicate nanostructure for efficient adsorption and removal of hemoglobin. Applied Surface Science, 2016, 375, 154–161.

[161] Wang J, Tan S, Liang Q, Guan H, Han Q, Ding M. Selective separation of bovine hemoglobin using magnetic mesoporous rare-earth silicate microspheres. Talanta, 2019, 204, 792–801.

[162] Song H, Yang C, Yohannes A, Yao S. Acidic ionic liquid modified silica gel for adsorption and separation of bovine serum albumin (BSA). RSC Advances, 2016, 6, 107452–107462.

[163] Qiu X, Yu H, Karunakaran M, Pradeep N, Nunes SP, Peinemann KV. Selective separation of similarly sized proteins with tunable nanoporous block copolymer membranes. ACS Nano. 2013, 7, 768–776.

[164] Liu S, Mukai Y. Selective adsorption and separation of proteins by ligand-modified

nanofiber fabric. Polymers, 2021, 13(14), 2313.

List of Publications

[1] Yasuhito Mukai, **Song Liu**, Eiji Amano. Preparation of nanocarbon-supported nanofiber fabric for purification of contaminated water. *Journal of Textile Engineering*, 2020, 66(1), 7-15.

[2] **Song Liu**, Takuro Sumi, Yasuhito Mukai. Development of Cibacron Blue-enhanced affinity nanofiber fabric for protein adsorption. *Journal of Fiber Science and Technology*, 2020, 76(10), 327-334.

[3] **Song Liu**, Yasuhito Mukai. Dynamic adsorption behaviors of protein on Cibacron Blue-modified PVA nanofiber fabrics. *Journal of Textile Engineering*, 2021, 67(1), 1-11.

[4] **Song Liu**, Yasuhito Mukai. Selective adsorption and separation of proteins by ligand-modified nanofiber fabric. *Polymers*, 2021, 13(14), 2313.

International Conferences

[1] **Song Liu**, Takuro Sumi, Yasuhito Mukai. Development of cibacron blue-enhanced affinity nanofiber fabric for protein separation. *The 47th Textile Research Symposium*, June 17-19, Leberec (Czech) 2019.

[2] **Song Liu**, Takuro Sumi, Yasuhito Mukai. Selective adsorption and separation of protein with ligand-enhanced electrospun nanofiber membrane. *18th Asian Pacific Confederation of Chemical Engineering Congress (APCChE 2019)*, September 23-27, Sapporo (Japan) 2019.

[3] Yasuhito Mukai, Tomoaki Tanabe, **Song Liu**, Yoshiyuki Bando, Tatsuya Masui. Development of selective adsorption and recovery process of gold ions by electrospun nylon membrane. *18th Asian Pacific Confederation of Chemical Engineering Congress (APCChE 2019)*, September 23-27, Sapporo (Japan) 2019.

Acknowledgement

During my study in Japan, I received a great deal of encouragement and help from the academic advisor, the leaders of Morimatsu company, and my family and friends. I would like to express my sincere gratitude to them.

I would like to thank my academic advisor Associate Professor Mukai Yasuhito for the continuously kind guidance during my doctoral course. Mukai Sensei's serious scientific attitude, rigorous academic spirit, and perfect work style deeply motivated and inspired me, which guided me into the door of academic research. I would also like to thank Professor Ito Akira, Professor Goto Motonobu, Associate Professor Kobayashi Nobusuke for their enthusiastic support and help during my research.

I am grateful to Sumi Takuro, Kurimoto Yuki, Shimoda Koya, Ito Shoji, Nakayama Satoru in the Mukai research group for helping me solve problems during the experiments and providing great help for the research.

I would like to thank Bando Yoshiyuki, Masui Tatsuya, and Zhou Jinsong of Morimatsu company for their help in my life, study, language, and work during my stay in Japan. I would like to thank the leaders and colleagues of Morimatsu company: Nishimatsu Koei, Nishimura Kyoko, Sheng Ye, Xu Sheng, Xiao Honghai, Mizutani Eiichi, Li Ying, Chen Hongwei, Wang Yufei, Wei Sijie, Zhu Yujun, Mei Longjie.

I would like to express my warmest gratitude towards my friends Benjamin, Liu Sifan, and Seulgee. With their help and companionship, I went through the difficult times, and my study life became colorful and wonderful.

Finally, I am highly grateful to my grandmother, parents, wife, and my daughter Liu Weiqiao. With their great support and dedication, I was able to complete the study.